THE USE OF SPECTRAL METHODS IN QUASI-GEOID MODELLING

Submitted in fulfillment of the academic requirements for the degree of

MASTER OF SCIENCE IN ENGINEERING

by

AMEER AMOD

Department of Geomatics

University of Cape Town
Cape Town

March 2001

DEDICATION

In memory of Professor Herman van Gysen

(1952 – 1998)

Former Head of Department of Surveying at the

University of Natal, Durban.

Acknowledgements

This research thesis was carried out from February 1999 to February 2001 under the supervision of Professor Charles Merry, Department of Geomatics, University of Cape Town, South Africa.

I am deeply grateful to Professor Charles Merry for his excellent supervision, assistance and encouragement throughout the duration of this work.

A special thanks to:

- Patrick Hicks and Cameron McInroy, Chief Directorate: Surveys and Mapping, Cape Town, for their assistance with the use of the *MICROSOFT ACCESS* software

- Dr. Fred Nicols, Department of Electrical Engineering, University of Cape Town, for his time and assistance in helping me understand the mathematics of the Fourier transform

- Derek Clarke, Richard Wonnacott, Thomas Krieg and Barbara van Geems of the Chief Directorate: Surveys and Mapping, Cape Town, for their support during this research

Last but not least, I would like to express my gratitude to my wife, Yasmin Jadwat, for her love and support during my studies.

Abstract

The Global Positioning System (GPS) has become a fast and effective tool for the horizontal and vertical control of large scale surveying and engineering projects. While GPS is generally considered a three dimensional system, the ellipsoidal heights obtained from such are impractical for surveying, engineering or geophysical applications – as the physical force of gravity is not taken into account. The heights that are found on South African topographic maps are essentially normal heights which are related to the earth's gravity field. The surface that provides the link between ellipsoidal heights and normal heights is defined as the quasi-geoid.

This thesis investigates the determination of a quasi-geoid by the application of spectral techniques to Molodensky's formula. The evaluation of the Molodensky G_1 term by means of quadrature, convolution and FFT is initially investigated. While the evaluation methods provide results which are not significantly different, the computational time varies considerably: for a grid resolution of one minute, the convolution/FFT method utilised less than one minute of computational time while the quadrature approach almost 52 hours. Grid differencing between different grid resolution shows that there is a tendency for the RMS difference to converge as the grid sizes being compared become more dense. For the test area of the South Western Cape, the G_1 contribution to the quasi-geoid for a one minute grid size is approximately 43cm.

The 2D planar FFT, 2D SFFT and 2D multi-band SFFT methods were applied to Molodensky's formula for quasi-geoid determination. Implementation of the 1D SFFT was unsuccessful in this thesis, however this is not a serious drawback as the test areas considered in this thesis are located in mid-latitude regions where the various spectral methods produce similar results. Quasi-geoids for the South Western Cape, Gauteng and South Africa have been computed. The quasi-geoid for South Africa was computed by generating the gravity anomalies from the EGM96 geopotential model and the results were compared to the quasi-geoid derived from the same geopotential model. This was merely a simulation to test the efficiency of the various spectral methods over a larger area. The 2D spherical FFT method seems a more promising method to consider for quasi-geoid/geoid computations in mid latitude regions.

TABLE OF CONTENTS

List of Figures

List of Tables

Units and Acronyms

ACRONYMS

BVP	Boundary Value Problem
DEM	Digital Elevation Model
DFT	Discrete Fourier transform
EGM96	Earth Gravity Model 1996
FFT	Fast Fourier Transform
GPS	Global Positioning System
NASA	National Aeronautical and Space Association
NIMA	National Imagery and Mapping Agency
NRL	Naval Research Laboratory
OSU	Ohio State University
PSD	Power Spectral Density
RMS	Root Mean Square
SFFT	Spherical Fast Fourier Transform
WGS84	World Geodetic System 1984

UNITS

mm	millimetre
m	metre
km	kilometre
mgal	milligal
mgal/m	milligal per metre
arcsec	arcsecond
min	minute
deg	degree

Chapter One

Introduction

The geoidal undulation or geoid-ellipsoid separation, N, can be determined from terrestrial observations combined with a high degree spherical harmonic geopotential model. Global Positioning Systems (GPS) provide an ellipsoidal height, h, that is related to the World Geodetic System 1984 (WGS84) datum and as such have no physical meaning as the earths gravity field is not considered. Gravimetric geoid models augment the third dimension to GPS (see figure 1-1 below) so that the resulting orthometric height, H, can be practically useful.

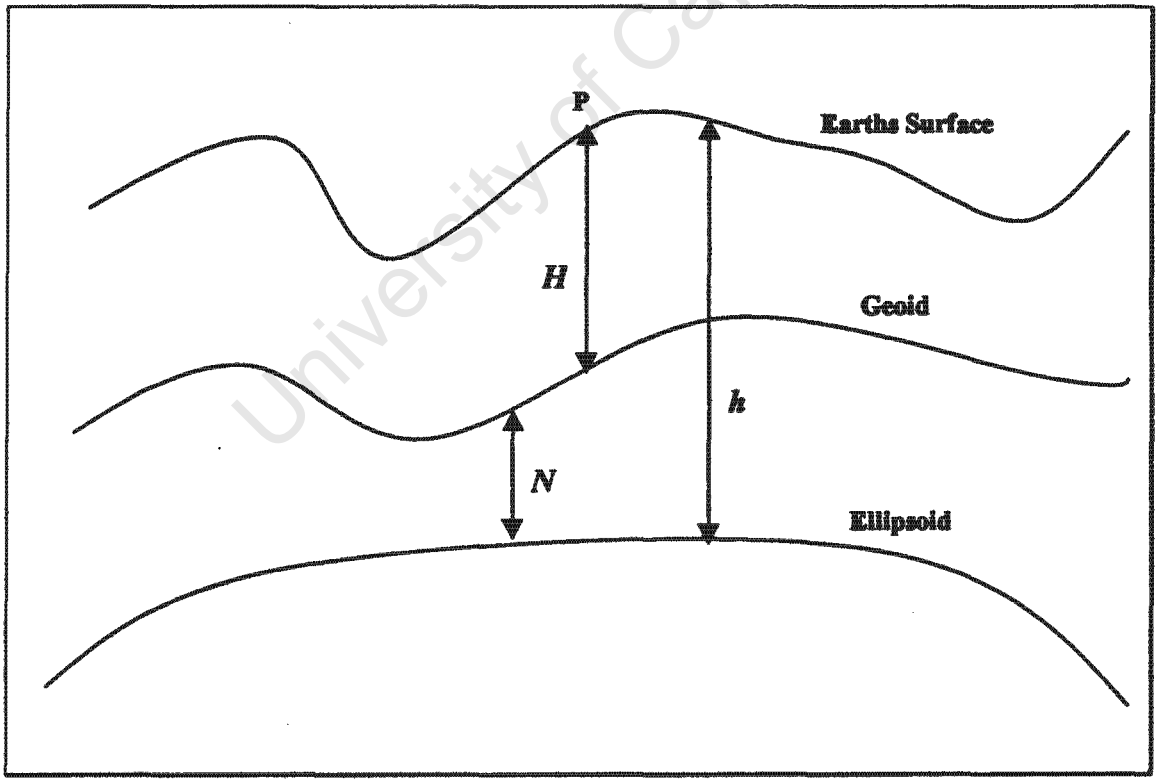

Figure 1-1: Orthometric, Geoidal and Ellipsoidal Heights (Krynski, 1995)

In the past spirit levelling has been used to determine this orthometric height with high accuracies but with severe implications: spirit levelling is time consuming, weather dependent, financially expensive and laborious. Gravimetric models are capable of achieving the same level of accuracies but the computational procedure is mathematically intensive and rigorous. The mathematical tool which has received much attention over the last two or three decades is the Fourier transform.

The fast Fourier transform (FFT) has become a popular computational tool in science and engineering applications. Over the last decade there has been an immense interest in the application of the FFT to gravity field modelling. Most integrals of physical geodesy such as the Molodensky series, terrain correction integrals and Stokes' formula can be expressed as convolution integrals and their implementation are well suited to FFT techniques. Computationally FFT methods are fast and efficient demanding data sets at gridded intervals. Fourier transform techniques are burdened with the effects of enforced periodicity, aliasing and leakage. However, with the aid of windows, zero-padding and a high degree spherical harmonic reference field these effects are significantly reduced.

In this thesis, the application of the various spectral techniques namely the planar FFT, spherical FFT and multi-band spherical FFT approaches to Molodensky's formula for quasi-geoid determination have been examined. An analysis of the Molodensky G_1 term using the methods of quadrature, convolution and FFT have further been investigated. Routines for the computational method have been developed by the author using the software package *MATLAB*.

In chapter two an outline of geodetic theory and the conceptual development toward Stokes' formula and the first order Molodensky series is documented. The development of the EGM96 geopotential model are further discussed. Chapter three examines the geodetic research and current status of quasi-geoid modelling in South Africa. Chapter four gives a comprehensive study of the Fourier transform and its associated properties. Chapter five examines the theoretical aspects of the

Molodensky G_1 term, the spectral methods proposed for quasi-geoid modelling by (Schwarz et al., 1990; Strang, 1990; Forsberg & Sideris, 1993) and the validation procedure for the quasi-geoid models. Numerical investigations of the G_1 term and quasi-geoid modelling for the Western Cape and Gauteng areas as well as the analysis of the quasi-geoid for South Africa are documented in chapter six. Conclusions and recommendations for quasi-geoid modelling inferred from the numerical investigations are highlighted in chapter seven.

Chapter Two

Techniques for Geoid Determination

2.1 Introduction

In order for Global Positioning System (GPS) derived differences in ellipsoidal height to be translated into orthometric height via the relationship $\Delta H = \Delta h - \Delta N$ the computation of a geoid is essential. To utilise the full potential of GPS, the accuracy level of the geoidal height differences, ΔN, must be consistent with the desired accuracy of the orthometric height difference, ΔH. It is unlikely that ellipsoidal height differences, Δh, will be used for practical surveying, engineering or geophysical applications as they have no physical meaning. When using ellipsoidal heights there is the possibility of water appearing to flow uphill as the physical force of gravity is not taken into account. The need to transform GPS derived ellipsoidal heights to orthometric heights using the knowledge of the position of the geoid with respect to the World Geodetic System 1984 (WGS84) ellipsoid is thus required. Surveying measurements are made in relation to the geoid because the equipment used in surveying is aligned with the local gravity vector (Heiskanen and Moritz, 1967).

Traditionally there have been two techniques from which precise geoid maps of a country could be derived. The first of these makes use of the deflections of the vertical, which provide horizontal gradients of the geoid undulation field. Integration over the surface of the earth produces the height of the geoid in all points provided a datum value is defined for an initial point. This technique is termed astrogeodetic levelling (Torge, 1991). The second technique is based on the principle of Newton's law of gravitation (Vermeer, 1998).

The reference surfaces defined above are illustrated in the following figure:

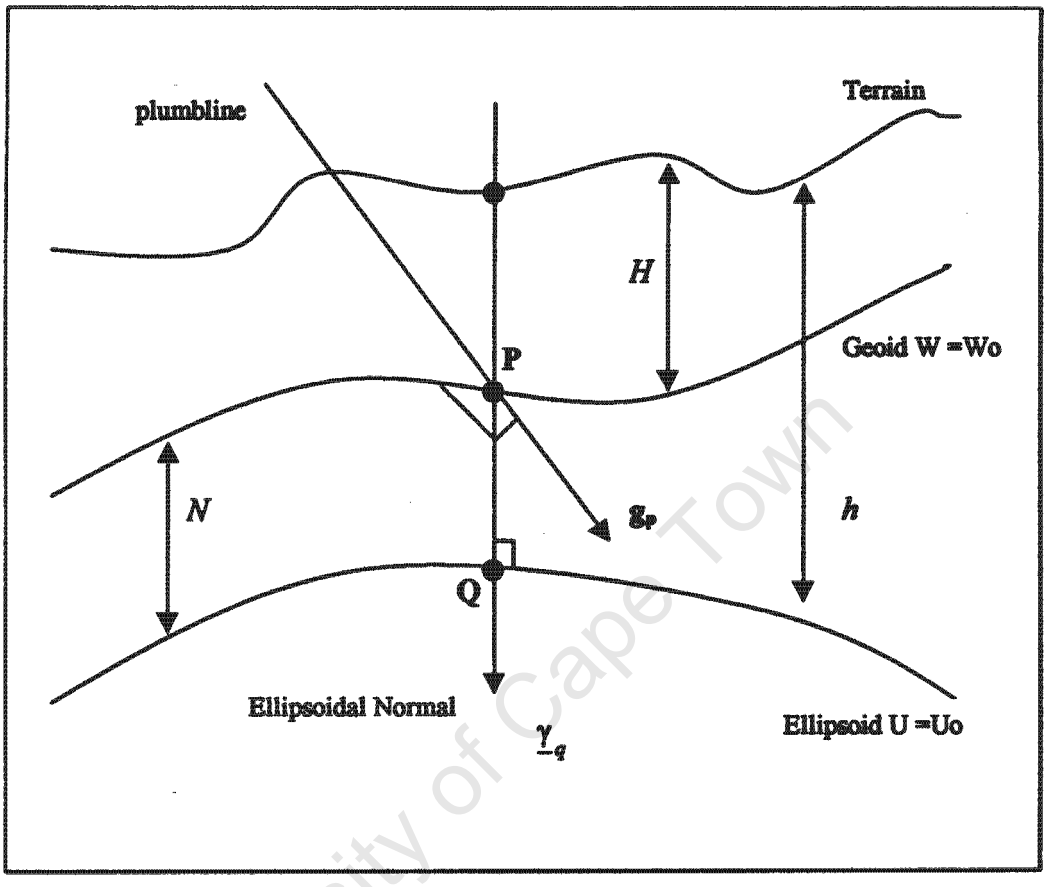

Figure 2-1: Reference Surfaces (Moritz, 1989)

The distance PQ between the geoid and the ellipsoid is called the geoidal height or geoidal undulation and is denoted by N. In the figure above: h is the ellipsoidal height, and H represents the orthometric height. Geoidal heights can be determined from the relation:

$$N = h - H \qquad (2\text{-}1)$$

The difference above is significant and can be as much as tens of meters and globally geoid heights vary from +75 to –100 meters (Merry, 1993). Apart from this magnitude the variation is extremely complex - the complexity relates to topographic

relief and subsurface rock density variations. It is a simple algebraic procedure to subtract the geoidal height N, from a GPS ellipsoidal height h, to obtain the orthometric height H. When this is done on a point by point basis, a systematic offset in the orthometric height is obtained mainly due to datum definition (Milbert and Smith, 1996). The height information defined by the three quantities in (2-1) differ in terms of physical meaning, the definition and realisation of the reference surface, observational methods and accuracies. Theoretically, they should fulfil the geometric relationship defined in (2-1) but this is cannot be fully attained practically owing to (Kotsakis and Sideris, 1999):

- random noise in the values of H, h and N;
- inconsistencies in the datum and systematic distortions inherent in H, h and N such as the long wavelength systematic errors in the geoid heights;
- geodynamic effects such as post-glacial rebound;
- theoretical approximations in the computation of either the orthometric or geoidal height such as improper density modelling in the geoid solution and the omission of sea surface topography at the tide gauges.

The gravity anomaly vector Δg, is the difference between the gravity vector $\underline{g}_p$ and normal gravity vector $\underline{\gamma}_q$:

$$\Delta g = \underline{g}_p - \underline{\gamma}_q \qquad (2\text{-}2)$$

The difference in the magnitude of equation (2-2) is termed the gravity anomaly and the difference in the direction, is the deflection of the vertical (Heiskanen and Moritz, 1967).

2.2 TECHNIQUES FOR GEOID DETERMINATION

2.2.1 Stokes' Concept

The geoidal height N is related to the disturbing potential T, by Bruns's formula:

$$N = \frac{T}{\gamma} \tag{2-3}$$

where $T = W_Q - U_Q$. Further T and Δg are related by:

$$\frac{\partial T}{\partial h} - \frac{1}{\gamma}\frac{\partial \gamma}{\partial h} T + \Delta g = 0 \tag{2-4}$$

Equation (2-4) above is denoted the *fundamental equation of physical geodesy* as it relates the measured quantity Δg to the unknown disturbing potential T (Heiskanen and Moritz, 1967; Moritz, 1989). This equation could only be solved as a real partial differential equation if Δg were known throughout space. Since Δg is only known on the geoid equation (2-4) can only be used as a boundary condition which is insufficient for computing T (shape of the earth is required to be known). The problem can be solved for the simplest possible case, where in dealing with small quantities, we assume that the earth is a sphere with radius r. With:

$$\gamma = \frac{GM}{r^2}, \quad \frac{\partial \gamma}{\partial r} = -\frac{2GM}{r^3} = -\frac{2\gamma}{r} \tag{2-5}$$

(M is the mass of the earth given by $M = 5.98 \times 10^{24}$ kg) equation (2-4) becomes:

$$\Delta g = -\frac{\partial T}{\partial r} - \frac{2}{r} T \tag{2-6}$$

$\nabla^2 T = 0$ (∇ is the vector derivative) is required to be solved subject to the boundary condition (2-6) (Krynski, 1995).

The solution of the boundary value problem in the case of a known spherical boundary reduces to Stokes' integral. This solution can be simply written as:

$$T(\mathrm{P}) = \frac{R}{4\pi}\iint_{\sigma} \Delta g S(\psi) d\sigma \qquad (2\text{-}7)$$

where R is the mean radius of the earth, σ is sphere with radius R, ψ is the spherical distance between the computation point P and the data points Q, $S(\psi)$ is Stokes' function given by:

$$S(\psi) = \csc(\psi/2) - 6\sin(\psi/2) + 1 - 5\cos(\psi) - 3\cos(\psi)\ln[\sin(\psi/2) + \sin^2(\psi/2)]$$

or alternatively by,

$$S(\psi) = \sum_{n=2}^{\infty} \frac{2n+1}{n-1} P_n(\cos\psi) \qquad (2\text{-}8)$$

where $P_n(\cos\psi)$ is the Legendre polynomial of degree n. The disturbing potential (2-7) is determined from the gravity anomalies only (Heiskanen and Moritz, 1967; Schwarz et al., 1990).

By Bruns' formula, equation (2-3), geoid heights can be determined from gravity data via:

$$N = \frac{R}{4\pi\gamma}\iint_{\sigma} \Delta g S(\psi) d\sigma \qquad (2\text{-}9)$$

Equation (2-9) is known as Stokes' formula published by G.G. Stokes in 1849. Stokes' formula applies to a sphere from which all the external masses have been removed and for which gravity is known as a continuous function over this surface. By modifying the kernel function, applying corrections to the free-air gravity anomalies, the employment of global geopotential models and digital terrain models these restrictions can be overcome. Stokes' formula is based on a spherical approximation of the reference ellipsoid which causes relative errors of the order $3\text{x}10^{-3}$m and absolute

errors of the order 1m in the geoidal undulations. These errors can be neglected for most practical purposes (Heiskanen and Moritz, 1967). The computed geoidal height N is always referred to the 'best fitting' geocentric reference ellipsoid.

2.2.2 The Molodensky Approach

Gravity reductions entail assumptions regarding the density distribution of the earth. To avoid the reduction problems in Stokes' approach, Molodensky put forth the concept of a telluroid, i.e., an auxiliary surface separating the ellipsoid height into the height anomaly ζ, and the normal height H^N. Figure (2-2) illustrates this concept:

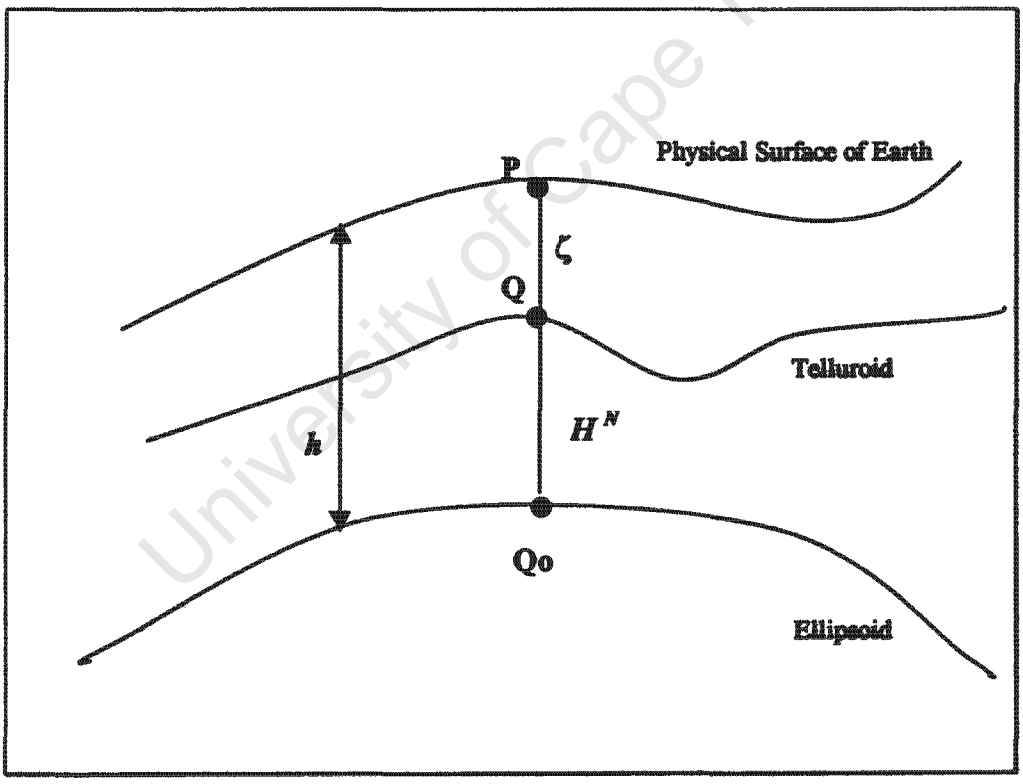

Figure 2-2: The Telluroid (Heiskanen and Moritz, 1967)

The telluroid is defined as the surface whose height above a geocentric ellipsoid corresponds to that of the physical surface above the quasi-geoid. The normal

potential of a point on the telluroid is equal to the potential at a corresponding point on the physical surface of the earth. From the figure the following expression for the geometric height h can easily be deduced:

$$h = H^{N} + \zeta \tag{2-10}$$

here h is the ellipsoidal height, H^{N} the normal height and ζ the quasi-geoidal height. In the Molodensky approach, a geoid is not used nor required. The topographic surface of the earth is used as a reference surface. Hence, no assumption regarding the internal structure of the earth is made. Molodensky defines a quasi-geoid, a superficial surface which has no physical interpretation and does not depart too far from the geoid (Vanicek, 1974).

From equations (2-1) and (2-10) we have:

$$N - \zeta = H^{N} - H \tag{2-11}$$

The quasi-geoid and the geoid coincide at sea level where the two surfaces are equal. The difference $N - \zeta$ is highly correlated with topography and may depart by a few meters on land where the topography is mountainous in nature. Equation (2-11) implies that the difference between the geoidal undulation and height anomaly is equal to the difference between the normal and orthometric height. The height anomaly is an undulation of the quasi-geoid and this difference is a distance between the quasi-geoid and the geoid which can further expressed as:

$$N - \zeta = \frac{\bar{g} - \bar{\gamma}}{\bar{\gamma}} H \tag{2-12}$$

where the quantity $\bar{g} - \bar{\gamma}$ is approximately equal to the Bouguer anomaly and H is the orthometric height. The difference $\zeta - N$ is usually positive over land where the Bouguer anomaly is generally negative (Heiskanen and Moritz, 1967).

The height anomaly given by Bruns' formula:

$$\zeta = \frac{T}{\gamma} \tag{2-13}$$

(T, is the disturbing potential and γ the normal gravity on the spheropotential surface) reasonably approximates the geoidal heights.

Molodensky's first order approximation to the solution for the height anomaly is:

$$\zeta = \frac{R}{4\pi\gamma}\iint_{\sigma}(\Delta g + G_1)S(\psi)\,d\sigma \tag{2-14}$$

with

$$G_1 = \frac{R^2}{2\pi}\iint_{\sigma}\frac{H^{N'} - H^N}{l_0^{\,3}}\Delta g\,d\sigma, \quad l_0 = 2R\sin\frac{\psi}{2} \tag{2-15}$$

The G_1 term corresponds to the gravimetric terrain correction. $S(\psi)$ represents Stokes' function, $H^{N'}$ and H^N are the normal heights of the telluroid points, Q' (attracting point) and Q (attracted point), represent the normal heights of the corresponding surface points (see figure 2-3), l_0 is the distance between the running point and the computation point. A plot of the height anomaly over the geocentric ellipsoid yields the quasi-geoid. Convergence of the Molodensky series where equation (2-13) constitutes the zero and first order terms is guaranteed for a much smoothed topography and test computations show that satisfactory results can be obtained from the first order approximations (Vanicek, 1974; Sjöberg, 1994; Torge, 1991).

In the classical boundary value problem (BVP), the geoidal heights are calculated from the gravity anomalies defined on the geoid by $\Delta g_o = g_{Po} - \gamma_{Qo}$. The quantity g_{Po} is usually computed from the gravity measured at point P (figure 2-3 below), by using the gradient of normal gravity γ to approximate the actual gradient of gravity:

$$g_{Po} \approx g_P - \frac{\partial\gamma}{\partial h}H, \quad H \approx \mathrm{PPo} \tag{2-16}$$

In the case of the Molodensky BVP, the height anomalies ζ are computed at ground level from free-air gravity anomalies defined by $\Delta g = g_P - \gamma_Q$, where, g_P is the gravity at point P and γ_Q is the normal gravity at point Q, as denoted in the figure (2-3):

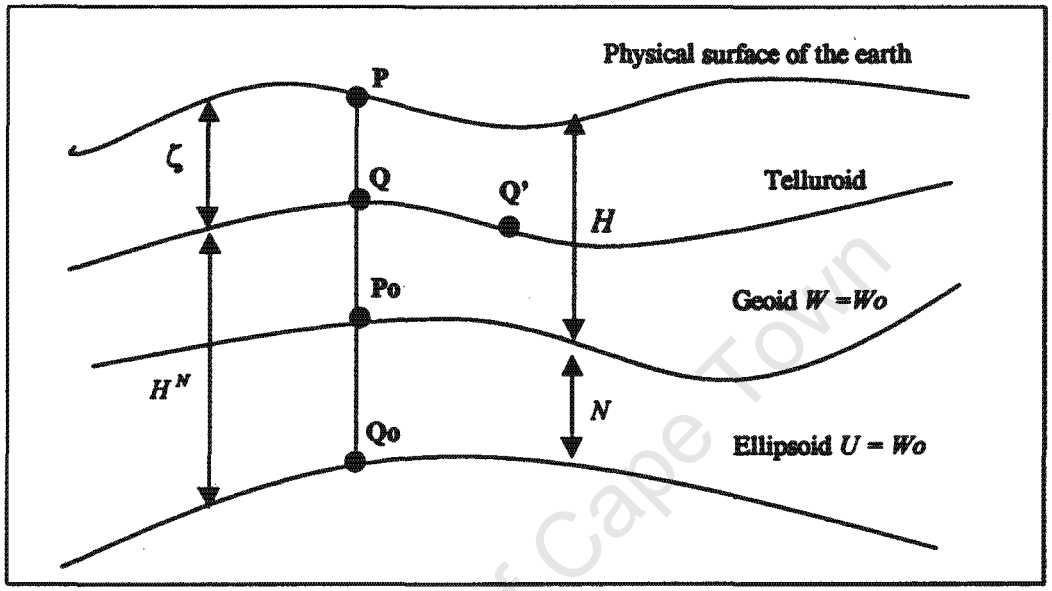

Fig 2-3: The Geometry of the Classical BVP and the Molodensky BVP (Sideris and Forsberg, 1990; Heiskanen and Moritz, 1967)

2.2.3 Geometric Method: GPS derived Geoids

In this method the orthometric heights of control points distributed homogeneously over an area are used to compute geoid heights. The ellipsoidal height of a control point is arbitrarily defined and the GPS vectors are adjusted using a least-squares minimum constraint adjustment. Relative geoidal heights at other control points can be estimated via (2-1). The geometric determination of the geoidal undulation along a short profile can be simply modelled using linear interpolation, however, since GPS surveys are seldom conducted along profiles it would be appropriate to fit a plane to (2-1):

$$N = a_0 + a_1 \Delta\lambda + a_2 \Delta\varphi \qquad (2\text{-}17)$$

where the coefficient a_0 represents a bias, a_1 and a_2 represent the tilts of the geoid or quasi-geoid plane in the directions of latitude and longitude. A minimum of three points are required to be occupied for GPS observations in order to solve for the coefficients above. If more than three points are occupied the coefficients in (2-17) can be obtained from a least-squares solution. Once the coefficients are obtained geoid/quasi-geoid heights can be interpolated at the required points. The method of interpolation could vary from that of a simple linear interpolation to collocation and bicubic spline interpolation (Merry, 1993).

The primary advantages of the geometric method are: (i) it ensures that ellipsoidal heights are consistent with the orthometric heights in the survey area and absorbs any biases in such area and (ii) it can model a small area using a simple linear interpolation. The disadvantages of the geometric method are: (i) it is subject to errors inherent in orthometric and GPS heighting which propagate through the process of interpolation and (ii) it makes the assumption that the geoid can be accurately modelled by a plane or a low-order polynomial surface (Featherstone, et al., 1998).

2.2.4 Fast Fourier Transform (FFT) Techniques

The amount of data available nowadays for the solution of gravity field convolution integrals has increased abundantly in size and type. This has called for more efficient data processing techniques and numerical solutions. Since much data is now available in gridded form the use of spectral techniques in gravity field modelling has become popular in recent years (Schwarz, et al., 1990).

Fast Fourier Transform (FFT) techniques permit the use of vast amounts of data over extended regions for improved results in local gravimetric geoid determination. Computationally FFT methods are very fast and efficient provided that gridded data are available. Stokes' formula (2-9), the Molodensky G_1 term (2-15), terrain correction integrals and deflections of the vertical, with some modification and

approximation can be written as convolution integrals which can be evaluated efficiently using the FFT methods (Schwarz et al., 1990). Using the properties of the Fourier Transform (cf. chapter four) there is no need for time consuming pointwise numerical summations and the evaluation of convolution integrals in the space domain is replaced by multiplication in the frequency domain. FFT provide results on the same grid on which the data were given (Forsberg and Sideris, 1993).

Over the last two decades works by (Sideris and Schwarz, 1986; Harrison and Dickinson, 1989; Schwarz et al., 1990), have introduced efficient algorithms for the FFT computation of terrain correction integrals, integral formulae of Vening Meinesz, planar form of Stokes' formula, the Molodensky series and deflections of the vertical. (Strang, 1990) shows that the spherical form of Stokes' formula can be expressed as a convolution integral which makes its evaluation possible via an FFT algorithm. (Forsberg and Sideris, 1993) generalise the concepts in (Strang, 1990) and propose the method of geoid computations by the use of a 'multi-band spherical FFT approach'. These methods are based on the two dimensional FFT procedure which can easily be implemented in software routines. (Haagmans et al., 1993) introduces a new method of one dimensional FFT evaluation on a sphere. In contrast to the other proposed methods, the approach of (Haagmans et al., 1993) results in an exact evaluation of convolution integrals on a sphere and not an approximate solution. The one dimensional spherical FFT approach can be applied to the integral formulae of Vening Meinesz, Hotine, Poisson and that of Stokes.

Considering all available geoid computation methods inclusive of the spherical form of Stokes' formula and modifications of it, the astrogeodetic method and the technique of least squares collocation, the FFT methods by comparison are the fastest.

2.3 THE EGM96 GEOPOTENTIAL MODEL AND EGM96 GEOID

Previously the application of Stokes' formula was limited to the classical method in which a discrete version was applied to the global numerical integration of gravity anomalies relative to the normal ellipsoid suitably weighted by Stokes' function. The effect of the gravity anomalies attenuate with increasing distance from the computation point. With the introduction of a geopotential model the integration can be restricted to a circular cap of limited radius around each computation point. In addition to this advantage, the gravity anomalies referred to the computation point are much smaller than those referred to the ellipsoid which in effect reduces the integration errors.

Geopotential models are usually made available with four components (Smith, 1998):
(a) a set of harmonic coefficients from degree 2 to N
(b) the gravity-mass constant (GM) used in the computation of the geopotential model
(c) the equatorial scale factor of the geopotential model and
(d) the permanent tide system of the model

Further description of these quantities as well as their magnitudes are to be found in (Anonymous, 1997a). The above information is sufficient to compute the gravitational potential outside a sphere (as well as inside the sphere) using equation (2-18) below (Smith, 1998):

$$V(r,\theta,\lambda)=\frac{GM}{r}\sum_{n=0}^{N}\left(\frac{a}{r}\right)^{n}\sum_{m=0}^{n}\left(\overline{C}_{nm}\cos(m\lambda)+\overline{S}_{nm}\sin(m\lambda)\right)P_{nm}(\cos\theta) \qquad (2\text{-}18)$$

V = gravitational potential to degree N from geopotential model
r,θ,λ = geocentric radius, co - latitude, longitude of computational point
a = equatorial scale factor
GM = gravity mass constant of geopotential model
$\overline{P}_{nm}$ = fully normalised Legendre functions
$\overline{C}_{nm}$, $\overline{S}_{nm}$ = fully normalised coefficients of geopotential model

A geopotential model together with additional information are combined in the generalised Bruns equation to produce a global geoid model. Gravimetric geoid determination has been successful in recent years owing to the accessibility of gravimetric data from the territory of the former Soviet Union and its satellite states, as well as China. Satellite altimetry missions provide a clearer indication of the figure of the geoid over marine areas.

Airborne gravity surveys by the National Imagery and Mapping Agency (NIMA) since 1990 over Greenland, parts of the Arctic and Antarctica surveyed by the Naval Research Lab (NRL) have helped to fill the remaining gaps. This new information combined with high quality satellite tracking results have been utilised in the global geoid model EGM96 (Vermeer, 1998; Anonymous, 1996a). The NASA (National Aeronautics and Space Association) Goddard Space Flight Centre, NIMA and Ohio State University (OSU) have collaborated to produce the NASA/OSU/NIMA EGM96 geopotential model, an improved spherical harmonic model of order 360 representing the earths gravitational potential. The use of terrestrial, airborne and altimetry data together with satellite tracking data from more than twenty satellites, including new data from GPS and TDRSS, as well as altimeter data from TOPEX, GEOSAT and ERS-1 have helped in the realisation of EGM96. EGM96 consists of a combination solution to degree and order 70, a block diagonal solution from degree 71 to 359 and a quadrature solution at degree 360 (Fashir et al., 1998). This new geopotential model has been used as a geodetic reference to update World Geodetic System 1984 (WGS84) and its application will encompass precise orbit determination, oceanographic and geophysical studies (Lemoine et al., 1996; Anonymous, 1996a).

The EGM96 geoid undulations are based on the height anomalies computed from the harmonic coefficients of the geopotential model. In order to reference the quasi-geoid to the WGS84 ellipsoid a correction of –0.53 metres has been applied. The value of -0.53 metres represents the difference between an 'ideal' earth ellipsoid in a tide free system and the WGS84 ellipsoid (Anonymous, 1997a). The EGM96 geoid gives a maximum variation of about 75 meters in the North East Atlantic and Indonesian

regions and a minimum variation of about –105 meters to the South of India and Sri Lanka. EGM96 geoid has a spatial resolution of about one degree in latitude and longitude (100 kilometers in extent) and is thus a smooth model which does not exhibit local variations in the geoidal undulations. The EGM96 geoid undulation on a fifteen minute grid appears in figure (2-4). Its statistics in units of metres on a global basis are as follows:

Mean	-0.57
Standard Deviation	30.56
Minimum	-106.99
Maximum	85.39

Table 2-1: Statistics of EGM96 Geoid (Units=m) (Anonymous, 1997a)

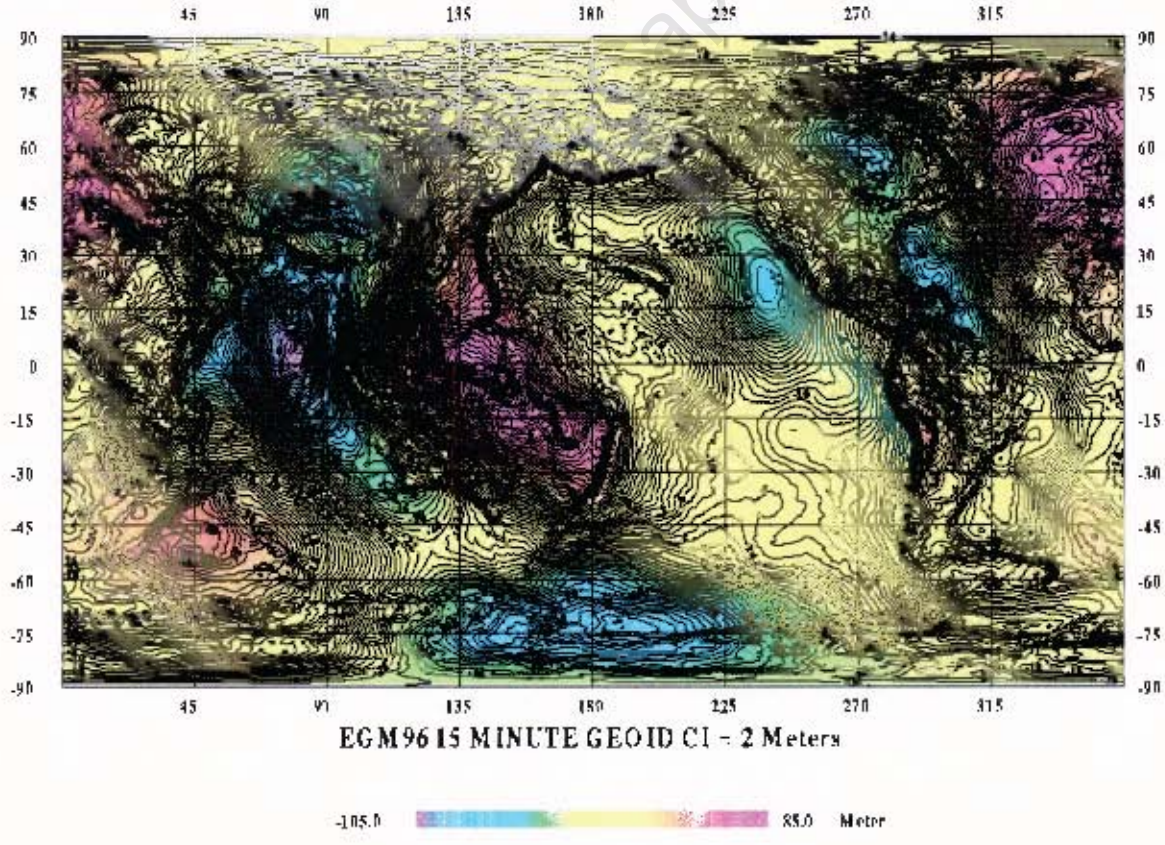

Fig 2-4: EGM96 Geoid (Anonymous, 1996b)

Chapter Three

The Geoid in South Africa

3.1 A Brief History of Geodetic Surveying in South Africa

Abbe de LaCaille made the first measurement of an arc of the meridian at the Cape in 1752. A short arc of meridian $1\frac{1}{4}^{\circ}$ in length was measured from Cape Town northwards. LaCaille's results being affected by gravity anomalies indicated that the curvature of the earth was less at southern latitudes than corresponding northern ones. A result contrary to Newton's theory. In 1820-21, Sir George Everest visited the Cape and examined LaCaille's survey. He showed that deflections of the plumbline caused by mountains adjoining the observation stations could account for the discrepancy in LaCaille's result. Between 1841 and 1848 Sir Thomas Maclear sought to verify and extend LaCaille's arc. Maclear made certain that his observations were not affected by the gravitational effect of mountain masses (Zakiewicz, 1997).

The measurements of the lengths of arcs increased in the 19th century. The determination of ellipsoids from the measurement of arcs, and from Struve's in particular, were already known and being utilised when the African Arc of the 30th meridian commenced. Sir David Gill initiated the measurement of the Arc of the 30th Meridian. In extending Maclear's triangulation chain to cover the Cape Colony, David Gill proposed to seek a datum point that would be free of large deviations of the plumb-line. Observations and calculations carried out by Gill were reduced to the Clark 1880 spheroid which was most recent at the time of the survey and in agreement with the figure of the earth in South Africa (Zakiewicz, 1997; van Gysen and Krynski, 1993).

The reference ellipsoid for the Cape Datum was the modified Clarke 1880 ellipsoid with semi-major axis $a = 6\,378\,249.145$ m, semi-minor axis $b = 6\,356\,514.967$ m and a flattening of 1/293.466. The Cape Datum is defined by the parameters of the Clarke 1880 ellipsoid and by the geodetic co-ordinates of the initial point, Buffelsfontein, of the datum. These co-ordinates derived indirectly from astronomical observations are $(\varphi_o, \lambda_o) = (-33^\circ\ 59'\ 32.000'', 25^\circ\ 30'\ 44.622'')$. This definition is by no means complete: the azimuth to a second point, the geoidal height and the deflection of the vertical at the initial point are required to complete the definition. The azimuth is explicitly defined and with Buffelsfontein being close to the sea, it is reasonable to assume a geoidal height of zero. Studies comparing Gill's geodetic co-ordinates with the satellite Doppler results of the South African contribution to the African Doppler Survey (ADOS) and Doppler translocation between these ADOS points has shown a consistent scale of between 4 and 5 parts per million (ppm) (van Gysen and Krynski, 1993; Merry and Rens, 1989; Wonnacott, 1986).

In 1960 the former Department of Land Surveying, at the University of Natal, sought to determine a geoid profile along the parallel 30° south. Astronomic latitude and longitude at 20 km intervals were determined at points of the South African and Lesotho geodetic networks. The profile was continued across the southern Orange Free State, northern Cape and Namaqualand, to reach the Atlantic Ocean close to the area of Port Nolloth. The east-west components of the deflection of the vertical were determined from the astronomic longitudes. An east-west geoid profile by the integration of these deflections over distance could then be obtained (van Gysen and Krynski, 1993). The interest in a geoid for South Africa emanating from the above investigations has led to significant contribution by South African geodesists towards the study of geoid modelling.

3.2 THE SOUTH AFRICAN HEIGHT SYSTEM

In general three height systems may be defined namely the orthometric, normal and dynamic height systems which may be expressed by the following formulae respectively (Heiskanen and Moritz, 1967):

$$H_{\text{orth}} = \frac{C}{\bar{g}}$$
$$H_{\text{norm}} = \frac{C}{\bar{\gamma}} \qquad (3\text{-}1)$$
$$H_{\text{dyn}} = \frac{C}{G}$$

$\bar{g}, \bar{\gamma}$ and G respectively represent the mean actual gravity along the plumbline, the mean normal gravity along the plumbline and a standard gravity value. C is the geopotential number (a potential difference) which is common to all three height systems and its value is independent of the route used by the levelling line to relate a point to sea level.

Heights are determined by applying corrections to observed height differences. In this respect the dynamic corrections are much larger than the orthometric and normal corrections and will not be discussed further. A rigorous computation of orthometric heights requires the gravity observations be made along a levelling route and requires the actual gravity along the plumbline of the point being levelled to. Practically it is difficult to measure this and the various methods used to approximate $\bar{g}$, make assumptions regarding the density of the earths crust and the effects of topography. To circumvent this difficulty we need to have gravity within the earth and hence the need for assumptions about the densities along plumblines by replacing the actual gravity field by a normal gravity field. Heights obtained in this manner are termed normal heights. The reference surface for normal heights is the quasi-geoid while orthometric heights are referred to the geoid.

The system of heights used in South Africa is based on the theory of Rune. This is approximately an orthometric height system in which the correction to height differences is made up of (i) a spheroidal orthometric correction and (ii) a geoidal orthometric correction. Heights based on these correction are identical to Vignal normal heights which are used in Europe. This system has been investigated by (Merry, 1977) and is considered to be a 'poor' approximation to the true orthometric height hence it is generally termed 'approximate orthometric', 'normal orthometric' or 'spheroidal orthometric' system of heights. The spheroidal orthometric correction has been applied to all South African geodetic levelling while the geoidal orthometric correction has been applied only to a few levelling lines prior to 1965. The difference between the orthometric and spheroidal orthometric heights is on average 10 centimetres across South Africa and has a maximum value of about 32 centimetres near Harrismith. The difference between the normal and spheroidal orthometric heights is at most 3 centimetres. Theoretically, the spheroidal orthometric height of a point is path dependent resulting in its loop closures not being zero. Practically this system of heights is a poor approximation to the orthometric and normal height systems leading to larger loop closures than those obtained from methods employing actual gravity (Merry, 1977).

3.3 Geoid Modelling In South Africa

3.3.1 The UCT86A Quasi-Geoid

Early attempts in computing a regional quasi-geoid for South Africa is described in (van Gysen and Merry, 1985). The method employed for the quasi-geoid computation was the least squares spectral weighting technique which combines data from the RAPP78 geopotential model and the UCT83 data set of 15' x 15' free air gravity anomalies. A weighted Stokes' function, $W(\psi)\sin\psi$, is employed. The estimated standard errors of the spectral components of each data set are used to weight the contribution of each data set. For a comprehensive description of the data sets used, the interested reader is referred to (van Gysen and Merry, 1985). The

quasi-geoid determined by this method as well as the quasi-geoid heights implied by the RAPP78 geopotential model were compared at 7 points with Doppler derived quasi-geoid heights. The 'overall fit' of the results are reproduced in the table below:

QUASI-GEOID	RAPP78	UCT86A
Mean Difference	0.08	-0.18
R.M.S Difference	1.74	1.44
Standard Error Difference	1.74	1.43

Table 3-1: Comparison of Doppler Derived Quasi-geoidal Heights with the Quasi-Geoid implied by RAPP78 and the UCT86A Quasi-Geoid computed using the Spectral Weighting Technique (Units=m)
(van Gysen and Merry, 1985)

The statistics above are plausible and an improvement would be noticed if the longer wavelength error sources such as the effects of the atmosphere and the eccentricity of the Cape Datum (Cape Datum not being geocentric) on gravity anomalies had been considered. A further source of error to be considered are the effects of terrain which could produce localised errors of up to 2 metres. The figures for the computed quasi-geoids are not reproduced here, however, an inspection of these figures in (van Gysen and Merry, 1985) show that the long wavelength features implied by the RAPP78 quasi-geoid are dominant in the quasi-geoid obtained from the method of spectral weighting. The latter, however, characterises the short wavelength features as is expected.

3.3.2 The UCT87A Quasi-Geoid

The UCT87A (figure 3-1 below) quasi-geoid was computed from a combination of UCT86 and the OSU81 geopotential model. Gravity anomalies deduced from the geopotential coefficients are combined with terrestrial data into a conventional integration of Stokes' formula. UCT87A uses an approximation to the function $S(\psi)\sin\psi$ giving greater weight to the gravity anomalies than the function employed

in the computation of UCT86A. The computations of the UCT86A and UCT87A quasi-geoids use the same data sets in different forms. Although the method of computation of the quasi-geoids differ, the results to be expected should be similar. (Merry and van Gysen, 1987) note that this is not the case owing to the UCT86 and OSU81 gravity anomalies not being compatible.

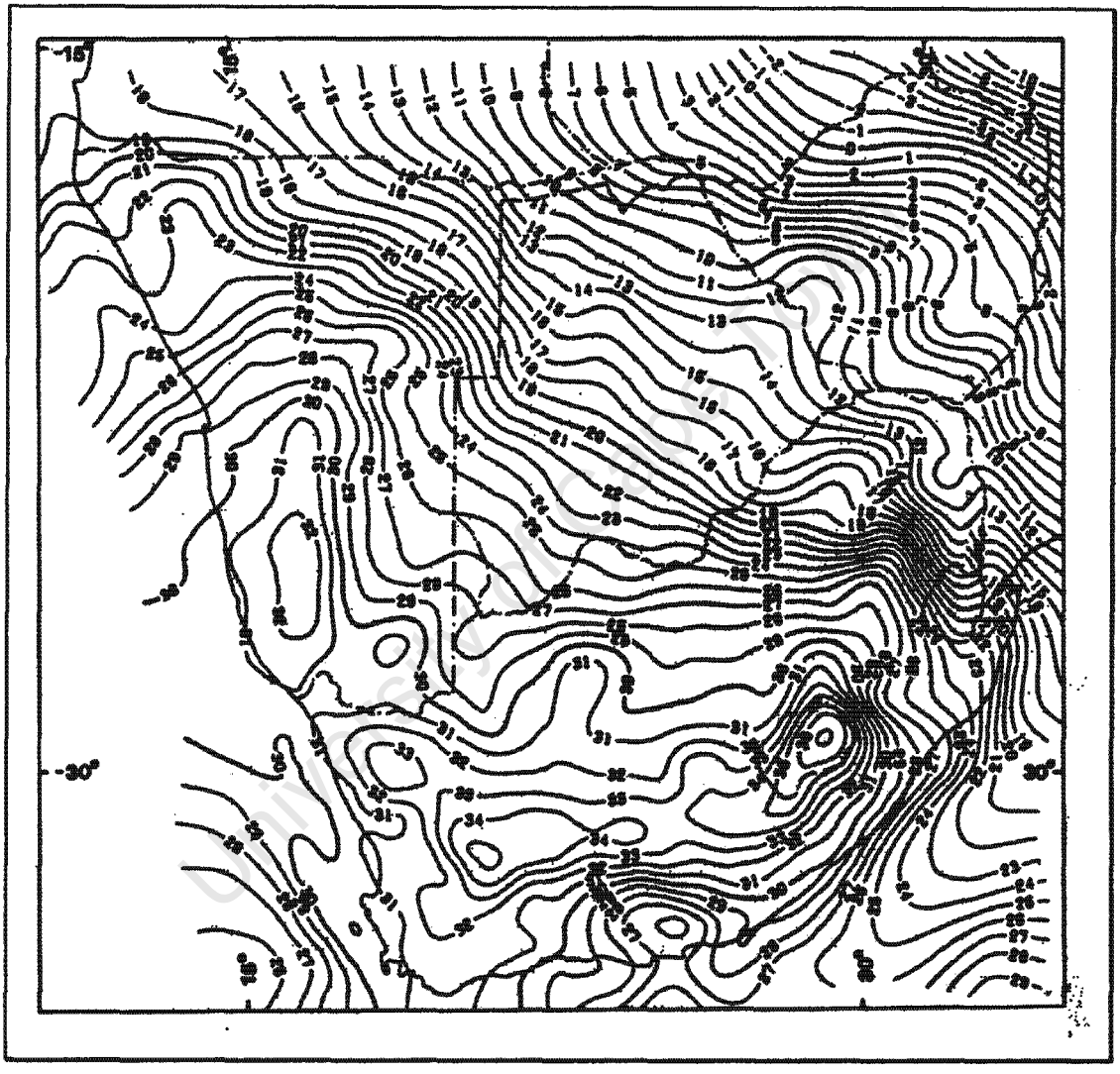

Figure 3-1: UCT87A Quasi-Geoid – Contour Interval 1 m

(Merry and van Gysen, 1987)

A comparison of the UCT86A and UCT87A quasi-geoids with a Doppler derived quasi-geoid were made to examine the quality of the quasi-geoid models. Certain points with a suspected bias were excluded. The table below gives an indication of the 'overall' statistics:

QUASI-GEOID	UCT86A	UCT87A
Mean Difference	-1.66	0.67
Standard Error Difference	2.58	1.33

Table 3-2: Comparison of Doppler Derived Quasi-geoidal Heights with the Quasi-Geoids UCT86A and UCT87A (Units=m)
(Merry and van Gysen, 1987)

A significant improvement of the mean difference and the standard error difference of the UCT87A quasi-geoid as opposed to the UCT86A quasi-geoid with the Doppler derived quasi-geoidal heights is notable. The statistics of each country tabulated in (Merry and van Gysen, 1987) further indicate that the UCT87A quasi-geoid is more consistent with the Doppler derived quasi-geoid.

A recent study (Crone and Merry, 1996) compared the UCT86A and UCT87A quasi-geoid models directly with a GPS-derived quasi-geoid for the Cape Peninsula. These results once again indicate that the UCT87A quasi-geoid conforms significantly better than the UCT86A quasi-geoid with respect to the GPS-derived quasi-geoid. The statistics reproduced from (Crone and Merry, 1996) follow in table (3-3):

DIFFERENCES IN QUASI- GEOIDS	Mean Difference	R.M.S Difference	R.M.S Difference (bias and tilts removed)
GPS-UCT86A	-2.22	2.21	0.06
GPS-UCT87A	0.17	0.07	0.05

Table 3-3: Comparison of UCT86A and UCT87A Gravimetric Quasi-Geoids with GPS-derived quasi-geoid (Units=m)
(Crone and Merry, 1996)

3.3.3 A Precise Quasi-Geoid for the Western Cape

In (Merry, 1998) a precise quasi-geoid for the Western Cape is computed by the application of convolution to the planar form of Stokes' integral. The global geopotential model used is the EGM96. The basis for the quasi-geoid computation is the 'remove-restore' technique. Here, the long wavelength component is removed from the gravity anomalies to produce the reduced anomalies. The G_1 correction term (computed from a 1'x1' digital elevation model in combination with a corresponding grid of predicted free-air anomalies) is added to the residual anomalies and the result is applied to a convolution of Molodensky's formula to predict quasi-geoidal heights for the test area. This represents the short wavelength contribution to the quasi-geoid. The final quasi-geoid is determined by 'adding back' the long wavelength component of the quasi-geoidal heights implied by the same geopotential model to the short wavelength component.

The results of this computation are not reproduced in this part of the thesis as a detailed analysis is done at a later stage with the quasi-geoid computed in this thesis. However, to mention in passing, a 6 centimetre root mean square difference was obtained between the (Merry, 1998) quasi-geoid against a GPS/Levelling derived quasi-geoid.

Chapter Four

Introduction to the Fourier Transform

4.1 Introduction

The Fourier transform has become a popular application in science and engineering. It is used in linear systems analysis, antenna studies, optics, random process modelling, probability theory, quantum physics and boundary value problems (Brigham, 1988). In recent years the Fourier transform has been extensively applied to gravity field modelling. The extensive application of the Fourier transform to convolution and spectrum analysis is due to the rediscovery in the nineteen sixties by Cooley and Tukey of a fast algorithm to compute the discrete Fourier transform. This algorithm is known as the fast Fourier transform (FFT) with the number of required complex multiplications proportional to $n\log_2 n$ in comparison to the complex n^2 multiplication's required by the conventional Fourier transform (Sideris, 1994). The time saving advantage allows for its use in the computation of large dense data sets and implementation in a small computer. Many variations exist in the formulation of the FFT algorithm and the interested reader is referred to (Sideris, 1994; Bracewell, 1978; Jackson, 1986) *inter alia*. Convolution integrals of physical geodesy can be evaluated very efficiently by the use of the FFT provided that gridded data are available. The FFT technique provides a homogeneous coverage of results on the same grid on which the data were given thus making interpolation convenient.

4.2 The Fourier Transform and Its Properties

4.2.1 Definition of the Fourier Transform

The Fourier transform decomposes or separates a waveform or function into sinusoids of different frequency which sum to the original waveform or function. It

distinguishes the different frequency sinusoids and their respective amplitudes (Brigham, 1988). The Fourier transform of a function $f(t)$ is defined as (Weaver, 1983):

$$F(\omega) = \int_{-\infty}^{\infty} f(t) e^{-i2\pi\omega t} dt \tag{4-1}$$

Transforming $F(\omega)$ by the same formula yields:

$$f(t) = \int_{-\infty}^{\infty} F(\omega) e^{i2\pi\omega t} d\omega \tag{4-2}$$

where t is time (usually represents the distance in geodetic applications), i is the imaginary unit ($i = \sqrt{-1}$) and ω is the cyclical frequency. The cyclical frequency is related to the period, T, and the linear frequency, f, by the expression $\omega = 2\pi/T = 2\pi f$. Equation (4-1) is called the direct Fourier transform of $f(t)$ and equation (4-2) is the inverse Fourier transform of $F(\omega)$. Conditions for the existence of the above integrals are to be found in numerous texts on the subject of Fourier transforms such as (Bracewell, 1978). There are functions for which the Fourier transform does not exist, however most physical functions have a Fourier transform, especially if the transform represents a physical quantity. Notationally, equations (4-1) and (4-2) can be expressed as:

$$\begin{aligned} F(\omega) &= \mathrm{F}[f(t)] \\ f(t) &= \mathrm{F}^{-1}[F(\omega)] \end{aligned} \tag{4-3}$$

where F and F^{-1} denote the direct and inverse Fourier transforms respectively.

4.2.2 The Two Dimensional Fourier Transform

The Fourier transform pair of a two dimensional function $f(x,y)$ is defined by:

$$F(u,v) = \int \int_{-\infty}^{\infty} f(x,y) e^{-2\pi i(ux+vy)} dxdy$$
$$f(x,y) = \int \int_{-\infty}^{\infty} F(u,v) e^{2\pi i(ux+vy)} dudv \qquad (4\text{-}4)$$

In analogy to the definition of the one dimensional Fourier transform, the first of equations (4-4) represents the direct Fourier transform of the function $f(x,y)$, and the second equation is the inverse Fourier transform of $F(u,v)$, ux, vy are the wave-numbers or spatial circular frequencies corresponding to the x and y spatial co-ordinates respectively and i is the imaginary unit. This can be expressed as:

$$F(u,v) = \mathrm{F}[f(x,y)]$$
$$f(x,y) = \mathrm{F}^{-1}[F(u,v)] \qquad (4\text{-}5)$$

here F and F^{-1} being the two dimensional (2D) direct and inverse Fourier transforms respectively (Weaver, 1983; Bracewell, 1978).

4.2.3 Properties of the two dimensional Fourier Transform

This section lists some properties of the Fourier transform which will be required in chapters to follow. A further listing of properties can be found in (Weaver, 1983; Schwarz et al., 1990) and for the proofs the reader is referred to (Bracewell, 1978). We follow (Schwarz et al., 1990) for the list of required properties:

(a) Linearity

$$af(x,y) + bg(x,y) \Leftrightarrow aF(u,v) + bG(u,v)$$

(b) Scaling

$$f(ax,by) \Leftrightarrow \frac{1}{|ab|}F\left(\frac{u}{a},\frac{v}{b}\right)$$

(c) Shifting

$$f(x-a,y-b) \Leftrightarrow e^{-2\pi(au+bv)}F(u,v)$$

(d) Convolution

$$f(x,y) * g(x,y) \Leftrightarrow F(u,v)G(u,v)$$

where $*$ is the convolution operator.

(e) Correlation

$$f(x,y) \otimes g(x,y) \Leftrightarrow F(u,v)G^{*}(u,v)$$

where $G^{*}(u,v)$ is the complex conjugate of $G(u,v)$ and $\otimes$ denotes correlation.

4.2.4 The 2D Discrete Fourier Transform (DFT)

In physical geodesy applications, function values are given only at discrete values of the independent variable in a finite domain, $-X/2 \le x \le X/2, -Y/2 \le y \ge Y/2$, hence the definitions of equations (4-4) and (4-5) cannot be applied. In the numerical evaluation of the transforms we speak of the discrete Fourier transform which can be considered as an approximation to the continuous Fourier transform.

With the data known only at discrete points of a regular grid with sampling intervals, Δx and Δy we may express the record lengths of the data by:

$$X = M\Delta x, \quad y = N\Delta y \tag{4-6}$$

where M and N represent the number of points along the x and y directions respectively.

Using the discretised data, the 2D Fourier transform integral may be approximated by the sum:

$$F(m\Delta u, n\Delta v) = \sum_{k=0}^{M-1}\sum_{l=0}^{N-1} f(k\Delta x, l\Delta y) e^{-2\pi\left(\frac{mk}{M}+\frac{nl}{N}\right)} \Delta x \Delta y \qquad (4\text{-}7)$$

where $m = 0, 1, 2, \ldots, M-1$ and $n = 0, 1, 2, \ldots, N-1$

with inverse:

$$f(k\Delta x, l\Delta y) = \sum_{k=0}^{M-1}\sum_{l=0}^{N-1} F(m\Delta u, n\Delta v) e^{2\pi\left(\frac{mk}{M}+\frac{nl}{N}\right)} \Delta u \Delta v \qquad (4.8)$$

where $k = 0, 1, 2, \ldots, M-1$ and $l = 0, 1, 2, \ldots, N-1$

The approximations (4-7) and (4-8) form the basis for connecting the 2D continuous and 2D discrete Fourier transforms. Assuming the function to be periodic, with periods X and Y in the x and y directions, then the Fourier transform (spectrum) becomes discrete with frequency spacings at:

$$\Delta u = \frac{1}{X} = \frac{1}{M\Delta x}, \quad \Delta v = \frac{1}{Y} = \frac{1}{N\Delta y} \qquad (4\text{-}9)$$

in units of cycles per sampling interval over the range $-M/2\Delta u \le u \le M/2\Delta u$ and $-N/2\Delta v \le v \le N/2\Delta v$. Due to the discreteness of the data the highest recoverable frequencies are:

$$u_M = \pm\frac{M}{2}\Delta u = \pm\frac{1}{2\Delta x}, \quad v_N = \pm\frac{N}{2}\Delta v = \pm\frac{1}{2\Delta y} \qquad (4\text{-}9a)$$

u_M and u_N in the above equation are called the Nyquist frequencies and are the highest frequencies that can be resolved from the given discrete data set (Sideris, 1994).

4.2.5 The Fast Fourier Transform (FFT)

The fast Fourier transform (FFT) is a discrete Fourier transform (DFT) algorithm developed by J. W. Cooley and J. W. Tukey in 1965. The FFT reduces the number of computations from something of the order n^2 to $n\log n$. The algorithm sequentially combines progressively larger weighted sums of data samples so as to produce the DFT (Weaver, 1983). There are basically two types of Tukey-Cooley FFT algorithms in use, decimation in time and decimation in frequency. An intuitive development of the FFT algorithm is given in (Bracewell, 1978).

4.3 Convolution and Correlation

4.3.1 Convolution

The convolution of two functions $f(x)$ and $g(x)$ is defined by:

$$g(x) * f(x) = \int_{-\infty}^{\infty} g(s) f(h-s) ds \qquad (4\text{-}10)$$

The function $g(x)$ can be considered as a filter that is applied to the function $f(x)$. Equation (4-10) can be written as:

$$f(x) * g(x) = \int_{-\infty}^{\infty} f(s) g(h-s) ds \qquad (4\text{-}11)$$

hence the convolution can be interpreted as the filtering of one function by another. A powerful tool in the analysis of discrete data is the convolution theorem which states

that 'convolution in the space domain can be replaced by multiplication in the spectral domain and vice versa' (Schwarz, 1984). Mathematically this can be expressed as:

$$\begin{aligned} f(x) * g(x) &\Leftrightarrow F(u)G(u) \\ f(x)g(x) &\Leftrightarrow F(u) * G(u) \end{aligned} \tag{4-12}$$

where $\Leftrightarrow$ denotes the Fourier transform pair. Most integrals in gravity field approximation such as Stokes' integral and the terrain correction integral can be expressed as convolution integrals. The convolution theorem replaces the integration in the space domain by multiplication in the frequency domain. The theorem gives an insight into the operations performed on sampled data such as averaging and smoothing. In two dimension, the convolution integral is defined as (Bracewell, 1978):

$$f(x,y) * g(x,y) = \int_{-\infty}^{\infty}\int_{-\infty}^{\infty} f(x',y')g(x-x',y-y')dx'dy' \tag{4-13}$$

The convolution is obtained by rotating one function 180 degrees about the origin (by reversing the signs of x and y), displacing and multiplying with the other function. The product is integrated to obtain the value of the convolution integral for that particular displacement.

Discretisation of equations (4-11) and (4-13) yield:

$$\begin{aligned} f(x) * g(x) &= \sum_{x'=0}^{N-1} f(x')g(x-x')\Delta x' \\ f(x,y) * g(x,y) &= \sum_{y'=0}^{M-1}\sum_{x'=0}^{N-1} f(x',y')g(x-x',y-y')\Delta x'\Delta y' \end{aligned} \tag{4-14}$$

which represent the one and two dimensional discrete convolutions respectively.

4.3.2 Convolution Properties

The two dimensional convolution is defined in the same way and enjoys the same properties as in the one dimensional case. The properties for the one dimensional case are stated below without proof (Weaver, 1983):

(a) associativity

$$f(x)*[g(x)*h(x)]=[f(x)*g(x)]*h(x)$$

(b) commutativity

$$f(x)*g(x)=g(x)*f(x)$$

(c) distributivity

$$f(x)*[g(x)+h(x)]=f(x)*g(x)+f(x)*h(x)$$

4.3.3 Covariance and Correlation

For two dimensional stationary data the cross-correlation is defined as (Schwarz et al., 1990):

$$R_{fg}=\lim_{\substack{X\to\infty\\Y\to\infty}}\frac{1}{XY}\int_{-X/2}^{X/2}\int_{-Y/2}^{Y/2}f(x',y')g(x+x',y+y')dx'dy' \qquad (4\text{-}15)$$

Using the relation from section (4.2.3) (e) we can express (4-15) as:

$$R_{fg}(x,y)=\lim_{\substack{X\to\infty\\Y\to\infty}}\frac{1}{XY}f(x,y)\otimes g(x,y) \qquad (4\text{-}16)$$

The cross-correlation describes the degree of linear dependence between the two functions a distance (x',y') apart. In computing the cross-correlation of two functions, the complex conjugate of the second function is taken and displaced by an

amount $-x$. In the case of a convolution the second function is rotated and then displaced. The cross-correlation is associative and distributive with respect to addition, but unlike convolution it is not commutative (Weaver, 1983). The spectrum of the cross-correlation function is the power spectral density given by:

$$S_{fg}(u,v) = \mathrm{F}[R_{fg}(x,y) = \lim_{\substack{X\to\infty \\ Y\to\infty}} \frac{1}{XY} F^*(u,v)G(u,v) \tag{4-17}$$

F is the 2D Fourier transform operator and F^* the complex conjugate of F. The power spectral density (PSD) describes the general frequency composition of the data. The correlation function, R_{fg}, can be obtained from the PSD via the relation:

$$R_{fg}(x,y) = \mathrm{F}^{-1}[S_{fg}(u,v)] \tag{4-18}$$

If the mean of the two functions, $f(x,y)$ and $g(x,y)$ are known, that is,

$$\mu_f = \lim_{\substack{X\to\infty \\ Y\to\infty}} \frac{1}{XY} \int_{-X/2}^{X/2} \int_{-Y/2}^{Y/2} f(x,y)dxdy$$

$$\mu_g = \lim_{\substack{X\to\infty \\ Y\to\infty}} \frac{1}{XY} \int_{-X/2}^{X/2} \int_{-Y/2}^{Y/2} g(x,y)dxdy \tag{4-19}$$

then the covariance function can be defined by:

$$C_{fg} = R_{fg}(x,y) - \mu_f \mu_g \tag{4-20}$$

When the function $f(x,y)$ and $g(x,y)$ are equal, that is, $f(x,y) = g(x,y)$, we call (4-16), (4-17) and (4-20) the autocorrelation, auto power spectral density and auto-covariance respectively (Schwarz, 1984; Schwarz et al., 1990).

4.4 Errors In The Discrete Fourier Transform

4.4.1 Circular Convolution and Zero Padding

For discrete data sequences as opposed to theoretically defined data sequences the Fourier transform cannot in general be computed. In this respect, the discrete Fourier transform (DFT) is defined for N samples at N uniformly spaced frequencies around a unit circle. Multiplication of two DFT sequences corresponds to convolution of the two sequences, but this convolution is circular and has to be appropriately implemented (Jackson, 1986). The properties of the DFT are similar to the Fourier transform except that the shifts and convolutions are circular. The convolution of two N element sequences, cannot be contained in an N element sequence. Zero padding is the operation of extending a sequence of length N_1 to a length $N_2 > N_1$, by appending $N_2 - N_1$ zero samples to the given sequence. The two prime reasons for doing this are:

- circular convolution can be used to implement linear convolution if the two sequences contain sufficient zero samples to prevent circular wrap-around or overlapping of the result.
- The density of the DFT samples are increased from N_1 to N_2. Therefore, the spectrum between the DFT samples can be interpolated to an arbitrary density by sufficient zero padding (Jackson, 1986).

4.4.2 Aliasing

Sampling of discrete data is performed at equally spaced intervals. Sampling of data points which are too close together results in correlated and highly redundant data which could be time consuming and laborious. Sampling at data intervals too far apart results in confusion between the high and low frequency components of the original data. High frequency components can 'mimic' low frequency components for large sampling intervals. This phenomenon is known as aliasing. Aliasing can be removed if the sampling rate is chosen to be at least twice as high as the highest

frequency present in the data, that is, twice the Nyquist frequency (cf. equation (4-9)) (Bendat and Piersol, 1971; Schwarz et al., 1990).

4.4.3 Leakage

Owing to a signal having a limited data length discontinuities become inherent at the boundaries of the signal. The finite data record length does not permit the long wavelength components to be accurately represented. This effect is called leakage because some energy leaks from the main lobes to its side lobes. Leakage can be overcome by the use of a windowing function such as the Hamming or Hanning window. Windows are applied to the data in order to reduce the discontinuities at the boundaries of the data set. Windowed data sets are smoothly truncated to zero at the boundaries so that the periodic extension of the data becomes continuous (Harris, 1978).

4.5 The Split Cosine Window

The split cosine window is basically a cosine lobe of width $\frac{\alpha}{2}N$ that is convolved with a rectangular window of width $(1-\frac{\alpha}{2})N$. The window smoothly tapers the data values at the edges of a data set reducing them to zero (Harris, 1978). The edge tapering is customarily done in the spatial domain. However this is also possible in the spectral domain by applying a series of transfer functions such as Stokes' kernel to the data.

For the data sets used in this thesis the cosine taper is used to suppress the signal content at all frequencies in a particular spatial domain namely the edges of the data sets. In this respect the cosine window is applied only to the data edges. This is typically the reason for it being termed a 'split cosine filter' as it uses 'ones' in the middle of the data set, hence no attenuation of the data in the middle.

The window is defined by (Harris, 1978):

$$w(n) = \begin{cases} 1.0 & 0 \le |n| \le \alpha \frac{N}{2} \\ 0.5\left[1.0 + \cos\left(\pi \frac{n - \alpha\frac{N}{2}}{(1-\alpha)\frac{N}{2}}\right)\right] & \alpha\frac{N}{2} \le |n| < \frac{N}{2} \end{cases} \qquad (4\text{-}21)$$

A two dimensional plot of a typical 10% cosine taper window is illustrated in figure (4-1) below (note the edge tapering):

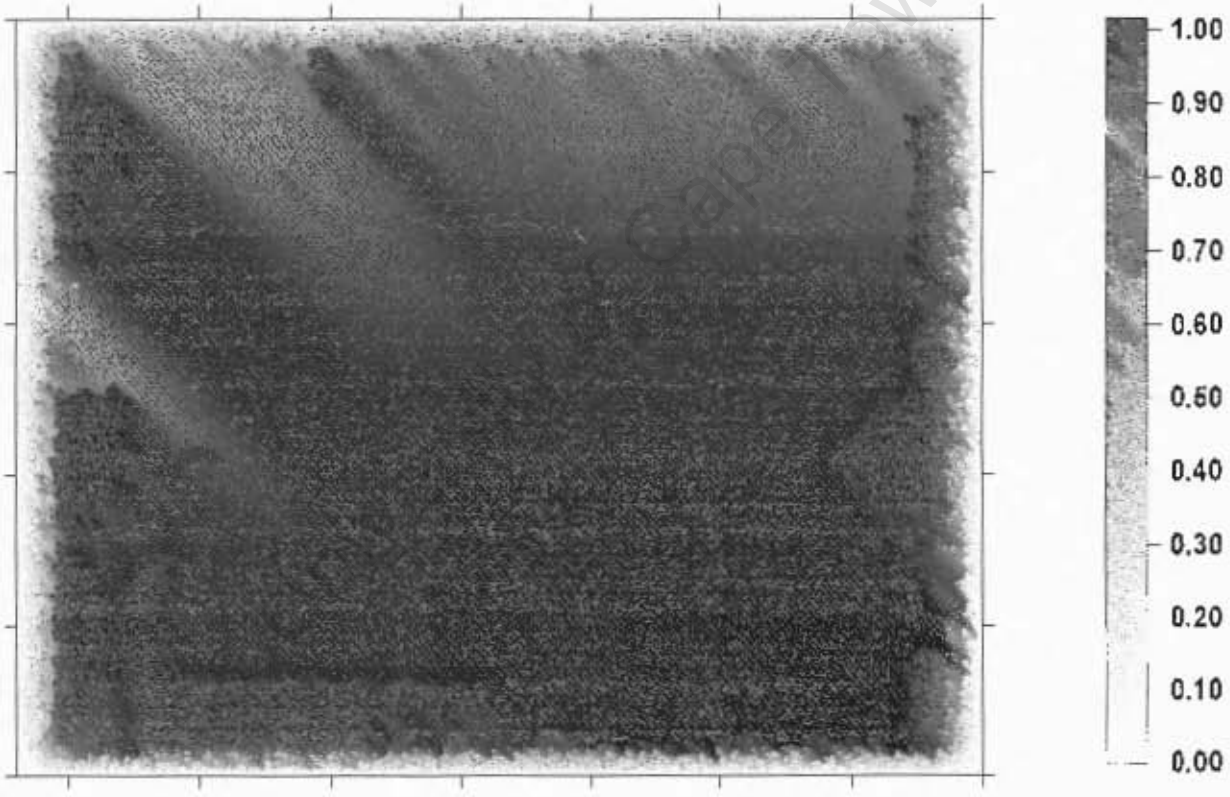

Figure 4-1: A Two Dimensional Split Cosine Window

Chapter Five

Theoretical Development Towards a Quasi-Geoid

5.1 The Molodensky G_1 Term

5.1.1 Introduction

Assumptions regarding the density distributions of the masses within the upper layer of the earth are required when geoidal heights are computed from terrestrial data, which weaken the confidence in the computed entities. Molodensky put forth the concept of a quasi-geoid to circumvent the practical problems associated with geoidal computations. Quasi-geoidal heights, generally termed the height anomaly, are computed without assumption and in theory can be computed exactly. The quasi-geoid has no physical meaning: it is purely a mathematical abstraction and is not an equipotential surface of the earth's gravity field. There is no disadvantage in using the quasi-geoid as a reference system for heights and has been adopted in many Eastern European countries, the former U.S.S.R and South Africa (Vanicek and Krakiwsky, 1987; Merry, 1977).

Expanding equation (2-14) , the height anomaly can be expressed as:

$$\zeta = \zeta_0 + \zeta_1 = \frac{R}{4\pi\gamma}\iint_\sigma \Delta g S(\psi)d\sigma + \frac{R}{4\pi\gamma}\iint_\sigma G_1 S(\psi)d\sigma \qquad (5\text{-}1)$$

In its first approximation the Molodensky's solution yields Stokes' integral (see equation, 2-9). In addition we have a small correction, ζ_1, which can be considered a correction term to Stokes' formula. G_1 is the correction term which

largely represents the effect of topography. Reformulating (2-15), the G_1 term can be expressed on the plane by:

$$G_1 = \frac{1}{2\pi}\iint_E \frac{h(x,y)-h(x_p,y_p)}{l^3(x,y)}\Delta g(x,y)\,dxdy \qquad (5\text{-}2)$$

where the horizontal distance l, between the two points is given by:

$$l(x,y) = \begin{cases} \left[(x_p-x)^2+(y_p-y)^2\right]^{1/2} & , \text{ for } x_p \neq x \text{ or } y_p \neq y, \\ 0 & , \text{ for } x_p = x \text{ and } y_p = y \end{cases} \qquad (5\text{-}3)$$

$h(x_p,y_p)$ is the normal height of the point of interest, $h(x,y)$ and $\Delta g(x,y)$ represent the normal height and the free-air gravity anomaly at the dummy point in the integration (Merry, 1998; Sideris and Schwarz, 1986). Free air gravity anomalies can be represented by a linear relationship, $\Delta g = a + bh$, where a is essentially the Bouguer anomaly which is independent of irregularities in the topography and b is equal to the Bouguer gradient of approximately 0.1119 mgal per metre. Statistically, this represents a linear correlation of the free-air anomalies with height. The solution for the height anomaly, equation (2-14) assumes this relationship (Moritz, 1966; Moritz, 1968). To a first approximation the G_1 term corresponds to the gravimetric terrain correction (Torge, 1991).

5.1.2 Practical Evaluation of the G1 Term

5.1.2.1 Quadrature

Practical evaluation of the G_1 term is an exercise in numerical integration (quadrature). The G_1 term can be determined as such by the expression:

$$G_1 = \frac{1}{2\pi}\sum \frac{h-h_p}{l^3}\Delta g\, dxdy \qquad (5\text{-}4)$$

where $dx = R\,d\lambda\cos\varphi_p$ and $dy = R\,d\varphi$, $d\varphi, d\lambda$ correspond to the spatial resolution of the data which are generally available in gridded form. Numerical integration of (5-4) can be quite time consuming for areas which are large in extent or where there is a high spatial resolution of the data. The principal limitation is that the summation has to be repeated for each and every point at which the G_1 contribution is required. From a computational point of view this can be numerically intensive requiring large amounts of memory and computational time. The availability of gridded height and gravity anomaly data, the development of the FFT algorithm and the convolution form of many geodetic integrals, have led to attractive alternatives in computational methods. In the next section the computation of the G_1 term via the FFT is examined.

5.1.2.1 The FFT Approach

The integral (5-2) can be expressed as a convolution integral and as such can be efficiently evaluated via the FFT. Equation (5-2) can be expressed in convolution form as follows (Sideris and Schwarz, 1986):

$$G_1 = \frac{1}{2\pi}\{\,[h(x,y)\Delta g(x,y)]_p * r(x_p,y_p) - h(x_p,y_p)[\Delta g(x_p,y_p) * r(x_p,y_p)]\,\} \qquad (5\text{-}5)$$

where * denotes the 2D convolution operator and $r(x_p,y_p) = l^{-3}(x_p,y_p)$.

Convolution in the space domain can be replaced by multiplication in the frequency domain by simply multiplying the spectra. The G_1 correction term can be evaluated in the frequency domain by:

$$G_1(x,y) = \frac{1}{2\pi}\Big[F^{-1}\{\ F\{h(x,y)\Delta g(x,y)\ \}F\{r(x,y)\}\ \} - h(x,y)F^{-1}\{\ F\{\Delta g(x,y)\}F\{r(x,y)\}\ \}\ \Big] \tag{5-6}$$

where F and F^{-1} denote the two dimensional direct and inverse Fourier transforms respectively (Sideris and Schwarz, 1986).

When dealing with real data there is usually some type of limited spatial extent. Implementation of the FFT assumes periodicity of the data. If the data is just 'fed' into the FFT algorithm, a cyclic convolution will result since the gridded data set is treated as if it has a torodial geometry. To avoid cyclic convolution a fifty percent pad is generally applied to the data sets, that is, double data length in each dimension. Usually a zero pad is applied (see section 4.4). A discontinuity exists where the data transitions into the padded region. This generates a Gibbs phenomenon and a 'ringing effect' can be seen around the circumference if a synthesis is done after the FFT analysis (Milbert, 1999; Bracewell, 1978). To remove this effect windows are applied to the data which smooth out the existing discontinuities at the boundaries of the data sets, thus eliminating from the spectrum any frequencies which are not really in the data. Windowed data sets are smoothly truncated to zero at the data edges so that the periodic extension of the data becomes continuous. A popular choice for such a window is the split cosine filter previously discussed in chapter four (Sideris and Schwarz, 1986; Milbert, 1999).

5.2 GRAVIMETRIC QUASI-GEOID

5.2.1 The Remove-Restore Approach

The remove-restore approach has become a popular method in the computation of gravimetric geoids/quasi-geoids. In this approach most of the long and medium wavelength components which are provided by a global geopotential model are removed from the gravity anomalies according to:

$$\Delta g_r = \Delta g_f - \Delta g_L \tag{5-7}$$

where Δg_r is the reduced gravity anomaly, Δg_f are the free-air anomalies and Δg_L is given by the following spherical harmonic expansion:

$$\Delta g_L = \frac{GM}{ar}\sum_{n=2}^{k}\left(\frac{a}{r}\right)^n (n-1)\sum_{m=0}^{n}\left(\overline{C}_{nm}\cos m\lambda + \overline{S}_{nm}\sin m\lambda\right)\overline{P}_{nm}(\cos\theta) \qquad (5\text{-}8)$$

where G is the Newtonian gravitational constant, M is the mass of the solid earth, oceans and atmosphere, r is the radial distance to the computation point, a is the length of the semi-major axis of the reference geocentric ellipsoid, $\overline{C}_{nm}$ and $\overline{S}_{nm}$ are the fully normalised harmonic coefficients of degree n and order m, $\overline{P}_{nm}$ is the fully normalised Legendre function, θ, λ are the geodetic co-latitude and longitude of the computation point and k is the maximum degree of the summation. The global geopotential model is assumed to have the same origin, mass and surface potential as the geocentric reference ellipsoid removing the need for the zero and first degree terms.

The residual gravity anomalies in equation (5-7) can be used to compute the short wavelength contribution to the quasi-geoid also termed the 'residual quasi-geoid' using the formula given in (5-1). The medium and long wavelength quasi-geoid heights computed from the same global geopotential model are restored to this 'residual quasi-geoid' solution. The spherical harmonic expansion of the medium and long wavelength contributions to the quasi-geoid heights is given by:

$$\zeta_L = \frac{GM}{\gamma r}\sum_{n=2}^{k}\left(\frac{a}{r}\right)^n \sum_{m=0}^{n}\left(\overline{C}_{nm}\cos m\lambda + \overline{S}_{nm}\sin m\lambda\right)\overline{P}_{nm}(\cos\theta) \qquad (5\text{-}9)$$

with γ being the normal gravity. The quasi-geoidal height is thus the sum of both the long wavelength, ζ_L, and short wavelength, ζ_s, contributions, that is, $\zeta = \zeta_L + \zeta_s$ (Merry, 1998; Vella and Featherstone, 1999; Fotopoulos et al., 1999).

There are two important advantages in using the remove-restore approach:

- The residual quantities are numerically much smaller than the original ones. Globally, gravity anomalies could be hundreds of milligals and geoid undulations as much as one hundred metres. In removing, a priori, the global spherical harmonic model, the residual quantities will be only tens of milligals or submetre respectively. Error sources such as the oblateness of the earth and numerical round-off errors are significantly reduced.
- Long range correlation's are also significantly reduced. Practically no global model is perfect and some long range correlation's will still exist, however, with an appropriately chosen global model these can be ignored (Vermeer, 1992).

5.2.2 Spectral Techniques for Geoid Computation

5.2.2.1 Planar Approximation of Stokes' Formula

In order to express Stokes' formula as a convolution integral, the spherical surface must be approximated locally by a tangent plane. In this case, the spherical distance, ψ, is small and Stokes' function (2-8) can be derived as a flat earth approximation:

$$S(\psi) = \frac{1}{\sin \frac{1}{2}\psi} + \ldots = \frac{2R}{l} + \ldots \qquad \text{(5-10)}$$

Substituting (5-10) into Stokes' integral (5-1), we can express the quasi-geoidal height as a two dimensional convolution integral (Schwarz et al., 1990; Strang, 1990):

$$\begin{aligned} \zeta &- \frac{1}{4\pi R\gamma} \iint \Delta g S(\psi)\, dx dy \\ &= \frac{\Delta x \Delta y}{4\pi R\gamma} \left(\frac{2R}{l} * \Delta g \right) \\ &= \frac{\Delta x \Delta y}{2\pi\gamma} \left(\frac{1}{l} * \Delta g \right) \end{aligned} \qquad \text{(5-11)}$$

where * denotes the two dimensional convolution operator, $l = (x^2 + y^2)^{-1/2}$ is the integral kernel function, Δg are the reduced gravity anomalies (including the G_1 term), $\Delta x = R\Delta\varphi$, $\Delta y = R\cos\varphi\Delta\lambda$ (φ is the mean latitude) and γ is the normal gravity which can be computed from the closed formula of Somigliana given by (Anonymous, 1997a):

$$\gamma = \gamma_e \frac{1 + \left(\frac{b\gamma_p}{a\gamma_e} - 1\right)\sin^2\varphi}{\sqrt{1 - e^2\sin^2\varphi}} \tag{5-12}$$

where:

a, b represent the semi-major and semi-minor axes of the reference ellipsoid respectively

γ_e, γ_p represent the theoretical gravity at the equator and poles, respectively

e^2 is the first numerical eccentricity

φ is the geodetic latitude

Equation (5-11) can be evaluated in the frequency domain by a two dimensional FFT (Sideris, 1994):

$$\zeta = \frac{\Delta x \Delta y}{2\pi\gamma} F^{-1}\left\{ F\left(\frac{1}{l}\right) F(\Delta g) \right\} \tag{5-13}$$

The singularity of the integral kernel is evaluated separately at the computation point. The central area or the inner zone contribution is considered to be the four innermost blocks with the radius of a circle having the same area as the four blocks. The inner zone contribution ζ_i is given by:

$$\zeta_i = \frac{r}{\gamma}\Delta g \tag{5-14}$$

where $r = R\sqrt{\frac{\Delta\varphi\Delta\lambda\cos\varphi}{\pi}}$, with φ being the mean latitude of the area of interest.

Equations (5-11) and (5-13) can be conceptualised in terms of 'input-output' relations. As discussed in chapter four, section (4.3.1), the convolution of two functions can be interpreted as the filtering of one function by the other. In this respect we can express the equations (5-11) and (5-13) by:

$$\zeta(x,y) = l(x,y) * \Delta g(x,y) \Leftrightarrow \zeta(u,v) = L(u,v)\Delta G(u,v) \qquad \textbf{(5-15)}$$

In the context of linear systems, the gravity anomalies, $\Delta g(x,y)$, can be considered the input function and the kernel, $l(x,y)$, the filtering function. $\zeta(x,y)$ is the output function which in this case represents the quasi-geoid heights. The spectrum of the kernel denoted by $L(u,v)$ is referred to as the transfer function. These relations can be expressed by means of a simple diagram depicting the input-output relations:

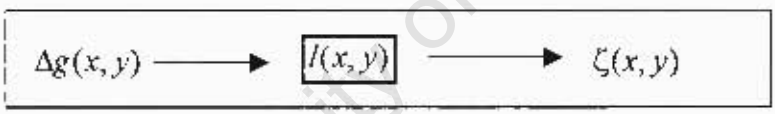

Fig 5-1: A single-input-single-output system

For further examples of single and multiple input-output systems the interested reader is referred to (Schwarz et al., 1990; Bendat and Piersol, 1971).

5.2.2.2 The 2D Spherical FFT Approach

Stokes' integral is valid for the exterior of the earths sphere and can be expressed in geographical co-ordinates as (Strang, 1990):

$$\zeta(\varphi_P,\lambda_P) = \frac{R}{4\pi\gamma}\int_{\varphi_Q}\int_{\lambda_Q}\Delta g(\varphi_Q,\lambda_Q)S(\upsilon_{PQ})\cos\varphi_Q d\varphi_Q d\lambda_Q \qquad \textbf{(5-16)}$$

this integral can be expressed as a convolution integral by representing ψ_{PQ} only in terms of $(\varphi_P - \varphi_Q)$ and $(\lambda_P - \lambda_Q)$:

$$\sin^2\frac{1}{2}\psi_{PQ} = \sin^2\frac{1}{2}(\varphi_P - \varphi_Q) + \sin^2\frac{1}{2}(\lambda_P - \lambda_Q)\left[\cos^2\bar{\varphi} - \sin^2\frac{1}{2}(\varphi_P - \varphi_Q)\right] \tag{5-17}$$

where $\bar{\varphi}$ is the mean latitude of the area. In (5-17), ψ, is expressed as a function of latitude and longitude differences only. As a result we can express (5-16) as a convolution in φ and λ of Stokes' function with $\Delta g\cos\varphi$. With $s = \sin\frac{1}{2}\psi$, Stokes' function can be evaluated by:

$$S(\psi) = \frac{1}{s} - 4 - 6s + 10s^2 - (3 - 6s^2)\ln(s + s^2) \tag{5-18}$$

and (5-16) can be transformed into the following convolution integral:

$$\zeta(\varphi_P, \varphi_P) = \frac{R\Delta\varphi\Delta\lambda}{4\pi\gamma}(S * \Delta g\cos\varphi) \tag{5-19}$$

where * is the two dimensional convolution operator. The convolution integral (5-19), can be evaluated via the FFT in the frequency domain by:

$$\zeta(\varphi_P, \varphi_P) = \frac{R\Delta\varphi\Delta\lambda}{4\pi\gamma}F^{-1}\{F(S)\,F(\Delta g\cos\varphi)\} \tag{5-20}$$

(5-19) and (5-20) make it possible to compute quasi-geoid heights over large areas on the sphere for all grid points using the two dimensional convolution or Fourier transform operator respectively. The contribution of the inner zone is computed from (5-14). The disadvantage is that large amounts of computer memory are

required since zero padding is applied in the latitude and longitude direction. Additional errors are introduced due to the approximations made on the kernel function (Sideris, 1994). Near the equator the error is minimum while at high latitudes these errors become more significant. The reason is that at high latitudes, the $\Delta\varphi, \Delta\lambda$ blocks are no longer rectangular blocks owing to meridian convergence. To circumvent this problem other block sizes need to be introduced instead of having equal $\Delta\varphi, \Delta\lambda$ blocks (Strang, 1990).

5.2.2.3 The 2D Multi-band Spherical FFT (SFFT) Approach

The two dimensional multi-band SFFT approach is an extension to the two dimensional spherical FFT technique proposed by (Strang, 1990). In the multi-band approach the area of interest is divided into an even number of equidistant latitude bands extending from the northern to southern limits. An improvement to the expression, $\sin^2 \frac{1}{2}\psi$, in (5-17) can be expressed as (Forsberg and Sideris, 1993):

$$\sin^2 \frac{1}{2}\psi_{PQ} = \sin^2 \frac{1}{2}(\varphi_P - \varphi_Q) + \sin^2 \frac{1}{2}(\lambda_P - \lambda_Q)\left[\cos^2 \varphi_p \cos \Delta\varphi + \cos\varphi_p \sin \varphi_p \sin \Delta\varphi\right] \quad (5\text{-}21)$$

The approximation (5-21) expresses Stokes' function as a P dependent function $S_p(\Delta\varphi, \Delta\lambda)$. Stokes' function may be evaluated correctly along a parallel, $\varphi = \varphi_p$, yielding an exact solution for quasi-geoidal heights computed either by (5-19) or (5-20) along this parallel. Spherical errors will still exist, however the magnitude of the errors will be much smaller closer to the reference parallel.

The area of interest is subdivided into an even number of overlapping zones each with mean latitude, $\overline{\varphi}$. The overlapping is required because of the need for zero padded extensions utilised in the FFT approach so that only the central part of the band is used (Blais, 2000). A composite solution result at a latitude φ, between

two consecutive reference bands φ_i and φ_{i+1} can be obtained by a linear interpolation of the geoidal heights obtained in each overlapping band (see figure 5-2):

$$N(\sigma) = \frac{\varphi - \bar{\varphi}_{i+1}}{\bar{\varphi}_i - \bar{\varphi}_{i+1}} N_i + \frac{\bar{\varphi}_i - \varphi}{\bar{\varphi}_i - \bar{\varphi}_{i+1}} N_{i+1} \qquad \textbf{(5-22)}$$

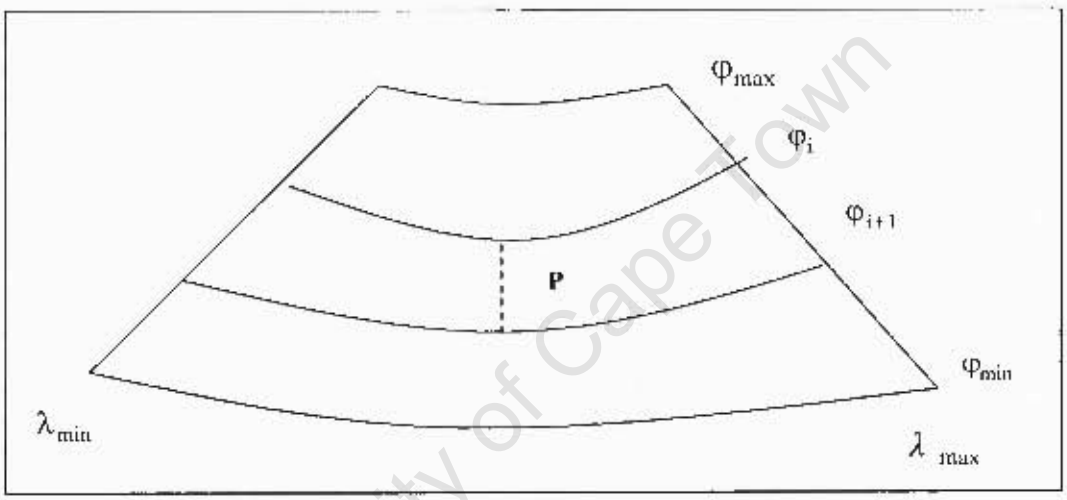

Fig 5-2: Linear interpolation of solutions from overlapping bands
(Forsberg and Sideris, 1993)

The desired accuracy depends on the number of reference bands selected. The two dimensional spherical FFT approach is equivalent to the multi-band SFFT technique with one band. In order to reduce the number of transforms required, the reference band structure may be limited to cover a particular latitude zone of interest, especially when zero padding is used to minimise the effects of cyclic convolution.

5.2.2.4 The 1D Spherical FFT (SFFT) Approach

(Haagmans et al, 1993) proposed a one dimensional spherical FFT method to produce exact geoidal heights for all points along a parallel. In this approach there is no need to approximate Stokes' kernel. The evaluation is implemented by use of the following formula:

$$\zeta(\varphi_p, \lambda_p) = \frac{R\Delta\varphi\Delta\lambda}{4\pi\gamma} F^{-1}\left\{ \sum_{\varphi_Q=\varphi_1}^{\varphi_M} F\left[S\left(\psi_{PQ}\right)\right] F\left[\Delta g\left(\varphi_Q, \lambda_Q\right)\cos\varphi_Q\right] \right\} \qquad (5\text{-}23)$$

with ϕ_p fixed.

The advantage of the 1D SFFT approach is that it is an exact evaluation of the quasi-geoidal heights along a parallel and yields the same results (when zero padding is applied) as direct numerical integration of Stokes' formula. It utilises less computational memory as opposed to its 2D counterparts since it deals only with one complex array at a time. However, it is burdensome in terms of computational time as each operation is performed parallel by parallel. (Tsiavos, 1996) showed that for a grid dimension of 512x512, the 1D SFFT used almost ten hours of computational time as opposed to the 2D SFFT which utilised about 23 minutes.

The implementation of the 1D SFFT algorithm was unsuccessful in this thesis. However, this is not a serious drawback since for areas in the mid latitude regions (as in the test areas used in this thesis) all the FFT methods outlined above yield similar results.

5.3 QUASI-GEOID VALIDATION

5.3.1 Bicubic Interpolation

The evaluation of the quality of a gravimetric quasi-geoid can be determined by interpolating the grid points of the gravimetric geoid ζ_{GRAV}, to a network of points where quasi-geoidal heights have been derived from the GPS/levelling observations, that is ζ_{GPS}. The interpolation method chosen for this study is the bicubic interpolation. The method fits a bicubic surface through the data points. The value of the interpolated point is obtained by a combination of the values of the closest sixteen points. The interpolation can be easily implemented on a standard package such as *MATLAB* (Anonymous, 1997b). Simple transformation models, such as the planar and four parameter transformation model can be used to determine the statistics of the residual quantity $\Delta\zeta = \zeta_{GRAV} - \zeta_{GPS}$. A discussion of these models follow.

5.3.2 Planar Transformation Model

The fitting of the gravimetric quasi-geoid to the GPS/levelling control points can be done via a planar transformation model of the form:

$$\Delta\zeta = A^T x + v = a_0 + a_1(\lambda - \lambda_m) + a_2(\varphi - \varphi_m) \qquad (5\text{-}24)$$

where x is the vector of unknown parameters, A is the vector of known coefficients, v denotes a residual random noise term, a_0 represents a bias in the vertical level, a_1 and a_2 are the tilts in the directions of longitude and latitude respectively, λ_m, φ_m respectively denote the mean longitude and mean latitude of the points at which the quasi-geoid is validated. The coefficients a_i (i = 0,1,2) can be determined from a simple parametric least squares adjustment. The maximum

tilt between the two surfaces can be computed by the application of distance formula to the values of a_1 and a_2.

5.3.3 Four Parameter Transformation Model

The four parameter transformation model can also be used to compare the quality of fit between the gravimetric quasi-geoid and the quasi-geoid determined from the GPS/levelling. Mathematically it is represented by the following expression (Heiskanen and Moritz, 1967):

$$\Delta\zeta = A^T x + v = a_0 + a_1 \cos\varphi\cos\lambda + a_2 \cos\varphi\sin\lambda + a_3 \sin\varphi \qquad \text{(5-25)}$$

The four parameter transformation model absorbs most of the datum inconsistencies among the height datasets as well as geoid biases due to the long wavelength component.

In both the models above, (5-24) and (5-25), the adjusted values for the residuals obtained from a least squares adjustment give a more realistic picture of the level of agreement between the gravimetric quasi-geoid and the GPS/levelling quasi-geoid. The final residual values are a combination of gravimetric quasi-geoid errors, levelling and the GPS errors. The parametric part $A^T x$, describes all possible datum inconsistencies and systematic effects in the data sets (Fotopoulos et al., 1999; Kotsakis and Sideris 1999).

Chapter Six

Numerical Investigations

6.0 Introduction

In this chapter the fast Fourier transform methods are applied to evaluate the Molodensky G_1 term, quasi-geoids for the test areas of the South Western Cape and Gauteng. A residual quasi-geoid for South Africa computed using the various spectral techniques from gravity anomalies generated by the program *GEOGRAV* is compared to the residual quasi-geoid generated by the same program.

For the G_1 term, we look at the different methods for its evaluation, namely, the quadrature approach, the convolution approach and the FFT approach. The G_1 term is evaluated on grid sizes of 5, 3, 2 and 1 minute respectively. The results obtained from the three methods as well as their computational time requirements are also compared. Grid differencing in order to determine convergence of the RMS discrepancy between the different grid resolutions compared is further investigated. The G_1 contribution to the quasi-geoid for a grid dimension of one minute is also computed.

In computing the quasi-geoid the planar, spherical and multi-band spherical FFT approximations are applied to Molodensky's formula. Differences between the methods were examined in order to determine the most efficient method that could be used to compute a South African quasi-geoidal model. The quasi-geoids for the South Western Cape and Gauteng were validated against GPS/Levelling derived quasi-geoids. Finally, a quasi-geoid for South Africa is calculated to test the accuracy of the different spectral methods over a larger area.

6.1 THE MOLODENSKY G_1 TERM

6.1.1 Description of Data used in the Computation

The initial test area for the computation of the G_1 term and the quasi-geoid (see section 6.2) made use of gravity and elevation data of the south western Cape, a coastal province of South Africa. The computation of the G_1 term requires a consistent set of gridded free air anomalies and a concomitant digital elevation model (DEM). The data was made available by Professor C. Merry of the Department of Geomatics at the University of Cape Town. We briefly discuss the compilation of the data sets used for the evaluation of the G_1 term and later in the computation of the quasi-geoid

Free-air gravity and elevation data are required on both land and sea as the test area is a coastal province. The land point gravity data are taken from the University of Cape Towns' gravity database which has been compiled from a variety of sources over many years (Van Gysen and Merry, 1987) and has been predominantly improved by data provided by the Council for Geoscience in 1997. The data are irregularly spaced and some interpolation is required to obtain a consistently gridded data set. The interpolation process simply extracts the Bouguer anomalies of a particular test area and this scattered data is interpolated onto a one minute grid using the Kriging method contained in the software package *Surfer* (Keckler, 1995).

Bouguer anomalies are used for the interpolation as they vary smoothly and are thus easily to interpolate. Free air anomalies are strongly correlated with elevation. The Bouguer anomalies are converted to free air anomalies using the Bouguer gradient of 0.1119 milligal per metre (mgal/m) and a one minute DEM. The DEM was compiled from a series of 1:50 000 topographic maps via manual interpolation. The marine data set on a three and a half minute grid was made available by the Danish National Survey and Cadastre (Anderson and Knudsen, 1998) and this was interpolated using Kriging onto a one minute grid (Merry, 1998; Merry and Amod 2001). Grids of size five, three and two

minutes were interpolated from the one minute grid for numerical and computational time comparisons. These grids were produced by simply deleting, for example, every second point to obtain a two minute grid. The grid resolution of one minute was the best available data set for the computations effected for the G_1 computation and the quasi-geoids for the test areas of the South Western Cape and Gauteng. Figures (6-1) and (6-2) are plots of the free air anomaly data and the digital elevation model of the test area respectively. Table (6-1) gives an indication of the data statistics.

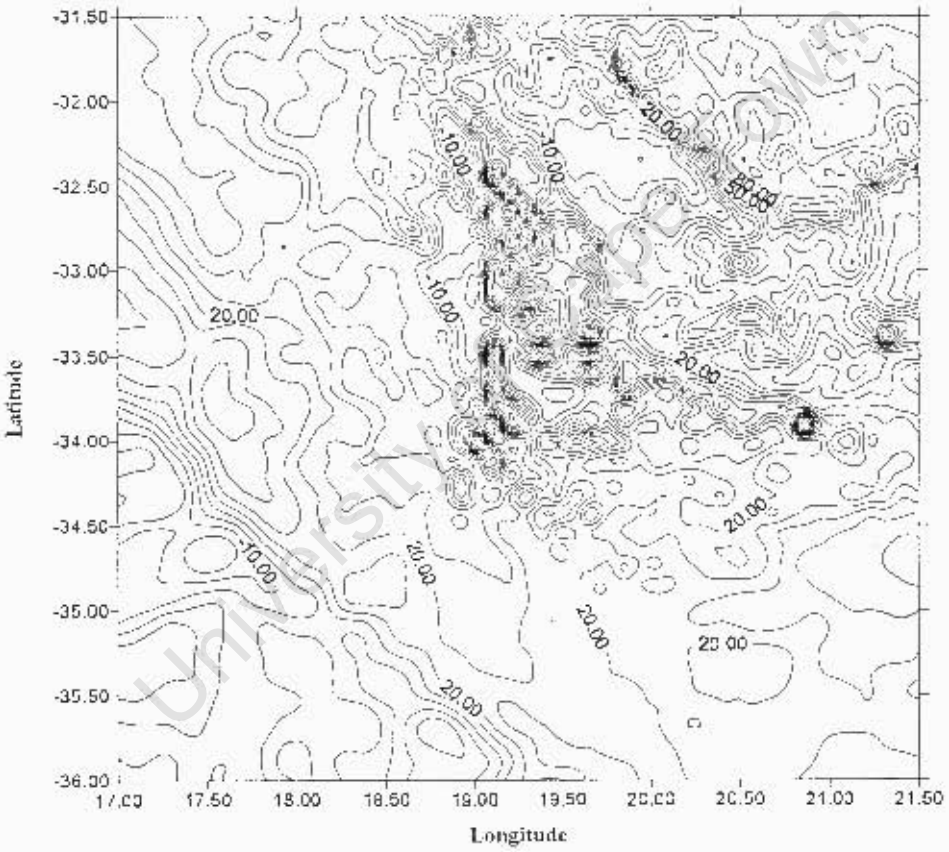

Figure 6-1: Free Air Gravity anomalies – South Western Cape (Contour Interval: 10mgal)

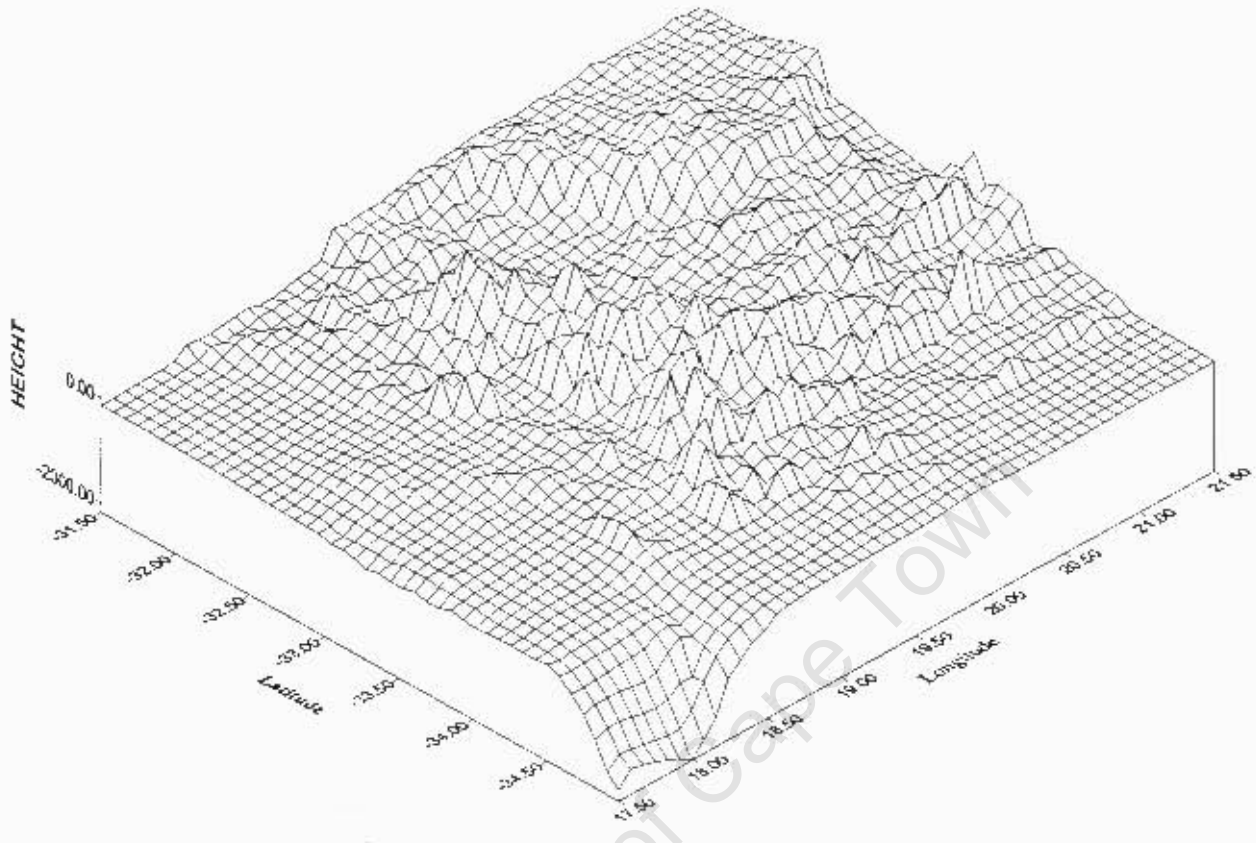

Figure 6-2: Digital Elevation Model – South Western Cape (Contour Interval 100m)

	FREE AIR ANOMALIES (mgal)	HEIGHTS (m)
Maximum	161.54	2180.00
Minimum	-47.82	0.00
Mean	18.05	409.51
Standard Deviation	25.67	533.54

Table 6-1: Statistics of the Free air anomaly and Height data for the South Western Cape

The South Western Cape is an area defined by mountainous topography with elevations close to 2500m and the relief in general is rather broken. The magnitudes of the free air anomalies vary from approximately –48 mgals to approximately 165 mgals. A glance at the figures (6-1) and (6-2) show that there exists a strong correlation between free air anomalies and topography and later we deduce same by an application of FFT correlation to these data sets.

6.1.2 Numerical Investigations of the Molodensky G_1 term

6.1.2.1 Comparisons between Quadrature, Convolution and FFT

From the original dataset of one minute, grid sizes of five, three and two minute were interpolated in order to compute the G_1 contribution for different grid resolutions. The G_1 term was computed using the techniques of numerical integration, two dimensional convolution and the two dimensional FFT. The procedure for each computational algorithm is briefly explained. In principal, a gridded data set of free air anomalies and an accompanying digital elevation model with latitude and longitude positions for the grid points are required for the evaluation of the G_1 term for each of the methods.

Numerical integration of the G_1 term is an application of formula (5-4). The summation, in theory, is carried out over the entire earth. The contribution of data points decreases rapidly as the points move further away from the computational point. In this regard, grid points within a vicinity of 10 kilometres of the computational point were used to determine the G_1 contribution of the computational point. The code for the algorithm was implemented using the *MATLAB* software package.

The implementation of formula (5-5) was used to determine the G_1 term for the convolution approach. The two dimensional convolution operator, conv2, available in

the *MATLAB* software package was used to evaluate equation (5-5). The advantage of the `conv2` function is that it automatically applies zero padding to the periphery of the data sets, effectively increasing the grid sizes from (p, q) to (2p-1, 2q-1) (Anonymous, 1997b). The algorithm developed to compute the G_1 term via the convolution approach also considers points within a vicinity of ten kilometres to determine the G_1 term for each of the grid points.

Implementation of equation (5-6) allows for the evaluation of the G_1 term using the fast Fourier transform (FFT). The implementation uses the *MATLAB* two dimensional fast Fourier transform operator `fft2`. To reduce discontinuities at the edge of the data sets, a split cosine taper (cf. 4.5, Chapter Four) was applied to the gridded data sets of heights and free air anomalies. As in the convolution approach, zero padding was applied to the periphery of the data sets. To maintain consistent dimensions for the purpose of the matrix operations involved, the entire kernel function was used in the evaluation of the G_1 contribution for each grid point and not just the points within a vicinity of 10 kilometres of the computational point.

We now examine the G_1 results for the individual grid sizes (5, 3, 2 and 1 minute respectively) for which the G_1 term was computed and examine the corresponding plots and statistics. Table (6-2) summarises the statistics of the computations for the G_1 term on the respective grid interval. Note that the matrix dimension of the grid sizes is required to be odd in order to implement the convolution. The statistics reflected in table (6-2) are computed after 10% of the data along the circumference of the border were removed. This was done since a 10% cosine window had been applied to the data set prior to the computation of the G_1 term using the FFT method. Computations were executed on a WINDOWS NT platform with 64 megabytes of random access memory (RAM) on a Pentium II with a 466 megahertz processor.

GRID DIMENSION	45 x 31 (1 395 data points)				
AREA	$-34.5^0 < \varphi < -32.0^0$, $17.8^0 < \lambda < 21.5^0$				$\Delta\varphi, \Delta\lambda = 5'$
	MAX. (mgals)	**MIN. (mgals)**	**MEAN (mgals)**	**STD DEV. (mgals)**	**COMP. TIME (in seconds)**
Quadrature	6.235	-4.284	0.516	1.008	166.31
Convolution	6.270	-4.335	0.530	1.020	0.27
FFT	6.553	-4.388	0.693	1.085	1.16
GRID DIMENSION	75 x 51 (3 825 data points)				
AREA	$-34.5^0 < \varphi < -32.0^0$, $17.8^0 < \lambda < 21.5^0$				$\Delta\varphi, \Delta\lambda = 3'$
Quadrature	15.870	-8.067	0.568	1.611	1 192
Convolution	16.746	-8.301	0.630	1.701	0.73
FFT	17.601	-9.245	1.021	1.961	2.29
GRID DIMENSION	111 x 75 (8 325 data points)				
AREA	$-34.5^0 < \varphi < -32.0^0$, $17.8^0 < \lambda < 21.5^0$				$\Delta\varphi, \Delta\lambda = 2'$
Quadrature	21.545	-13.843	0.836	2.355	6 169
Convolution	21.545	-13.942	0.863	2.385	1.82
FFT	22.184	-15.131	1.281	2.653	4.53
GRID DIMENSION	181 x 241 (43 621 data points)				
AREA	$-34.5^0 < \varphi < -31.5^0$, $17.5^0 < \lambda < 21.5^0$				$\Delta\varphi, \Delta\lambda = 1'$
Quadrature	40.720	-36.883	0.985	3.671	187 200
Convolution	40.363	-36.750	1.012	3.711	13.89
FFT	40.838	-38.874	1.453	3.988	45.91

Table 6-2: Statistical Analysis of the G_1 term in respect of Evaluation Methods

Examining table (6-2) we see that each computational method reveals similar values for the maximum, minimum, mean and standard deviation for the different grid sizes. The maximum value for the G_1 contribution increases positively (figure (6-3)) while the minimum value increases negatively (figure (6-4)) as the data sets become more dense. For a grid size of five minutes in which the points are approximately 8 kilometres apart the maximum and minimum value for the G_1 contribution are 6.235 mgals and –4.284 mgals respectively (quadrature method) while for a grid size of one minute in which the points have a spatial extent of about 1.6 kilometres these maximum and minimum values are 40.720 mgals and –36.883 mgals respectively. This is indicative of the nature of the G_1 term which in principle mirrors the topography (see figure (6-5), page 61). For grids with a low spatial resolution, where rugged and mountainous details of the topography are not well defined we would expect the maximum and minimum magnitudes of the G_1 contribution to be smaller than in grid resolutions where the features of topography are well depicted.

Contour plots of the G_1 contribution for each grid size evaluated using the methods of quadrature, convolution and FFT are illustrated in figures (A.1) to (A.12) in the appendix. The plots have been generated using the *Surfer* software using the process of Kriging for the data gridding (Keckler, 1995). Medium smoothing was selected as default for the contour lines. For each grid size, we see that each method of computation reveals similar plots of the G_1 contribution. Note that the contour plots of the FFT method show some of the edge effects along the north eastern border. Suffice it to say, a plot at a contour interval of one milligal or less, would reveal such edge effects along the periphery of the plot.

The plots further show the correlation of the G_1 term with topography. In areas of rugged and mountainous topography, from the north eastern to south eastern area of the contour plots we see that the G_1 contribution is quite significant. While the denser grids (one and two minute grids) reveal more local detail contributions of the G_1 term, the coarser grid

resolutions (three and five minute grids) nevertheless highlight the G_1 contributions in the areas coinciding with rough and mountainous topography.

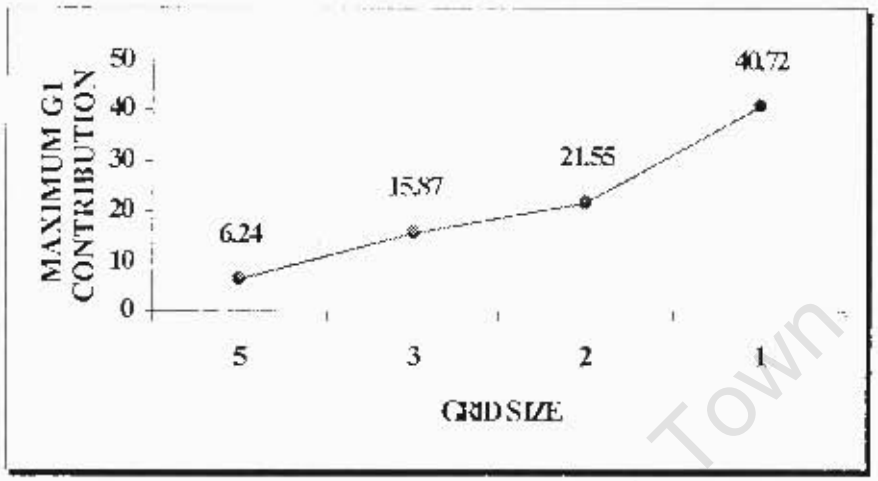

Figure 6-3: Graphical Illustration of the Maximum G_1 Contribution (Units=mgal)

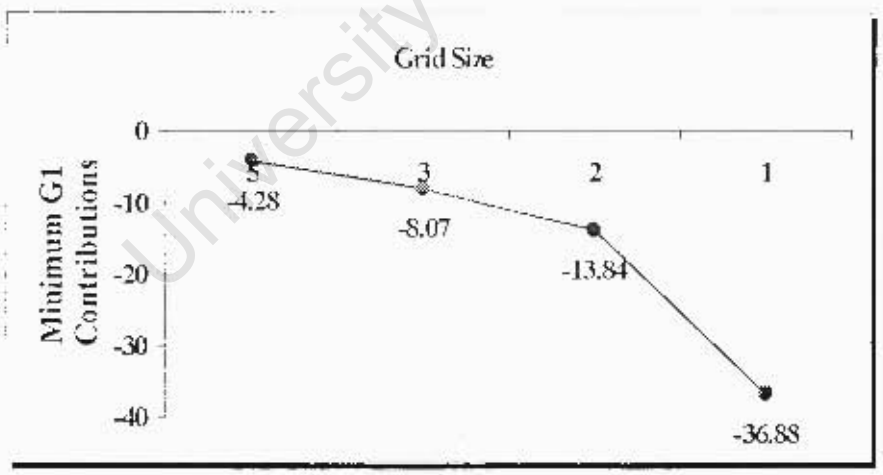

Figure 6-4: Graphical Illustration of the Minimum G_1 Contribution (Units=mgal)

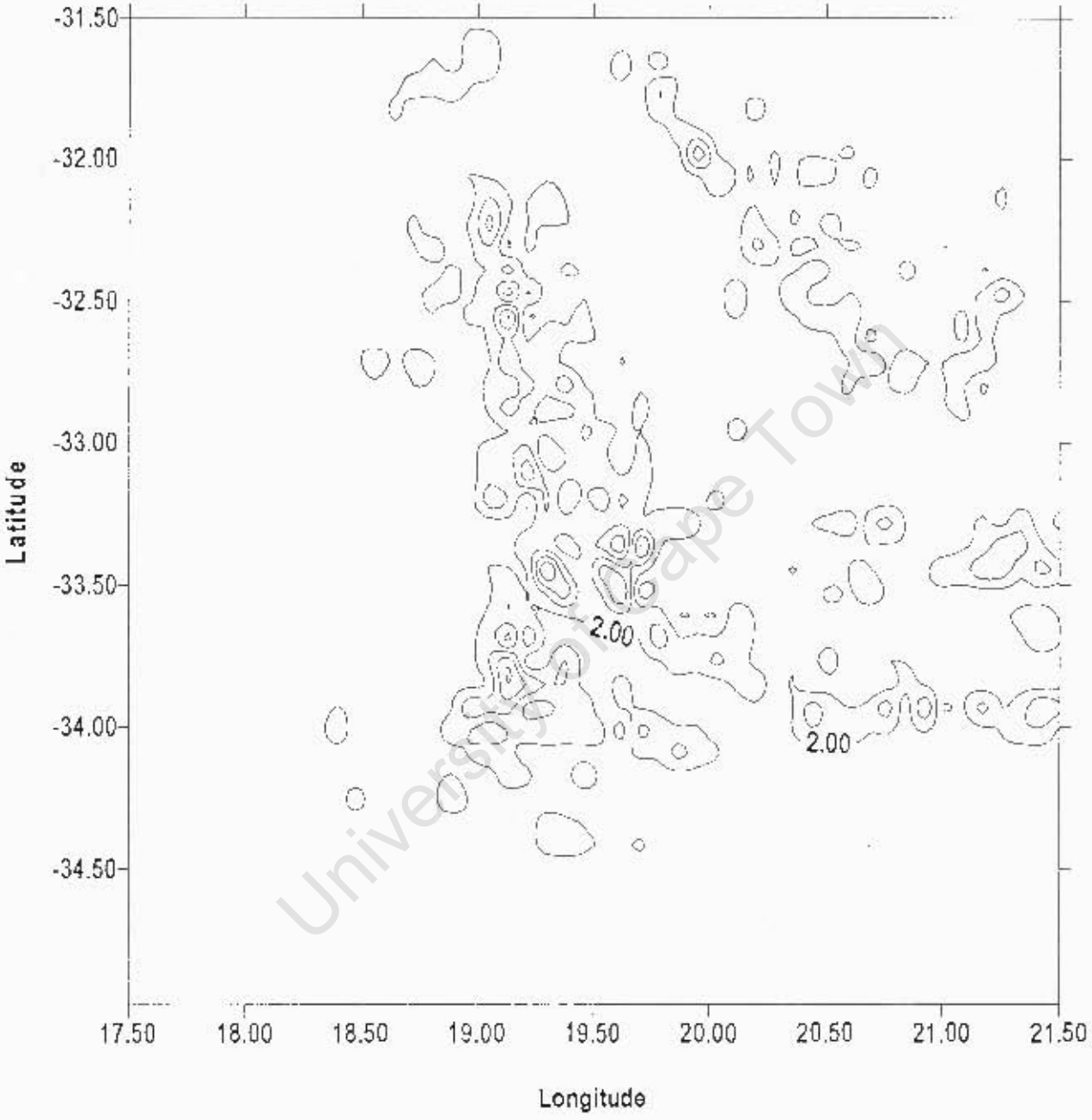

Figure 6-5: Evaluation of the G_1 Contribution via Quadrature
Grid Interval – 1 minute
(Contour Interval 5mgal)

The method of quadrature is demanding in terms of the computational time required for the evaluation of the G_1 term. For a grid dimension consisting of 1 395 data points (5 minute grid), evaluation of the G_1 contribution by quadrature is approximately three minutes while the methods of convolution and FFT require about 30 and 60 seconds respectively.

For high resolution grids the computational time requirement is quite stringent. On a one minute grid consisting of approximately 44 000 data points the quadrature method utilised about 52 hours of computational time for the evaluation of the G_1 term while the convolution and FFT methods took under a minute for the same computation. A further simulation (not tabulated in table (6-2)) was carried out on a 0.25 minute grid consisting of approximately 62 000 points. The convolution and FFT methods utilised 43 and 90 seconds of computational time respectively, while the quadrature approach a startling 96 hours! We briefly look at the graphical illustrations of the computational time required by the three methods in figure (6-6) below:

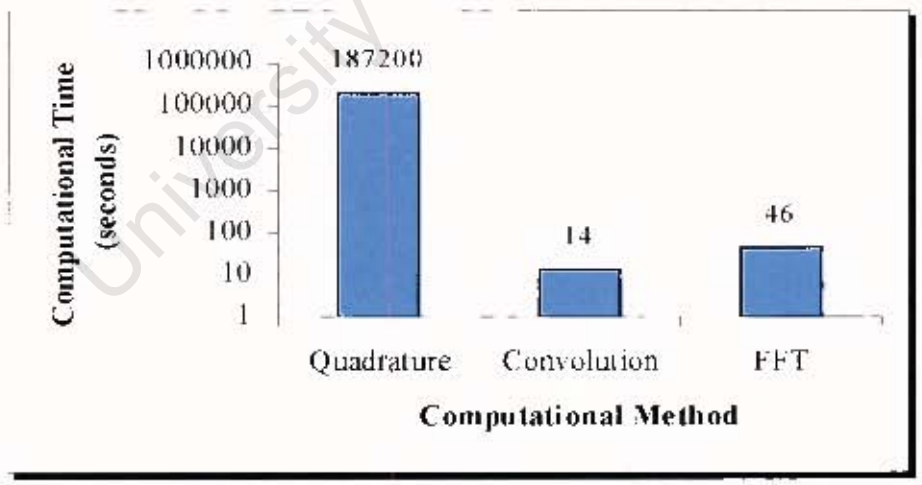

Figure 6-6: Computational Time Requirements for Different Methods for a Grid Resolution of one minute

The graph basically illustrates the large amount of computational time required by the quadrature method. There a minimal difference between the convolution and FFT method indicating that their computational time requirement does not differ significantly. Note that for the convolution method only data points within a ten kilometer radius from the computational point were used to evaluate the G_1 contribution while in the FFT method all the data points were used.

A comparison on the one minute grid was carried out using the convolution approach when points within a ten kilometer radius of the computation point are considered against that when all grid points are taken into account. The computational time required for use of the entire distance kernel was 300 seconds as opposed to the 13.89 seconds (table (6-2)) required when points within a limited radius are considered. It should be noted that the FFT computation on the same grid dimension which, as well, uses the entire distance kernel required 45.91 seconds of computational time (table (6-2)). This result highlights the computational efficiency of using FFT methods in gravity field modeling. Nevertheless, the statistics of the differences when using a full distance kernel and modified distance kernel are not very significant as illustrated in table (6-3) below.

GRID DIMENSION	181 x 241 (43 621 data points)			
AREA	$-34.5^0 < \varphi < -31.5^0$, $17.5^0 < \lambda < 21.5^0$			$\Delta\varphi, \Delta\lambda = 1'$
Convolution: full vs modified	**MAX. (mgals)**	**MIN. (mgals)**	**MEAN (mgals)**	**RMS (mgals)**
	2.866	-2.903	0.340	0.592

Table 6-3: Statistics of the Differences between Full and Modified Distance Kernel

The absolute value of the maximum and minimum discrepancies does not exceed more than 3mgals. The root mean square discrepancy (RMS) between the two computations is not significant and has a magnitude of approximately 0.6mgals. From a computational point of view, it would be beneficial to evaluate the G_1 contribution of a point from data points within a limited radius of the computational point. A plot of the differences, figure (A.13) in the appendix, shows that the maximum and minimum values occur at points on the sampling grid that coincide with mountain peaks and rugged topography.

6.1.2.2 Differences of Quadrature with respect to Convolution and FFT

In this investigation the differences between the method of numerical integration with respect to the methods of convolution and FFT are examined. Examining the statistics in tables (6-4) and (6-5) there is a general tendency in the magnitudes of the maximum, minimum, mean and root mean square values to increase from the low resolution grid of five minutes to the more higher resolution grid of one minute. This is primarily due to the higher resolution grids reflecting more details in the topography.

The statistics of the differences between the quadrature-FFT comparison are much larger than those of the quadrature-convolution differences. In particular, note the plot of the root mean square (RMS) differences figures (6-7) and (6-8). The RMS discrepancy of the quadrature-FFT comparison is approximately greater by a factor of 10 than the quadrature-convolution comparison. This is possibly due to the quadrature and convolution methods using only data points within a 10km radius of the computation point as opposed to the FFT method which uses all the data points. The effects of enforced periodicity, spectral leakage and aliasing errors associated with the Fourier transform are also possible sources of error. These sources of error cannot be completely eliminated but are significantly reduced by applying edge tapering windows as well as zero padding along the periphery of the data sets. A similar analysis between the convolution-FFT comparison yielded no discernible results: an RMS difference of 0.014miiligal.

GRID DIMENSION	45 x 31 (1 395 data points)			
AREA	$-34.5^0 < \varphi < -32.0^0$, $17.8^0 < \lambda < 21.5^0$			$\Delta\varphi, \Delta\lambda = 5'$
	MAX. (mgals)	**MIN. (mgals)**	**MEAN (mgals)**	**RMS (mgals)**
Quadrature – Convolution	0.061	-0.185	-0.014	0.028
GRID DIMENSION	75 x 51 (3 825 data points)			
AREA	$-34.5^0 < \varphi < -32.0^0$, $17.8^0 < \lambda < 21.5^0$			$\Delta\varphi, \Delta\lambda = 3'$
Quadrature – Convolution	0.523	-0.904	-0.062	0.1542
GRID DIMENSION	111 x 75 (8 325 data points)			
AREA	$-34.5^0 < \varphi < -32.0^0$, $17.8^0 < \lambda < 21.5^0$			$\Delta\varphi, \Delta\lambda = 2'$
Quadrature – Convolution	0.278	-0.462	-0.027	0.066
GRID DIMENSION	181 x 241 (43 621 data points)			
AREA	$-34.5^0 < \varphi < -31.5^0$, $17.5^0 < \lambda < 21.5^0$			$\Delta\varphi, \Delta\lambda = 1'$
Quadrature – Convolution	0.814	-0.625	-0.035	0.092

Table 6-4: Statistics of the Differences between Quadrature-Convolution Evaluation of G_1 term

GRID DIMENSION	45 x 31 (1 395 data points)			
AREA	$-34.5^0 < \varphi < -32.0^0$, $17.8^0 < \lambda < 21.5^0$			$\Delta\varphi, \Delta\lambda = 5'$
	MAX. (mgals)	**MIN. (mgals)**	**MEAN (mgals)**	**RMS (mgals)**
Quadrature – FFT	0.280	-0.715	-0.177	0.239
GRID DIMENSION	75 x 51 (3 825 data points)			
AREA	$-34.5^0 < \varphi < -32.0^0$, $17.8^0 < \lambda < 21.5^0$			$\Delta\varphi, \Delta\lambda = 3'$
Quadrature – FFT	1.685	-2.587	-0.453	0.699
GRID DIMENSION	111 x 75 (8 325 data points)			
AREA	$-34.5^0 < \varphi < -32.0^0$, $17.8^0 < \lambda < 21.5^0$			$\Delta\varphi, \Delta\lambda = 2'$
Quadrature – FFT	2.423	-2.530	-0.446	0.673
GRID DIMENSION	181 x 241 (43 621 data points)			
AREA	$-34.5^0 < \varphi < -31.5^0$, $17.5^0 < \lambda < 21.5^0$			$\Delta\varphi, \Delta\lambda = 1'$
Quadrature – FFT	3.210	-3.236	-0.605	0.765

Table 6-5: Statistics of the Differences between Quadrature-FFT Evaluation of the G_1 term

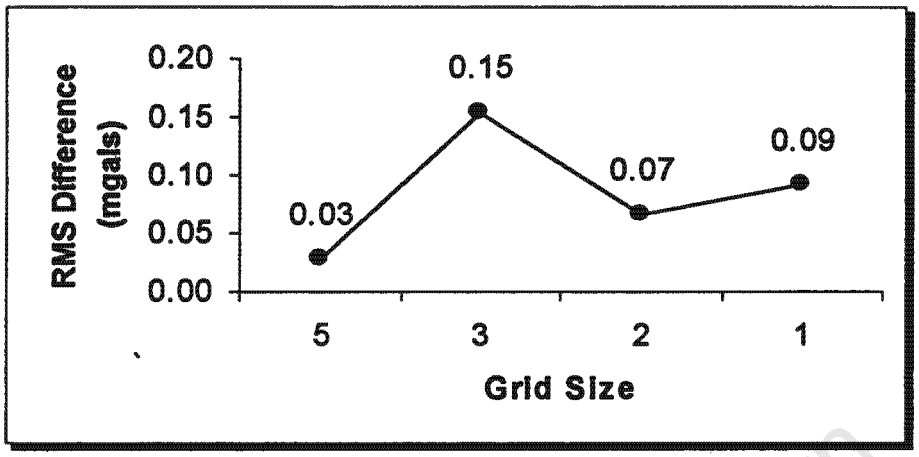

Figure 6-7: Root Mean Square Discrepancy between Quadrature-Convolution Evaluation of the G_1 term

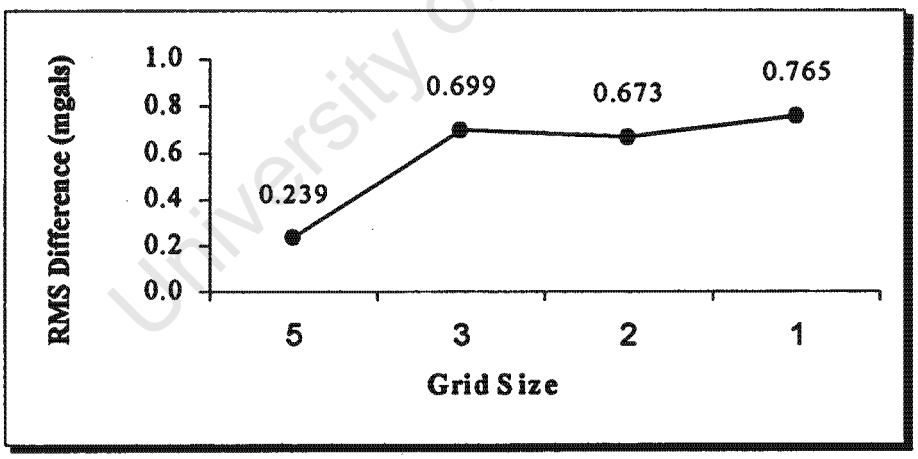

Figure 6-8: Root Mean Square Discrepancy between Quadrature-FFT Evaluation of the G_1 term

6.1.2.3 Comparison of G_1 Contribution between One minute and Coarser grid Resolutions

The statistics of the differences between the densest resolution grid (1' minute) with respect to the coarser grids (5', 3' and 2') is investigated in this section. Table (6-6) below reflects the differences in units of milligals:

Grid Size Comparison	1' ↔ 5'	1' ↔ 3'	1' ↔ 2'
No. of Common Points	1395	3825	8325
MAX.	30.060	30.880	29.180
MIN.	-28.820	-22.100	-17.520
MEAN	0.840	0.567	0.408
RMS	3.444	3.041	2.471

Table 6-6: Statistical Comparison for Differences in the G_1 term between 1' and Coarser Grid Resolutions (Units=milligals)

There is no significant reduction in the maximum difference of the 1' ↔ 5' grid comparison to that of the 1' ↔ 2' grid comparison: a difference of about one milligal. The statistics of the minimum and mean differences however do reflect a more noticeable decrease as the grid comparisons become more dense.

It is anticipated that the denser the resolution of the grid comparisons, one would expect to see a convergence in the value of the root mean square. Although such convergence is not apparent in figure (6-9) below, there is a slight decrease in the RMS value.

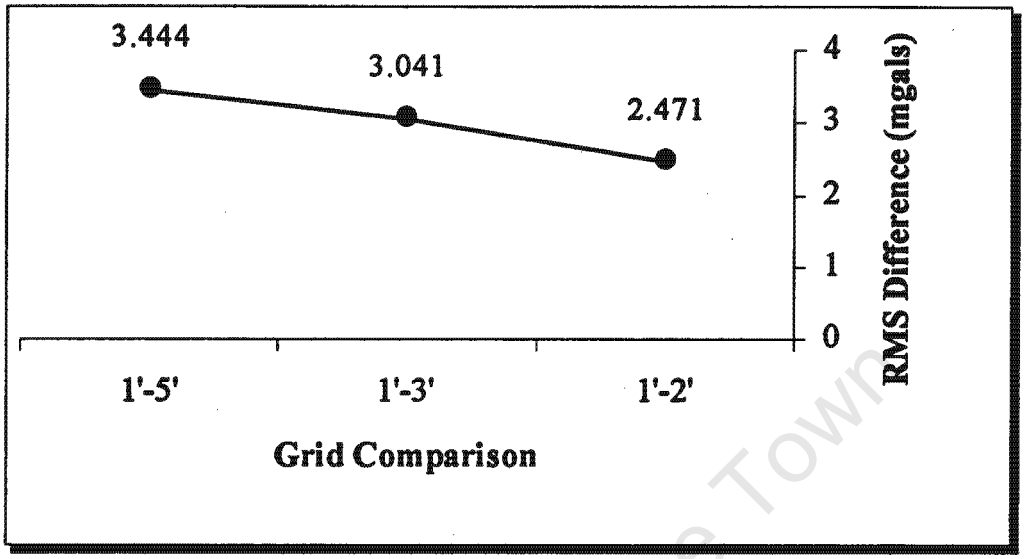

Figure 6-9: RMS Discrepancies of G_1 term between a 1' grid with respect to 2', 3' and 5' Grid Sizes

The convergence of the RMS difference depends largely on the nature of the topographical relief. In areas of rugged and mountainous topography such as the Western Cape, we would expect to see a convergence in the RMS value if detailed digital elevation models of 200 and 400 metres are employed in the analysis. For areas where the relief is in general smooth such as the Gauteng region, north east of South Africa, one could anticipate a convergence of the RMS difference on a grid comparison of $1' \leftrightarrow 2'$.

Such analysis is useful in order to determine the optimal grid resolution one would require to evaluate the G_1 term. While the data capacity becomes considerably large for dense grid resolutions, the evaluation of geodetic integrals are not insurmountable considering the computing power and techniques nowadays available.

6.1.2.4 G_1 Contribution to the Quasi-geoid

A simple investigation to determine the contribution of the G_1 term to quasi-geoidal heights is carried out by an application of formula (5-11) (cf. Chapter 5, section 5.2.2.1). In formula (5-11) the 'Δg' term was simply replaced by the 'G_1' values already computed for the various grid sizes previously mentioned. For a grid with a spatial resolution of 5' the contribution is as much as 15.5cm while the densest grid resolution of 1' yields a maximum contribution of 42.5cm with an RMS value of 7cm (table 6-7 below). A graphical illustration (figure (6-10)) of these tabulated results clearly indicate that the statistics of the G_1 contribution show a tendency to increase as the grid resolutions become more dense. This highlights the importance of the G_1 term especially in areas of rugged and mountainous topography. A plot of the G_1 contribution to the quasi-geoid for a grid size of one minute is shown in figure (A.14) in appendix A.

GRID RESOLUTION (minutes)	MAX. (m)	MIN. (m)	MEAN (m)	RMS. (m)
5	0.155	0.029	0.095	0.029
3	0.250	0.045	0.134	0.040
2	0.317	0.057	0.164	0.048
1	0.425	0.055	0.212	0.072

Table 6-7: Statistical Analysis of the G_1 Contribution to the Quasi-geoid

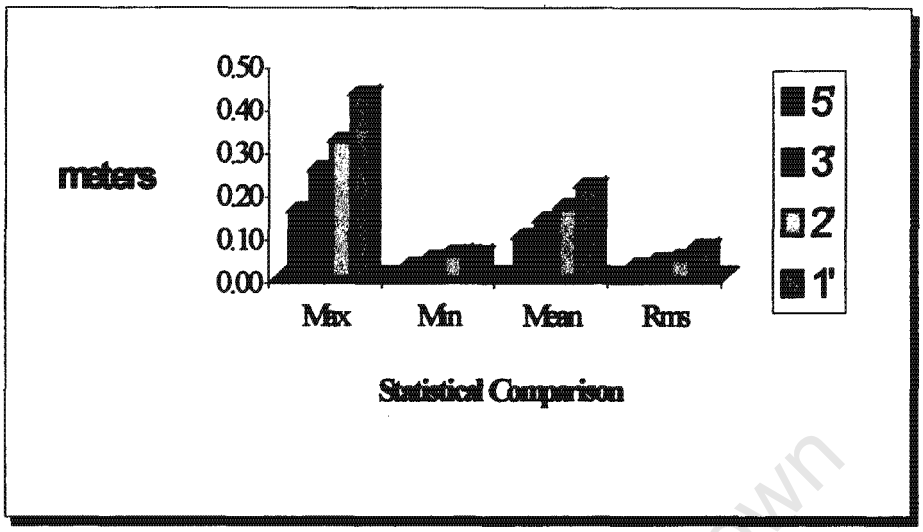

Figure 6-10: Graphical Illustration of Statistical Analysis of G_1 Contribution to the Quasi-geoid

Finally a comparison of the G_1 contribution to the quasi-geoid between a grid resolution of 1' with respect to the grid sizes of 2', 3' and 5' respectively was initiated. Table (6-8) gives an indication of these statistics in units of metres:

Grid Size Comparison	1 ↔ 5	1 ↔ 3	1 ↔ 2
No. of Common Points	828	2301	5133
MAX.	0.270	0.190	0.120
MIN.	0.050	0.040	0.030
MEAN	0.133	0.095	0.067
RMS	0.140	0.098	0.069

Table 6-8: Statistical Comparison of the Differences for the G_1 Contribution to the Quasi-geoid between 1' and Coarser Grid Resolutions (Units=m)

The statistics appearing in table (6-8) are not surprising. We note a decrease in the statistical differences as the comparison varies from a grid resolution of 5' to one of 2' - a significant decrease in the maximum difference from that of 27cm to 12cm with RMS discrepancies of 14cm and 6.9cm respectively.

It has been suggested that the G_1 term can be approximated by the terrain correction under the assumption that the free air anomalies are linearly dependent on elevation. An investigation by (van Gysen, 1991) found that use of the terrain correction had led to results much worse than that obtained when the terrain correction was excluded. (Sideris and Schwarz, 1986) carried out an investigation to determine the effect of the higher order terms (G_1 and G_2 terms) of the Molodensky series as well as the terrain correction on height anomalies and deflections of the vertical. The effects of these corrections were computed in the White Sands Area in New Mexico. The extent of the area was $6^0 \times 6^0$ covered with a five minute grid of free air anomalies and heights.

(Sideris and Schwarz, 1986) recommend that the G_2 term may be neglected when computing height anomalies as the maximum effect on the test area was about 0.2cm. However, the effect of this term on the deflections of the vertical amounted to a fraction of an arcsecond and hence it must be considered in this case. The effect of the terrain correction and the G_1 term on the height anomaly and deflection components are reproduced below from (Sideris and Schwarz, 1986):

	Terrain Correction			**G_1 term**		
	ζ (cm)	ξ (arcsec.)	η (arcsec.)	ζ (cm)	ξ (arcsec.)	η (arcsec.)
Max. Effect	4.0	0.6	1.0	8.0	1.9	2.9

Table 6-9: Effect of Terrain Correction and G_1 term on the Height Anomaly and Deflection Components (Sideris and Schwarz, 1986)

The results clearly indicate that the G_1 term has a greater effect on the height anomaly and the deflection components in comparison to the terrain correction. The computation of the terrain correction always yields positive values while the G_1 corrections could be positive and negative. For grids with a higher resolution the effects could be much larger and one would expect to see the importance of also considering the G_2 term which is affected by higher frequencies of the gravity field.

6.1.2.5 FFT Correlation

Autocorrelation and cross correlation functions have also been computed for the south western Cape region using the data from the grid resolution of one minute. Correlation functions are important in the processing and interpretation of geodetic and geophysical data.

Figure (B.1) in the appendix represents the height autocorrelation function. The digital elevation model (6-2) shows the topography of the South Western Cape to be pronounced in the northern and eastern directions. The height autocorrelation function reveals a plot which is isometric indicating that the northern and eastern trends of the topographic masses cancel each other. The same trend is further noticeable in figure (B.2) where the autocorrelation function of the G_1 term was determined. A relationship between the secondary features in figure (B.2) and the distribution of the G_1 term figure (6-5) can also be seen where the contribution of the G_1 term is quite significant. It was previously mentioned that a strong correlation exists between the free air anomalies and height data sets, this can further be inferred from the cross correlation function of these quantities presented in figure (B.3) in the appendix. Using *MATLAB'S* `corrcoef` function a strong linear correlation of 0.75 was obtained between the free air anomalies and heights.

6.2 A QUASI-GEOID FOR THE SOUTH WESTERN CAPE

6.2.1 Description of Data and Computational Methods

The quasi-geoid was computed on the densest grid resolution of one minute. The remove-restore technique (cf. 5.2.1, chapter five) was used in which the long wavelength contribution implied by the EGM96 geopotential model is removed from the free air gravity anomalies and the resulting reduced anomalies are processed to obtain residual quasi-geoidal heights. The long wavelength contribution to the residual quasi-geoid heights implied by the same geopotential model are then restored to obtain quasi-geoidal heights. The program *GEOGRAV* made available by Professor C. Merry of the Department of Geomatics at the University of Cape Town was used to compute the quasi-geoidal heights and gravity anomalies from the EGM96 geopotential coefficients.

The spectral methods employed for the quasi-geoid evaluation were the 2D planar approximation of Stokes' formula (equation 5-13), the 2D spherical FFT approach (equation 5-20) and the 2D Multi-band spherical FFT approach. These methods have been discussed comprehensively in chapter five. The computational routines for the these approaches have been developed by the author using the software package *MATLAB*. No window was applied to the reduced gravity anomalies as a global model was removed *a priori*. However, zero padding was applied to the data sets to avoid cyclic convolution. In section (6.2.2) we analyse the results of the residual quasi-geoids obtained after the application of the three spectral methods and in section (6.2.2.5) we go on to validate the quasi-geoids against a GPS/Levelling derived quasi-geoid.

6.2.2 Numerical Investigations of the Spectral Methods used in Residual Quasi-Geoid Evaluation

6.2.2.1 Comparison between Planar, Spherical and Multi-Band SFFT Approximations

For the planar and spherical FFT approximations a residual quasi-geoid is computed for the entire grid dimension while the multi-band SFFT requires the area of interest to be divided into equidistant overlapping bands. The test area which spans about 350x350 km was divided into two equidistant bands. The overlaps are required for the zero padded extensions associated with the application of the Fourier transform. Since we have 'two solutions' in each of the overlapping regions a linearly weighted distance interpolation (equation 5-22) is applied to the overlapping regions to obtain a composite solution. At this point, it was thought appropriate to investigate the effect of employing different sizes for the overlapping area and a full investigation (see section 6.2.2.4) was carried out in this respect. Nevertheless, we quote the statistics of the residual quasi-geoids in respect of a 20, 40, 60 and 80 minute overlap in table (6-10) to follow, as well as those obtained via the planar and spherical approximation.

The last column of the table reflects results of a residual quasi-geoid computed with an overlap of 80 minutes with no linear interpolation being performed in the overlapping regions. The intention here was merely to obtain a significant contribution of the gravity field when computing the residual quasi-geoid for each band.

The statistics indicate no significant difference in the methods employed. The RMS value of the planar and spherical FFT methods are almost equivalent and only differs from the multi-band SFFT approach by a maximum value of approximately 4cm in the RMS value. Figures (C.1), (C.2), (C.3) and (C.4) in the appendix depict the contour plots of the residual quasi-geoid computed via the planar FFT, spherical FFT, multi-band SFFT (20 minute overlap) and multi-band SFFT (80 minute overlap) respectively. All

the plots show similar features of the short wavelength content of the residual quasi-geoid.

AREA $-34.5^0 < \varphi < -31.5^0$, $17.5^0 < \lambda < 21.5^0$ $\Delta\varphi, \Delta\lambda = 1'$							
			Multi-Band FFT with 2 Bands				
			Overlap in minutes				
	Planar FFT	Spherical FFT	20	40	60	80	80 No Interp.
MAX.	0.679	0.639	0.647	0.663	0.653	0.652	0.656
MIN.	-1.141	-1.141	-1.173	-1.171	-1.267	-1.206	-1.168
MEAN	-0.208	-0.218	-0.199	-0.214	-0.235	-0.255	-0.251
STD.	0.312	0.308	0.328	0.325	0.328	0.331	0.325
RMS.	0.375	0.377	0.387	0.389	0.403	0.418	0.4111

Table 6-10: Residual Quasi-Geoid Heights via Planar, Spherical and Multi-band SFFT Approaches (Units=m)

Figures (6-11) and (6-12) below respectively represent the quasi-geoid from the EGM96 model and the final combination quasi-geoid via the planar FFT. The combination quasi-geoid represents the unification of the short wavelength (residual quasi-geoid) and long wavelength (EGM96 model) quasi-geoidal models. Figures (C.5) and (C.6), in the appendix, represent combination quasi-geoids computed by the spherical FFT and multi-band SFFT (two bands, 80 minute overlap) respectively. A comparison of figures (6-12), (C.5) and (C.6) with respect to figure (6-11) show the dominant features of the EGM96 model. The computational time was less than five minutes for the cases above indicating no significant discrepancies between the methods.

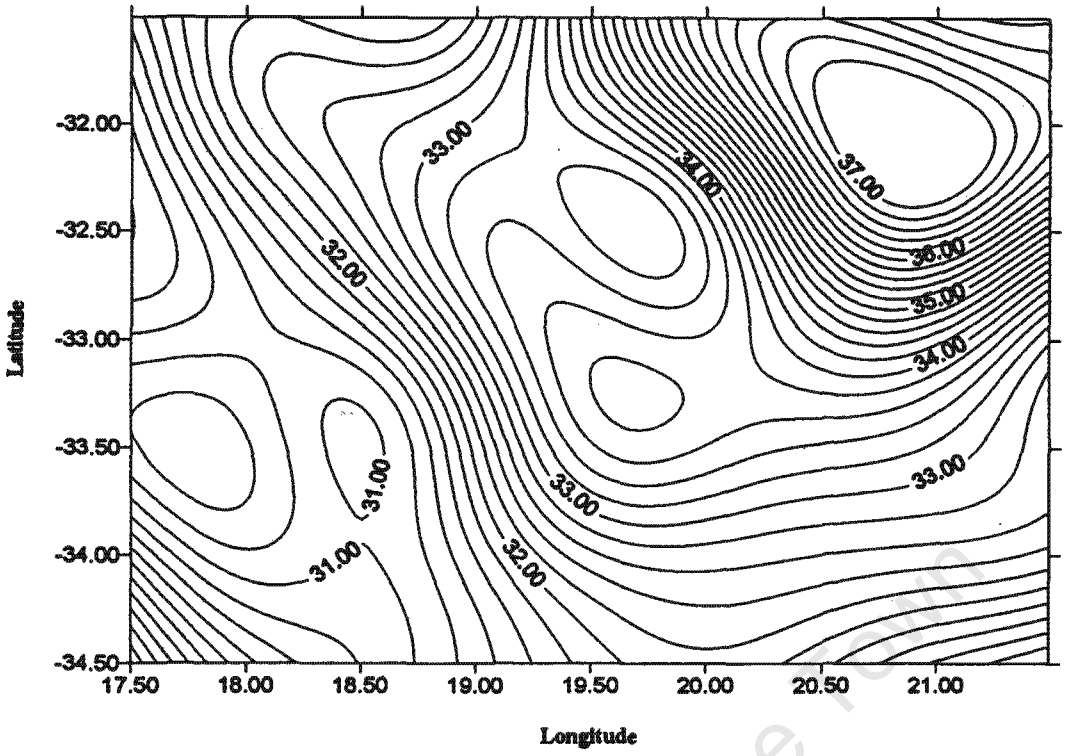

Figure 6-11: Quasi-Geoid EGM96 – South Western Cape (Contour Interval 0.2m)

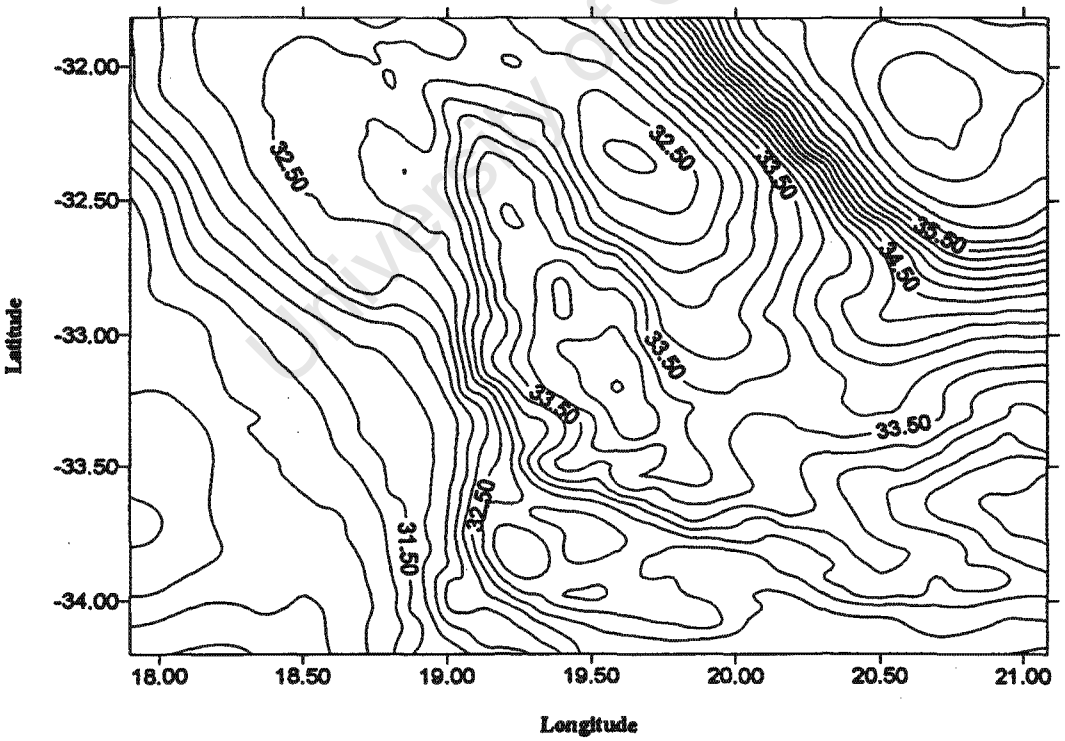

Figure 6-12: Quasi-Geoid via Planar FFT – South Western Cape (Contour Interval 0.2m)

6.2.2.2 Planar versus Spherical and Multi-Band SFFT Approximations

The quasi-geoidal heights obtained from the planar FFT were compared to those results obtained via the spherical FFT approach and the multi-band FFT approach (with the different sizes for the overlapping regions). Table (6-11) indicates the statistics obtained:

AREA $-34.5^0 < \varphi < -31.5^0$, $17.5^0 < \lambda < 21.5^0$ $\Delta\varphi, \Delta\lambda = 1'$					
		MAX	**MIN**	**MEAN**	**RMS**
Spherical FFT		0.053	-0.035	0.010	0.016
Multi-Band FFT	20'	0.084	-0.246	0.056	0.092
	40'	0.066	-0.177	0.037	0.061
	60'	0.145	-0.121	0.010	0.038
	80'	0.144	-0.100	0.009	0.032
	80' (No Interpol.)	0.083	-0.110	0.012	0.027

Table 6-11: Statistics of the Differences between the Planar FFT with respect to Spherical and Multi-Band SFFT Methods (Units=m)

The differences between the planar and spherical FFT method applied to the test area is reasonably small in magnitude – about 5cm and -3.5cm in the maximum and minimum differences with an RMS difference of about 1.5cm. With respect to the multi-band approach we note that there is a tendency for a decrease in the RMS values as the size of the overlapping area is increased. The magnitude of the maximum difference tends to be random as the extent of the overlap is increased while there appears to be a notable decrease in the minimum value as well as the mean value.

Of significance are the statistics of the multi-band approach when no interpolation of the overlapping regions is executed. The results in this case are much smaller than the case where a linear interpolation of the overlapping regions is carried out. One could surmise that, when a significant overlap is considered with no interpolation, then the statistics would be equivalent to that of the spherical FFT method for the particular test area. In summary, figure (6-13) re-iterates that, in case of the multi-band FFT approach with significant overlap (as well as significant overlap and no interpolation) the RMS differences obtained by the multi-band approach tend to converge to those obtained via the spherical FFT approach.

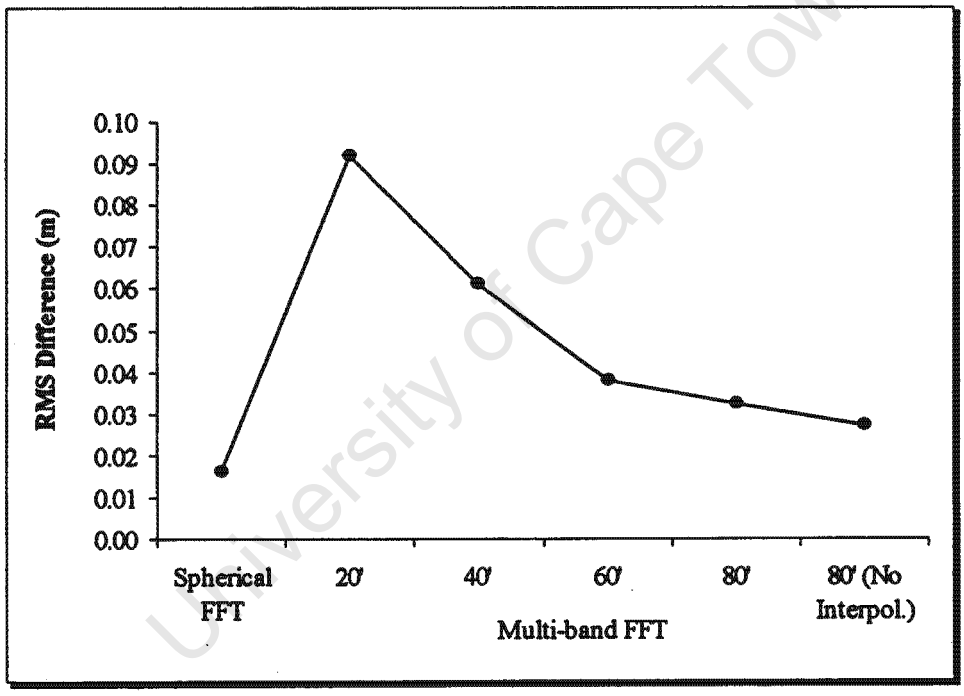

Figure 6-13: RMS Differences between the Planar FFT with respect to the Spherical and Multi-band SFFT Approaches

Figure (D.1) in the appendix depicts a contour plot of the quasi-geoid differences between the planar FFT and spherical FFT approaches. We note that the differences are reasonably small for the test area (as previously commented) but further note that the larger differences occur mostly along the north-eastern border and are more pronounced along the southern border. One would expect to see the spherical effects along both the northern and southern borders where we have a convergence of the meridians. We nevertheless infer that these effects are not significant for the particular test area and that both methods produce identical results.

Figures (D.2) to (D.4) (in the appendix) represent the quasi-geoid differences between the planar FFT approach with respect to the multi-band approach using overlapping regions of 20, 40 and 80 minute respectively. The differences appear to be 'stratified' layers with the larger differences occurring at the edges of the overlapping regions. This is due to the linearly distance weighted interpolation employed which gives a larger weight to the quasi-geoid solutions closer to the mean latitude of a particular band.

Figure (D.5) (appendix) represents the quasi-geoid differences between the planar and multi-band SFFT with an 80 minute overlap and no linear interpolation. We also note a 'stratified' dispersion of the contours but the larger discrepancies occur closer to the mean latitude of the test area rather than at the edges of the overlap.

6.2.2.3 Spherical FFT versus Multi-Band SFFT Approximations

As in section (6.2.2.2), a similar analysis was performed of the quasi-geoid differences between the spherical FFT and multi-band SFFT. Table (6-12) below reflects these statistics:

AREA $-34.5^0 < \varphi < -31.5^0,\ 17.5^0 < \lambda < 21.5^0$ $\Delta\varphi, \Delta\lambda = 1'$					
		MAX	**MIN**	**MEAN**	**RMS**
Multi-Band FFT	20'	0.089	-0.257	-0.067	0.101
	40'	0.062	-0.201	-0.046	0.071
	60'	0.145	-0.147	-0.019	0.045
	80'	0.141	-0.127	0.000	0.033
	80' (No Interpol.)	0.077	-0.138	0.002	0.025

Table 6-12: Statistics of the Differences between the Spherical FFT and Multi-Band SFFT Methods (Units=m)

We see a similar distribution of the results as those depicted in table (6-11) - a tendency for a smaller RMS value associated with an increase in the size of the overlap. We note that in both tables (6-11) and (6-12) the mean difference is almost zero when the overlap is greater than a degree. Contour plots of the differences between the spherical FFT and multi-band SFFT also appear to be 'stratified' with larger discrepancies occurring at the edges of the overlapping regions (linear interpolation employed), in the case of no interpolation these discrepancies occurring at the mean latitude of the area of interest - these plots have not been reproduced in the thesis.

6.2.2.4 Analysis of the Multi-band Solutions

In this section the results from using overlap sizes of 20', 40' and 60' were compared to that obtained using an 80' overlap. Such analysis to some extent allows one to determine the optimal overlap to be considered when employing the use of the multi-band SFFT approach. Table (6-13) reflects the results:

Grid Size Comparison	20' ↔ 80'	40' ↔ 80'	60' ↔ 80'
MAX.	0.245	0.136	0.105
MIN.	-0.029	-0.029	-0.077
MEAN	0.065	0.046	0.019
RMS	0.088	0.059	0.030

Table 6-13: Quasi-geoid Differences between 80 minute overlap with respect to overlaps of 20, 40 and 60 minutes respectively (Units=m)

The maximum discrepancy between a 20 minute overlap with respect to an 80 minute overlap is 24.5cm with an RMS difference of approximately 9cm. This is important and implies that the extent of the overlap must encompass a significant portion of the gravity field. A notable decrease is evident in the statistics as the size of the overlapping region is increased. For a comparison of the 40-80 minute overlap the maximum discrepancy drops to 13.6cm with an RMS of 5.9cm. The overlap of one degree compared to the 80 minute overlap yields results that are reassuring – an RMS difference of 3cm, almost three time smaller than the 20-80 minute overlap comparison.

The optimal overlap will depend on the frequency content of the data and the overlapping region would be required to be more than the sizes of the overlaps considered here. (Sideris, 2001) recommends that the size of the overlap should be one degree at minimum.

6.2.2.5 Quasi-geoid Validation

The quality of the gravimetric quasi-geoid computed in the previous section was evaluated against a GPS/Levelling derived quasi-geoid. The evaluation principally comprises the comparison of the interpolated values of the gravimetric quasi-geoidal heights at the points corresponding with the GPS/Levelling quasi-geoid. The comparison is made in a least squares sense by fitting a transformation model to the two surfaces. Examples of two such models have been given in chapter five (cf. 5.3). The coefficients (a_i) of the respective models are solved for by minimising the sum of the squares of the residuals and the adjusted values for the residuals give a more realistic indication as to the quality of fit between the two surfaces.

The GPS/Levelling quasi-geoid model was provided by Professor C. Merry in the Department of Geomatics at the University of Cape Town. A brief discussion of the model ensues. 42 GPS determined ellipsoidal heights were made at selected benchmarks and levelled town survey marks spanning the south western Cape area. This network of GPS points is tied to the International Terrestrial Reference Frame (ITRF) site at Hartebeeshoek resulting in absolute ellipsoidal heights for the respective points. The difference between the ellipsoidal and normal heights of these points yields their quasi-geoidal heights. For further discussion on the compilation of this data set, the interested reader is referred to (Merry, 1998).

Of the 42 points provided, only 40 of the points were interpolated to as we removed a 10% window from the periphery of our test area owing to edge effects, hence two of the points fell outside the interpolation region. The interpolation was executed on *MATLAB* using the `bicubic` interpolation option in which sixteen of the closest points are used to determine a value for the interpolated point. A planar transformation model was used to determine the quality of fit between the two surfaces. The statistics displayed in table (6-14) show the level of agreement of the different methods used to compute the gravimetric geoid with that of the GPS/Levelling quasi-geoid and table (6-15) reflects the statistics after the fit was

applied to the two surfaces. The last column of both tables represent the results of the spherical FFT computation of the quasi-geoid with the exclusion of the G_1 term.

	with G_1 term			excluding G_1
	Planar FFT	**Spherical FFT**	**Multi-Band FFT (80 min. Overlap)**	**Spherical FFT**
MAX	-0.327	-0.316	-0.318	0.000
MIN	-0.568	-0.564	-0.553	-0.420
MEAN	-0.452	-0.453	-0.454	-0.230
RMS (mean removed)	0.042	0.045	0.040	0.10

Table 6-14: Level of Agreement between Gravimetric and GPS/Levelling Quasi-geoids (Units=m)

	with G_1 term			excluding G_1
	Planar FFT	**Spherical FFT**	**Multi-Band FFT (80 min. Overlap)**	**Spherical FFT**
Coefficients	$a0$= -0.452 $a1$= 0.012 $a2$= 0.015	$a0$= -0.453 $a1$= -0.001 $a2$= 0.017	$a0$= -0.454 $a1$= -0.003 $a2$= -0.030	$a0$= -0.230 $a1$= 0.154 $a2$= 0.090
MAX.	0.108	0.108	0.108	0.143
MIN.	-0.129	-0.127	-0.125	-0.136
MEAN.	0.000	0.000	0.000	0.000
RMS	0.041	0.044	0.038	0.062
TILT (sec)	0.03	0.03	0.06	0.34

Table 6-15: Level of Agreement between Gravimetric and GPS/Levelling Quasi-geoids after Planar Transformation fit (Units=m)

Table (6-14) shows a significant bias of up to 45cm in all three methods when the G_1 term is considered. This bias is due to the zero-order term of the EGM96 geopotential model not being perfectly known as well as the South African vertical datum being biased by about 15-20cm with respect to the quasi-geoid (Merry and Amod, 2001). The statistics of the three methods are consistent with each other and basically imply that for regions of mid latitude the methods do not produce results which differ significantly. A recent study by (Tsiavos, 1996) confirms the last statement. The RMS difference using the multi-band approach yields the smallest value although it only differs from the planar and spherical approximations by about 2mm and 5mm respectively.

The planar transformation fit does not alter the RMS values of the three methods (with G_1 term) significantly – an improvement of about 2mm in the RMS value of the multi-band approach, the results are graphically illustrated in figure (6-14). However, it is the results of this fit, which generally gives us an indication of the quality of the gravimetric quasi-geoid. Nevertheless, such results are plausible in order to bring the quasi-geoid consistency with the GPS/Levelling data down to centimeter level. The maximum slope between the surfaces are 0.03 seconds for the planar and spherical FFT methods and about 0.06 seconds for the multi-band approach.

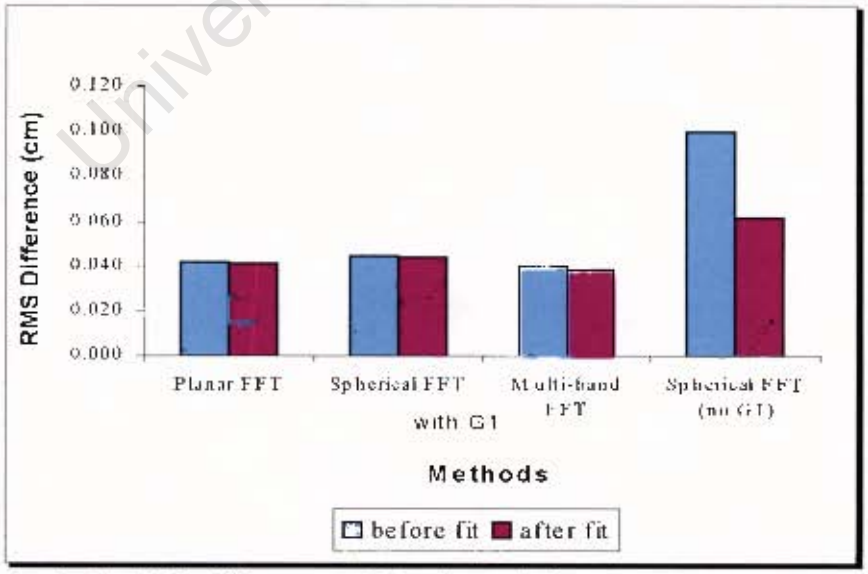

Figure 6-14: RMS differences of Gravimetric Quasi-geoid with respect to GPS/Levelling Quasi-geoid

A plot, figure (6-15), of the discrepancies between the gravimetric and GPS/Levelling derived quasi-geoids shows that the maximum residuals, not surprisingly, occur at the points situated in the mountainous terrain of the test area:

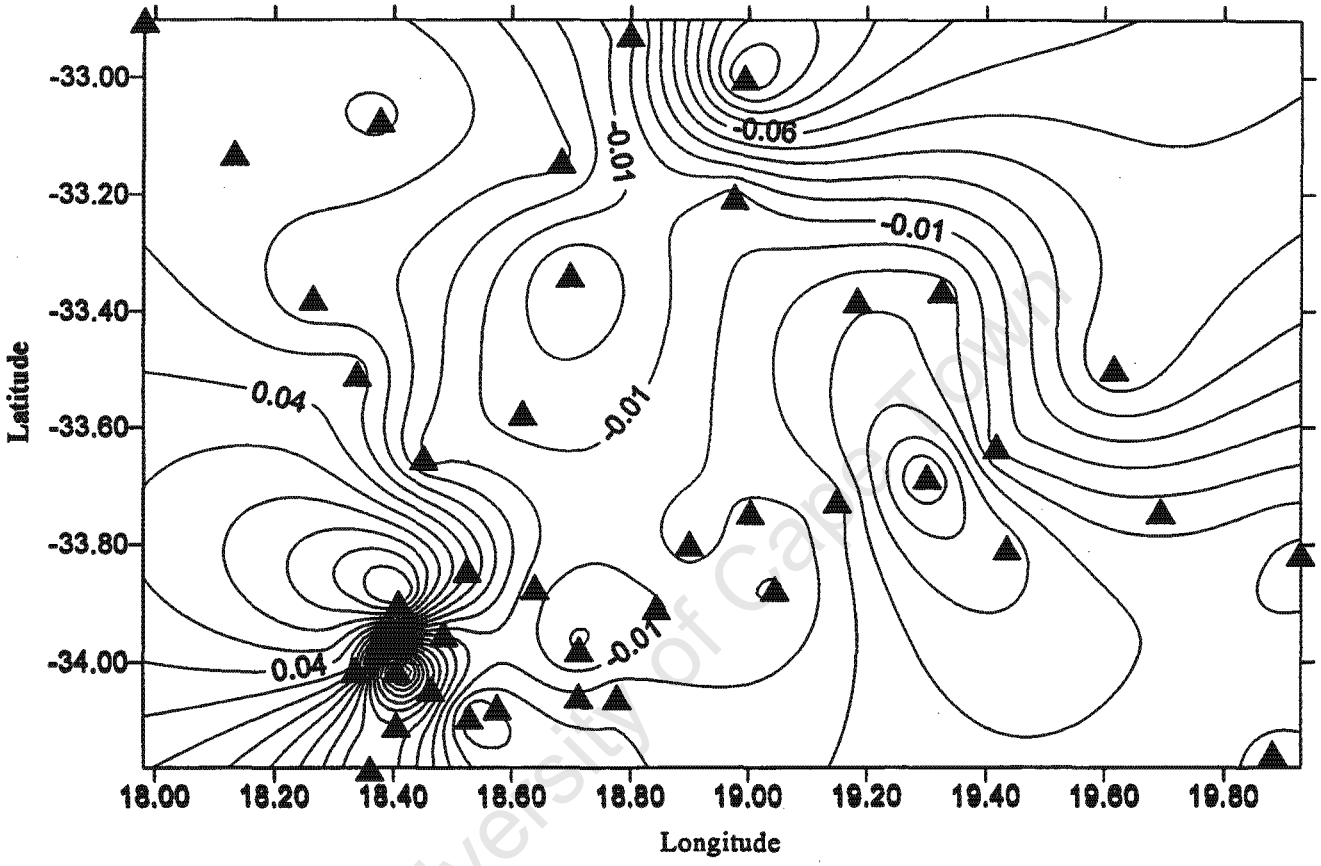

Figure 6-15: Residual Differences between Gravimetric and GPS/Levelling Quasi-geoids (Contour Interval: 0.02m)

In the last column of table (6-14)/(6-15), the computation of the spherical FFT method is executed without including the G_1 term. The results are rather interesting and we note that omission of the G_1 term yields higher RMS discrepancies in the quality of the gravimetric quasi-geoid: an RMS difference of 10cm (prior to fit) which is reduced to 6cm after a planar transformation fit (figure 6-15) with a significant tilt

of 0.34 seconds, – a tilt, greater by a factor of 10 in comparison to the planar and spherical FFT methods. The inclusion of the G_1 term displays two important facts: it implies that the South African height system is more tailored toward a normal height system and the use of the G_1 term significantly improves the quasi-geoid validation.

The results obtained here are an improvement to the quasi-geoid computed by (Merry, 1998) which we for convenience denote as UCT98WCape. UCT98WCape is computed via a two dimensional convolution to the planar approximation of Stokes' formula. A comparison with the 42 GPS/Levelling derived quasi-geoid points (previously discussed) yielded a bias of 47cm with an RMS of 10cm which reduced to 6cm after removal of a tilt. When the G_1 term was excluded in the computation of UCT98WCape, a bias of 30cm with an RMS of 16cm which reduced to 9cm after removal of the tilt was achieved.

The discrepancies between the quasi-geoid computed for the south western Cape in this thesis and UCT98WCape lies in the manner in which the G_1 term was computed. UCT98WCape evaluated the G_1 term from one minute data but for every fifth data point while we have computed the G_1 term for every data point. In this respect modelling the G_1 term at every grid point gives a better reflection of the high frequency content of the gravity field. Table (6-16) gives the statistics of the UCT98Wcape quasi-geoid differenced against the quasi-geoid computed in this thesis (denoted UCT2000WCape in the table):

	MAX.	MIN.	MEAN	RMS
UCT98WCAPE – UCT2000WCAPE	0.310	-0.260	0.043	0.115

Table 6-16: Differences between UCT98WCape and UCT2000WCape Quasi-Geoids (Units=m)

The discrepancies are significant with maximum and minimum values at the decimeter level. Figure (6-16) depicts a contour plot of these differences. Note that

the maximum and minimum differences occur in the areas of mountainous and rugged topography. In summary, it is important that the G_1 term adequately models the short wavelength features owing to its sensitivity to topography.

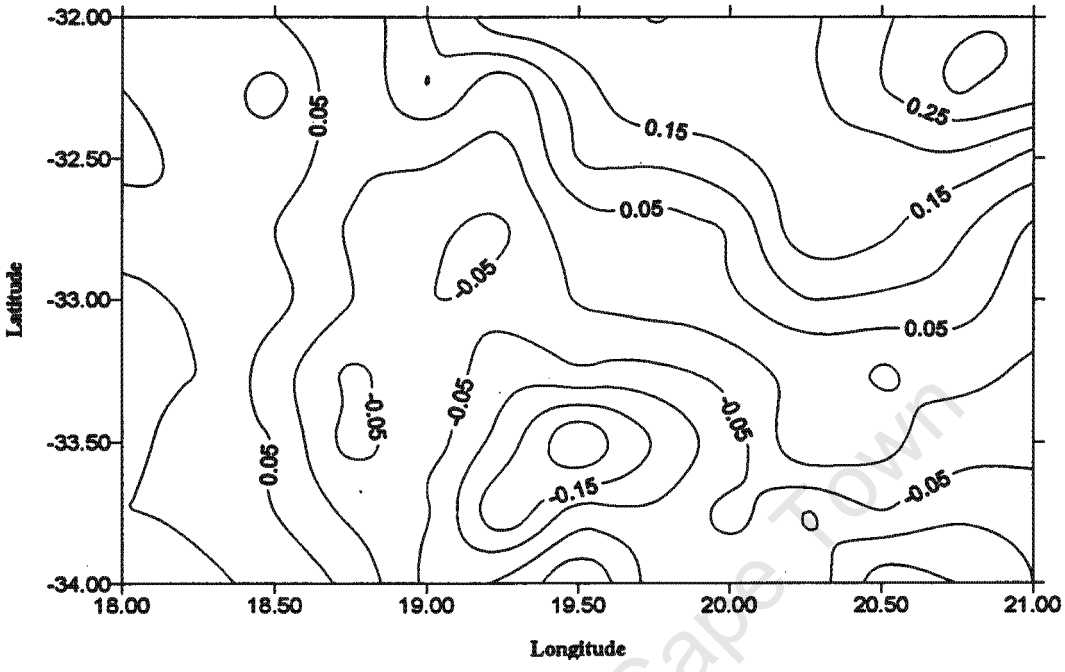

Figure 6-16: Differences between UCT98Wcape and UCT2000WCape Quasi-Geoids (Units=m)
(Contour Interval: 0.05m)

Similar results on much larger scales have also been reported in (Fotopoulos et al., 1999) and (Milbert and Smith, 1996). A new gravimetric geoid computed using a one dimensional FFT in Canada evaluated at 1300 GPS benchmarks yielded an RMS difference of 13cm after fitting the two surfaces to a four parameter transformation model. For the central part of Canada an RMS difference of 9cm was obtained (Fotopoulos et al., 1999). The GEOID96 model also computed using a one dimensional FFT for the United States was tested at 2729 GPS points on levelled benchmarks. After the removal of a bias, tilted plane and an empirical conversion surface an RMS error of 5.8cm was achieved (Milbert and Smith, 1996). These results once again highlight the possibilities of producing quality gravimetric geoids consistent with accuracies obtained via GPS.

6.3 A QUASI-GEOID FOR GAUTENG

6.3.1 Description of Data and Computational Methods

Gauteng is a province situated north east of South Africa, an 'economic powerhouse' and an area of rapid urban development. The infrastructural development owing to its population expansion over the last few decades has placed a significant demand on large scale engineering projects such as the construction of dams which require precise heighting.

A quasi-geoid for this area bounded by $-26.333 < \varphi < -26.0$, $27.667 < \lambda < 28.5$ was computed on a one minute grid using the planar FFT approximation. The G_1 term was first modelled: Bouguer anomalies provided by Professor C. Merry, Department of Geomatics at the University of Cape Town were converted to free air anomalies using the standard Bouguer gradient of 0.119mgal/m. A digital elevation model on the same grid as the gravity anomalies was made available by the Chief Directorate of Surveys and Mapping in Mowbray, Cape Town. Figure (6-17) depicts a contour plot of these elevations:

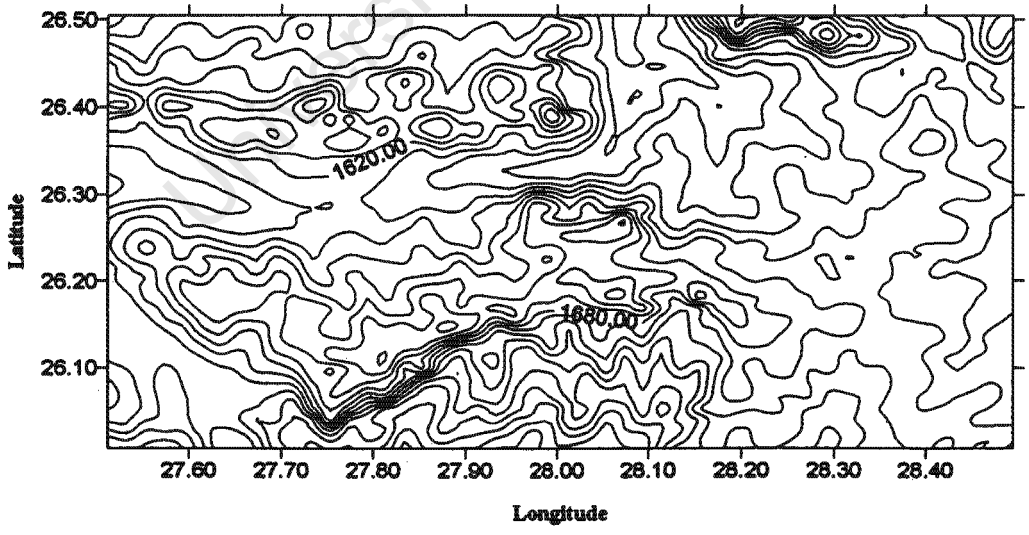

Figure 6-17: Contour Plot of Elevations - Gauteng

Gauteng is on average approximately 1200 meters above mean sea level with elevations close to 1700 meters. For our test area we note the maximum elevations at the north eastern and western half parts of the grid (figure 6-17). In general we note that the topography is quite smooth.

The elevation model with its accompanying map of free air anomalies was used to compute the G_1 correction for the test area. In the computation of the quasi-geoid, the gravity anomalies implied by the EGM96 geopotential model (computed by *GEOGRAV*) were removed from the free air anomalies (including the G_1 contribution), a residual quasi-geoid was computed via a planar FFT and finally the long wavelength contribution to the quasi-geoidal heights implied by the same geopotential model were restored to the residual heights. The gravimetric quasi-geoid was validated against 15 GPS/Levelling derived quasi-geoid heights distributed over the test area. These 15 points were made available by the Chief Directorate of Surveys and Mapping in Mowbray, Cape Town.

6.3.2 Discussion of Results and Quasi-geoid Validation

The statistics of the G_1 correction in table (6-17) show that the absolute maximum and minimum values of the G_1 contribution are about 2mgals with an RMS value of 0.44mgals. This is expected since the topography is generally smooth and unbroken. The contour plot (figure 6-18) indicates that the maximum values, although not significant occur in the western half of the test area where the terrain is rugged.

GRID DIMENSION 19 x 49				
AREA $-26.333 < \varphi < -26.0, 27.667 < \lambda < 28.5$ $d\varphi, d\lambda = 1'$				
Units = mgals	**MAX.**	**MIN.**	**MEAN**	**RMS**
	2.155	-1.887	0.099	0.444

Table 6-17: Statistics of the G_1 term – Gauteng

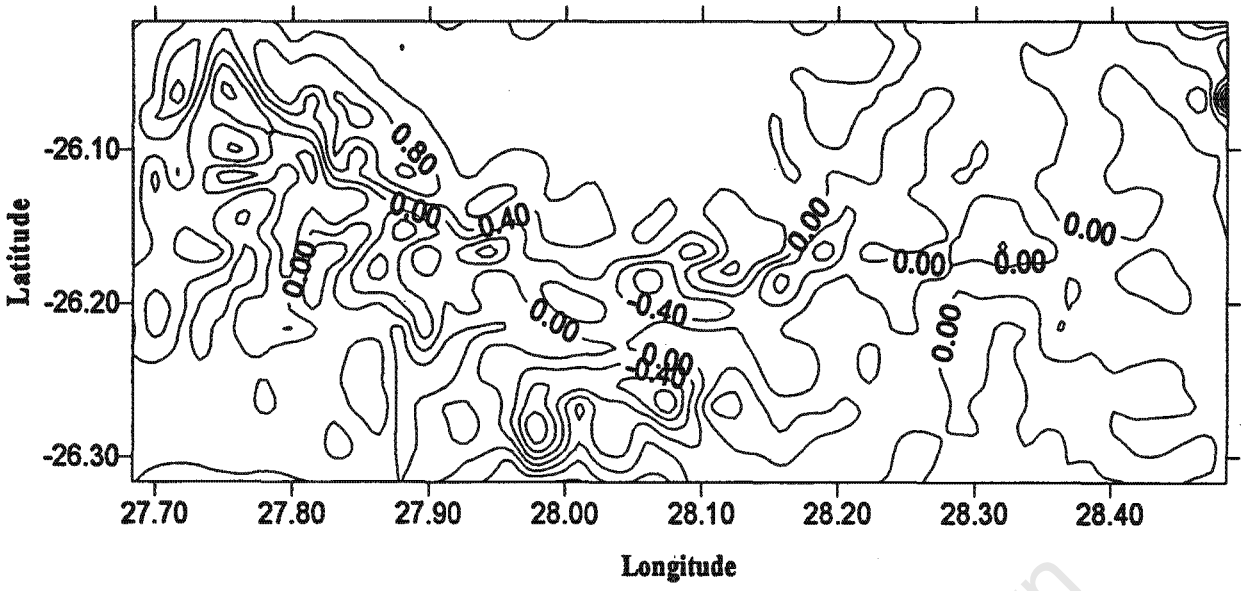

Figure 6-18: G_1 Contribution – Gauteng
(Contour Interval 0.4mgal)

The contour plot of the quasi-geoid, figure (6-19) below, reveals a surface of smooth quasi-geoidal heights over the test area.

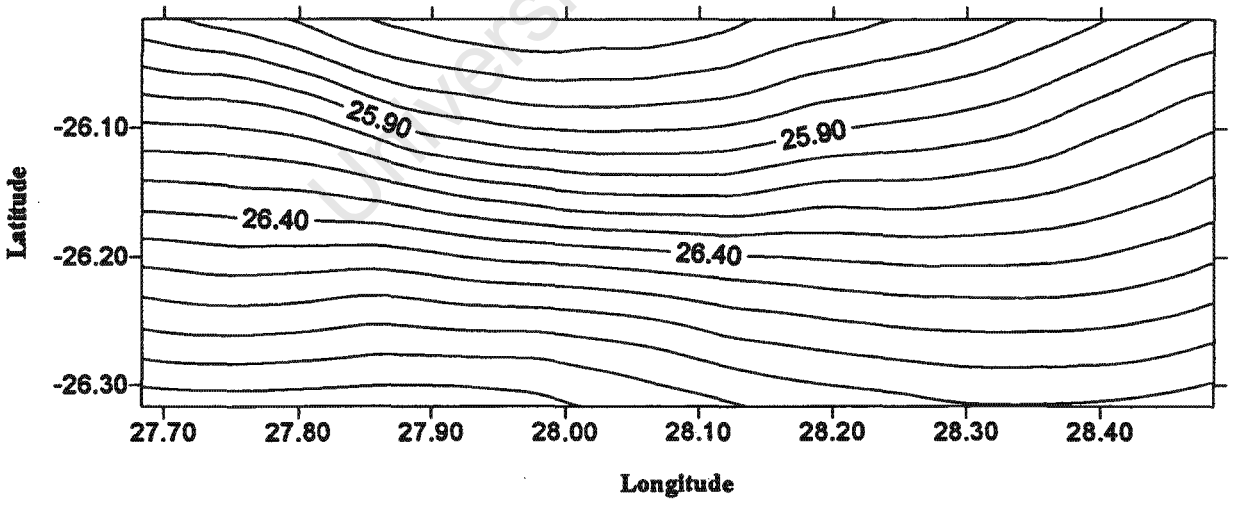

Figure 6-19: Quasi-geoid – Gauteng
(Contour Interval 0.1m)

The quasi-geoid above was validated against a quasi-geoid derived from 15 GPS/Levelling points well distributed over the test area (figure 6-20). The maximum and minimum differences are about 37cm and 27cm respectively with an RMS difference of 3.6cm. These statistics (in metres) appear in table (6-18) below. We note a bias of about 31cm. After removal of this bias by fitting a planar transformation model to the vector of quasi-geoid differences, the RMS difference is reduced to 1.3cm (table (6-19)). This result is encouraging and shows that the gravimetric quasi-geoid, by simply applying a tilt can yield results at the centimeter level in small areas with smooth topography.

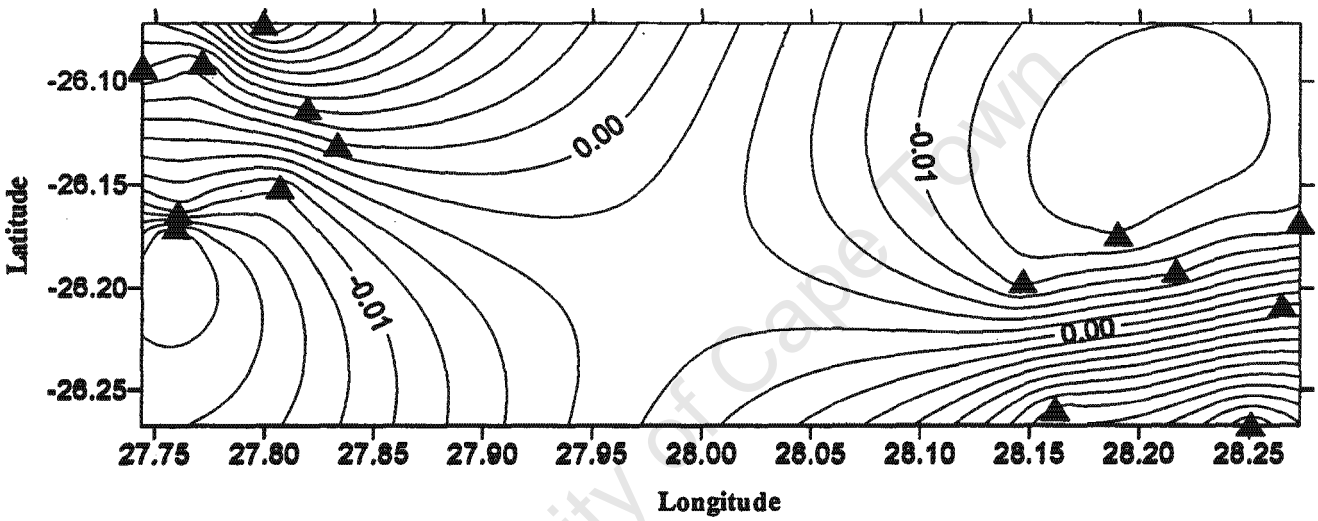

Figure 6-20: Residual Differences between Gravimetric and GPS/Levelling Quasi-geoids - Gauteng (CI: 0.002m)

MAX	MIN.	MEAN.	RMS (mean removed)
0.373	0.268	0.309	0.036

Table 6-18: Level of Agreement between Gravimetric and GPS/Levelling Quasi-geoids – Gauteng (Units=m)

MAX	MIN.	MEAN.	RMS (mean removed)	Tilt
0.024	-0.013	0.000	0.013	0.48 secs.

Table 6-19: Level of Agreement between Gravimetric and GPS/Levelling Quasi-geoids after Planar Transformation fit (Units=m) - Gauteng

6.4 ANALYSIS OF THE QUASI-GEOID FOR SOUTH AFRICA

6.4.1 Description of Data and Computational Methods

In the final investigation the various FFT methods previously discussed were used to compute a quasi-geoid for the region bounded by latitudes $-35.0 < \varphi < -22.0$ and longitudes $16.0 < \lambda < 33.0$. This region encompasses the whole of South Africa and overlaps onto part of the neighbouring countries. This is a much larger test area on which the FFT methods are now applied thus giving us a more realistic picture in order to infer the most suitable method for the quasi-geoid computation at mid latitude regions.

The computations were performed on points distributed at six minute intervals – resulting in a matrix/grid dimension of 131x171 or 22 401 'data' points. The gravity anomalies derived from the EGM96 geopotential model for degree (120-360) computed by *GEOGRAV* were used as input into the different FFT approximations of Stokes' formula to determine the quasi-geoid. By removing the first 120 harmonic coefficients we are basically using the high frequency part of the geopotential model. The spectral methods employed were the two dimensional planar FFT, spherical FFT and the multi-band SFFT. For the multi-band approach the calculation was done in three different ways: (i) the area of interest was divided into two bands with a two degree overlap (ii) the area of interest was divided into four bands with a two degree overlap and (iii) the area of interest was divided into two bands with a more significant overlap of three degrees but no linear interpolation of the overlapping region was executed.

The results from the computations above were compared to the height anomaly derived from the same geopotential model computed by *GEOGRAV*. In implementing the FFT techniques, zero padding was applied to the periphery of the data sets. The differences between the computed height anomalies and those implied by the geopotential model are not expected to be zero as the integration is carried out over a limited extent and not over the entire earth. The computational routines have been developed by the author using the *MATLAB* software package.

6.4.2 Statistics of the Quasi-geoid

Table (6-20) below indicates the statistics of the quasi-geoid computed using the different methods – note that the second column refers to the quasi-geoid derived from the EGM96 geopotential model computed by *GEOGRAV*.

AREA $-35.0 < \varphi < -22.0,\ 16.0 < \lambda < 33.0$ $d\varphi, d\lambda = 6'$ 131x171 data points

TRUNCATION 120 - 360

Units = m	EGM96 Quasi-geoid	Planar FFT	Spherical FFT	MULTI-BAND FFT		
				2bd/2deg.	4bd/2deg.	2bd/3deg. (no interpolation)
MAX.	2.981	3.155	3.090	2.822	2.829	3.004
MIN.	-2.743	-2.458	-2.322	-2.493	-2.407	-2.528
MEAN	0.015	0.148	0.162	0.131	0.088	0.132
RMS.	0.656	0.680	0.667	0.665	0.685	0.675

Table 6-20: Statistics of the Quasi-geoid – South Africa

The statistics reveal consistency in the different methods used for the computation of the quasi-geoid. The magnitude of the maximum and minimum values are on average about 3m and 2.5m respectively. Figure (6-21) represents a contour plot of the quasi-geoid obtained from the EGM96 geopotential model. The plot has been included for illustrative purposes.

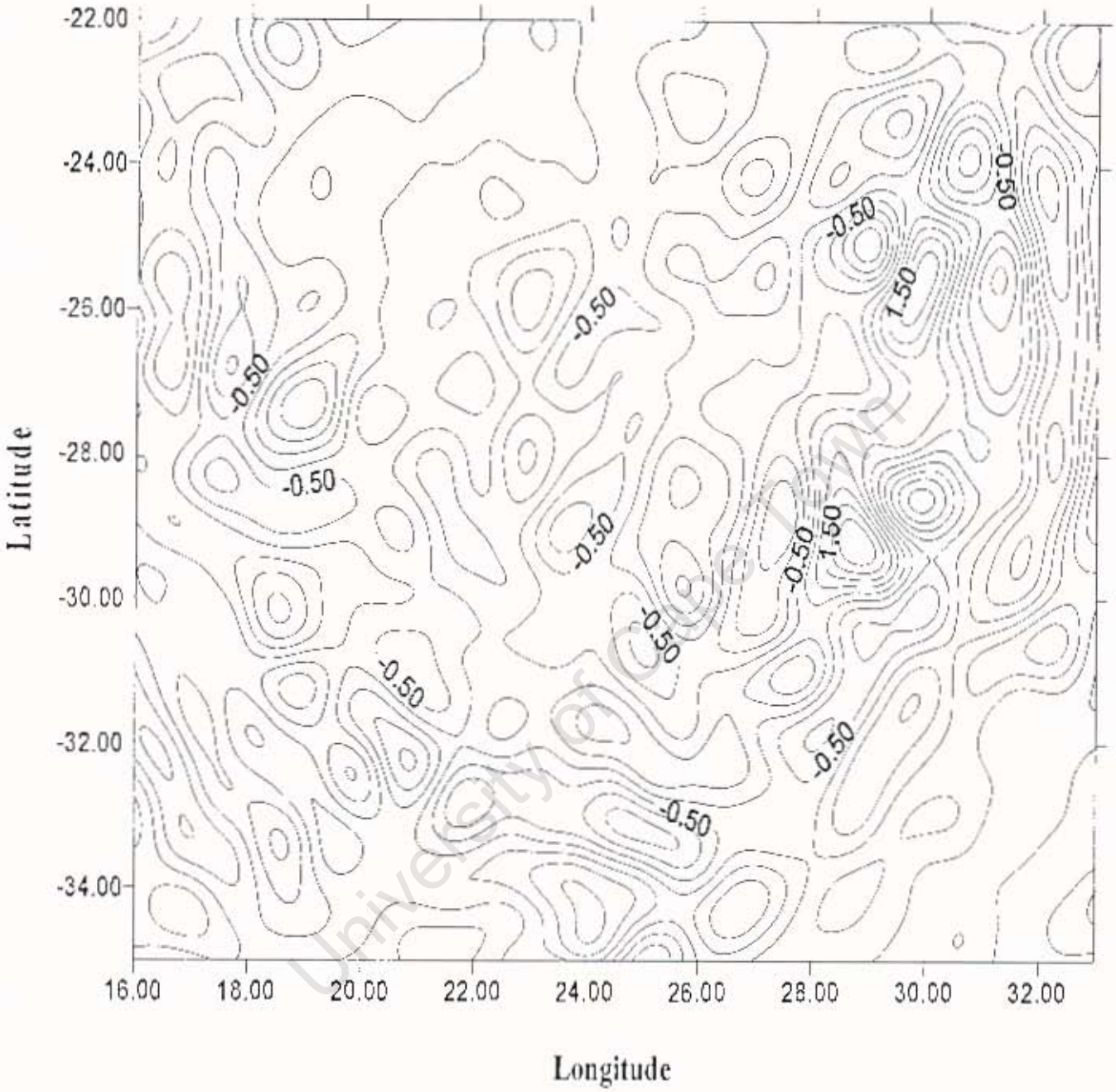

Figure 6-21: Contour Plot of Quasi-geoid – South Africa

(Contour Interval 0.5m)

Truncation: (120-360)

6.4.3 Comparison of the Quasi-geoid obtained from Spectral Methods to that derived from the EGM96 Geopotential Model

The quasi-geoid derived from the EGM96 geopotential model was used as a base to test the level of accuracy of the quasi-geoid derived using the planar, spherical and multi-band SFFT techniques. A truncation of (120-360) of the gravity anomalies were used in Molodensky's formula to produce the quasi-geoid. Although the investigation did not perform tests to assess different truncation errors, the examination of such can be used to determine the best truncation error to be optimally combined with gravity and height data to produce high resolution geoids (Tsiavos, 1996). Some error will still remain due to the integration being performed over a limited extent. Zero padding of the data sets was used to eliminate the effects of cyclic convolution. Table (6-21) reflects the statistics of the differencing and table (6-22) the results after a planar and four parameter transformation fit:

AREA $-35.0 < \varphi < -22.0$, $16.0 < \lambda < 33.0$ $d\varphi, d\lambda = 6'$ 131x171 data points
TRUNCATION 120 - 360

Units = m	Planar FFT	Spherical FFT	MULTI-BAND FFT		
			2bd/2deg.	4bd/2deg.	2bd/3deg. (no interpolation)
MAX.	0.694	0.690	0.719	0.852	0.738
MIN.	-1.083	-1.131	-1.226	-1.452	-1.244
MEAN	-0.132	-0.147	-0.116	-0.073	-0.117
RMS.	0.196	0.213	0.224	0.251	0.224

Table 6-21: Statistical Analysis of the Quasi-geoid derived from Spectral Methods differenced against EGM96 derived Quasi-geoid

AREA $35.0 < \varphi < -22.0$, $16.0 < \lambda < 33.0$ $d\varphi, d\lambda = 6'$ 131x171 data points

TRUNCATION 120 - 360

Units=m	Planar FFT	Spherical FFT	MULTI-BAND FFT		
			2bd/2deg.	4bd/2deg.	2bd/3deg. (no interpolation)
PLANAR TRANSFORMATION MODEL					
Coefficients					
a_1	-0.132	-0.147	-0.116	-0.073	-0.117
a_2	-0.006	-0.007	-0.003	-0.002	-0.006
a_3	0.007	0.007	0.003	-0.002	0.006
MAX.	0.900	0.928	1.083	1.368	1.073
MIN.	-0.822	-0.837	-0.837	-0.949	-0.862
MEAN	0.000	0.000	0.000	0.000	0.000
RMS	0.139	0.148	0.190	0.240	0.187
TILT (sec.)	0.018	0.019	0.008	0.005	0.016
FOUR PARAMETER MODEL					
Coefficients					
a_0	-0.294	0.135	-2.285	-4.750	-2.186
a_1	0.475	0.136	1.908	3.775	1.983
a_2	-0.211	-0.408	0.647	1.585	0.453
a_3	0.294	0.508	-0.876	-2.313	-0.690
MAX.	0.899	0.928	1.075	1.376	1.065
MIN.	-0.825	-0.837	-0.853	-0.983	-0.879
MEAN	0.000	0.000	0.000	0.000	0.000
RMS	0.139	0.148	0.190	0.240	0.187

Table 6-22: Statistical Analysis of the Quasi-geoid after Planar and Four Parameter Transformation Fit (Units=m)

Table (6-21) shows that the different approaches produce similar results and no method has produced results that significantly differ from the rest. We note that by removing the first 120 coefficients of the geopotential model the results for the methods are almost unbiased. The bias is much smaller when four bands with a two degree overlap is used for the computation but the planar and spherical FFT methods perform much better in an RMS sense than the multi-band SFFT approach. Using a significant overlap of three degrees with two bands produced almost identical statistics to that when two bands and a two degree overlap is used. (Forsberg and Sideris, 1993) points out that the number of bands to be used depends on the extent and location of the test area.

A planar and four parameter transformation model were fit to the difference of each computed quasi-geoid (emanating from the different methods) and the quasi-geoid produced by the geopotential model. Both the transformation models produced the same RMS statistics. We note that the magnitudes of the RMS showed an improvement of up to 6cm (after fit) for the planar and spherical FFT methods while we see a maximum of about 3cm in the improvement (after fit) of the multi-band SFFT approach. However, the multi-band approaches produced much smaller tilts in comparison to the planar and spherical FFT methods.

Figures (E.1) to (E.5) in the appendix shows the plots of the differences in the cases discussed above. A glance at each plot shows the edge effects around the borders associated with the Fourier transform. Although zero padding was used to minimise the edge effects, the effects will still remain adjacent to the zero padded area and the more realistic results will be in the central part of the test area. Larger errors in figure (E.4) (four bands/2 degree overlap) occurring at the edges of the bands are more conspicuous along the bottom half of the grid. This is apparent in figure (E.5) along the parallel where the area is divided into two bands. Surprisingly, the same pattern is not noticed in figure (E.3) where the area has also been divided into two bands. A possible reason for this is that owing to the linear interpolation applied to the overlapping regions of figure (E.3) there is some continuity where the bands meet.

Such interpolation was not applied to figure (E.5) as the intention was to use a significant overlap but disregard any interpolation.

Similar tests have been performed covering Europe and encompassing surrounding areas by (Tsiavos, 1996). (Tsiavos, 1996) considered the 2D planar FFT (analytical and discrete kernels) , 2D spherical FFT, 2D multi-band SFFT, 1D spherical FFT and the 2D FHT (fast Hartley transform). The latter two have not been investigated in this thesis and our discussion will not concern them. (Tsiavos, 1996) found that the spherical FFT's (2D spherical and multi-band) give much better accuracies at higher latitudes and all the methods produced similar results at mean and lower latitudes. To quantify the last statement, an RMS difference of 38cm and 10cm were respectively achieved, after a comparison of the planar and multi-band SFFT with respect to the geoid heights generated by the OSU91A geopotential model with the first 120 harmonic coefficients removed. The numerical tests carried out in this thesis conform to the conclusions of (Tsiavos, 1996). (Tsiavos, 1996) suggests that in order to properly transform longer wavelengths, spherical FFT's must be considered in all cases as they are theoretically superior .

A brief comment concerning the 1D spherical FFT technique: while this method is exact and produces better accuracies it requires much more computational time than its counterparts. In the test performed by (Tsiavos, 1996) the 1D spherical FFT utilised almost 10 hours of computational time as opposed to the 23 minutes used by the 2D spherical FFT. While the results of both methods were almost unbiased for the computational area, the 1D spherical FFT achieved an accuracy of 9cm as opposed to the 18cm obtained by the 2D spherical FFT. At mid latitudes the level of accuracy differed by only 2cm! Nevertheless, the 1D FFT has become a popular choice for geoid computations in different parts of the globe such as the United States (Milbert and Smith, 1996), East Africa (Gachari and Ollivier, 1998), Tasmania (Vella and Featherstone, 1999) *inter alia* – a possibility for consideration in the development of a southern African geoid model.

Chapter Seven

Conclusions and Recommendations

Conclusions

This thesis has considered the use of spectral techniques namely the planar FFT, spherical FFT and multi-band spherical FFT techniques for quasi-geoid modelling. In South Africa we have a height system which is approximately a normal height system and the appropriate reference surface to be determined is thus a quasi-geoid. Theoretical derivation of such, based on the theory of Molodensky has been discussed earlier.

The numerical investigations considered in this thesis have been centered around four main areas and the objectives of such investigations are outlined below:

1. Analysis of the Molodensky G_1 term

The G_1 contribution computed using the methods of quadrature, convolution and FFT for different grid resolutions were investigated. The results obtained using the different computational techniques did not differ significantly. However, the computational time required by the quadrature approach was rather stringent requiring approximately 52 hours for the evaluation of the G_1 term on a grid resolution of one minute as opposed to the convolution and FFT approach which took less than a minute for the same grid dimension.

The G_1 term, by nature is very sensitive to topography. For a coarse resolution grid of five minutes the maximum G_1 contribution was approximately 6.24mgals while the densest grid resolution of one minute yielded a maximum contribution of 40.72mgals. These maximum values translate to approximately 16cm and 43cm respectively with regard to their maximum contribution to quasi-geoidal heights for the area of the south western Cape.

In the FFT approach the entire distance kernel was used for the computation of the G_1 contribution of a grid point while for the quadrature and convolution methods only points within a radius of 10km in the vicinity of the grid point were considered. The results are all identical but the point to be stressed is that the convolution approach is computationally faster than the FFT approach by almost a factor of 3. In this regard a motivation is put forth to evaluate the G_1 term using the method of convolution and considering points within a limited radius of the computational point.

Comparisons were made by differencing the coarser grids (five, three and two minutes respectively) against the densest grid resolution of one minute in order to determine the optimal grid size, in particular, the highest resolution digital elevation model required to evaluate the G_1 term. From the differencing we found that as the grid resolutions become denser the RMS difference shows a tendency to converge. This convergence will depend on the nature of topographical relief – for a smooth terrain the optimal grid resolution could well be a one minute grid but much denser grids with resolutions of 0.25 minutes or less, may be required to model the G_1 term in areas of rough and mountainous topography.

2. A Quasi-geoid for the Western Cape

The methods of planar FFT, spherical FFT and the multi-band SFFT were applied to Molodensky's formula and then combined with the quasi-geoidal heights implied by the EGM96 geopotential model to determine the quasi-geoid for the south western Cape at a grid resolution of one minute. This test area was chosen owing to its mountainous topography and broken relief.

The three spectral methods produced the same results and the validation of the gravimetric quasi-geoid against a GPS/Levelling derived quasi-geoid produced an RMS discrepancy at roughly 4cm for each method. The quasi-geoid was re-computed by excluding the G_1 term and a bias of about 23cm was obtained. After a planar transformation fit this bias was reduced to 6cm. This re-iterates the importance of considering the G_1 term in quasi-geoid modelling. Nevertheless, the results are

encouraging and shows the potential of the gravimetric geoid/quasi-geoid to achieve accuracies at the centimetre level.

While the multi-band approach is not suitable for such a small area as the south western Cape, the method was used merely for comparative purposes - at a later stage the multi-band approach was used to determine the quasi-geoid for the whole of South Africa to give a more realistic picture of this method.

3. A Quasi-geoid for Gauteng

The planar FFT method was used to compute the G_1 term and subsequently determine a quasi-geoid for the Gauteng province, north east of South Africa. The rationale for choosing this area is that the topography is smooth and unbroken. The area is approximately 40x80 kilometres in extent. The statistics of the G_1 term for this area are almost insignificant – about 2mgals in magnitude for the maximum and minimum contributions. The gravimetric quasi-geoid validated against a GPS/Levelling derived quasi-geoid yielded a bias of 3.6cm, which after removal of this bias reduced to an RMS value of 1.3cm. These results indicate that centimetre accuracies in the gravimetric geoid are attainable in local geoid computations were the topographical relief is in general smooth.

4. Analysis of the Quasi-geoid for South Africa

The intention of this analysis was to determine which of the spectral methods give the better accuracy for an area almost 1300x1700km in extent encompassing the whole of South Africa. The quasi-geoid computed from the different spectral methods were tested against the quasi-geoid implied by the EGM96 geopotential model. The planar FFT, spherical and multi-band SFFT approaches produced identical results that were almost unbiased.

This bias was much better when the multi-band approach was used with four bands and a two degree overlap but the planar and spherical FFT methods performed better in an RMS sense.

Recommendations

A geoid for South Africa will entail the proper modelling of the G_t term. This would require high resolution free air anomalies and concomitant digital elevation models (DEM) covering the whole of South Africa and its neighbouring countries. The Chief Directorate: Surveys and Mapping in Mowbray, Cape Town have produced a DEM at a spatial resolution of 400m for the entire country. DEM's at spacings of 200m are also available for the main urban centers. The department of Geomatics at the University of Cape Town has an extensive gravity database covering most of South Africa and some of its neighbouring countries. The more reliable source of satellite altimetry can be used to provide marine gravity data (Merry and Amod, 2001). Systematic corrections to this gravity data such as the effect of the atmosphere, ellipsoidal corrections and the vertical gradient of normal gravity will have to be taken into account (Rapp and Pavlis, 1990). The short wavelength component of the gravimetric quasi-geoid is combined with the long wavelength component of the quasi-geoidal heights implied by the EGM96 geopotential model. A study into the errors of the different truncation levels can assist to optimally combine the geopotential model with gravity and height data.

The South African vertical datum, referred to as the land levelling datum (L.L.D) is constrained to four tide gauges based at Cape Town, Port Elizabeth, East London and Durban. At present there are nine tide gauges which could be incorporated for the vertical datum adjustment. In addition gravity corrections have not been applied to all levelling routes and the interpolation of existing gravity data to benchmarks could be used to calculate gravity corrections without the need for additional gravity surveys

(van Gysen, 1992). These adjustments would provide a consistent system of normal heights for the definition of the South African vertical datum.

The development of a corrector surface would be essential to optimally transform GPS ellipsoidal heights to normal heights with respect to the LLD. The National Geodetic Survey of the United States and the Geodetic Survey Division of Canada have developed such surfaces (Milbert and Smith, 1996; Kotsakis and Sideris, 1999). The adjusted values for the residuals are spatially modelled on a grid using some method of interpolation or collocation. The gridded values for the residuals are combined with the adjusted parameters (see equation (5-24), Chapter five) to produce a corrector surface. A more rigorous approach suggested by (Kotsakis and Sideris, 1999) is to examine the variance-covariance components of the ellipsoidal, orthometric and geoidal height data sets and include them in a least-squares adjustment. Two methods of a deterministic and collocation approach to such modelling are discussed in (Kotsakis and Sideris, 1999).

This thesis has shown the potential of the gravimetric quasi-geoid in achieving accuracy levels consistent with those obtained from GPS and that it can be efficiently evaluated over large regions using FFT techniques. Various authors have suggested different approaches to the modifications of Stokes' formula and the most popular amongst these methods is that of the 1D spherical FFT. With the increase in pace of technological developments, computer memory and computational speed no longer present a burden for large scale gravimetric geoid/quasi-geoid computations.

LIST OF REFERENCES

Anderson, O B & Knudsen, P (1998), "Global Marine gravity field data from the ERS-1 and Geosat geodetic mission altimetry", *Journal of Geophysical Research*, 103(C4):8129

Anonymous, (1996a) "EGM96 General Description" http://cddisa.gsfc.nasa.gov/926/egm96/gendesc.html

Anonymous, (1996b), "EGM96 15 Minute Geoid", http://cddisa.gsfc.nasa.gov/926/egm96/egm96.html

Anonymous, (1997a), *Department of Defense World Geodetic System 1984 – its definition and relationships with local geodetic systems*, National Imagery and Mapping Agency Technical Report NIMA TR8350.2, Third Edition.

Anonymous, (1997b), *MATLAB – the language of technical computing, version 5*, The Mathworks, Inc., Natick, Mass., USA.

Blais, R (2000), University of Calgary, Alberta, Canada, Personal Communication.

Bracewell, R (1978), *The Fourier Transform and Its Applications*, 2nd. edn, McGraw-Hill, New York.

Bendat, J S & Piersol A G (1971), *Random Data: Analysis and Measurement Procedures*, John Wiley & Sons, New York.

Brigham, E O (1988), *The Fast Fourier Transform and Its Applications*, Prentice Hall, Englewood Cliffs, New Jersey.

Crone, S M & Merry C L (1996), "A GPS-derived geoid for the Cape Peninsula", *South African Journal of Surveying and Mapping*, **23**(5), 263-267.

Fashir, H H, Majid A & Kadir A (1998), "The Sudanese Gravimetric Geoid 1997: Stokesian Approach", *South African Journal of Surveying and Mapping*, **24**(4), 175-182.

Featherstone, W E, Dentith M C & Kirby J F (1998), "Strategies for the Accurate Determination of Orthometric Heights from GPS", *Survey Review*, **34** (267): 278-296.

Forsberg, R & Sideris M G (1993), "Geoid Computations by the multi-band Spherical FFT Approach", *Manuscripta Geodaetica*, **18**: 82-90.

Fotopoulos, G, Kotsakis, C & Sideris M G (1999), "A new Canadian geoid model in support of levelling by GPS", *Geomatica*, Vol. 53, No.4, 53-62.

Gachari, M K & Ollivier J G (1998), "A High Resolution Gravimetric Geoid of the Eastern Africa Region", *Survey Review*, **34**(269).

Haagmans, R, de Min E & van Gelderen M (1993): "Fast Evaluation of Convolution Integrals on the Sphere using 1D FFT, and a Comparison with Existing Methods for Stokes' integral", *Manuscripta Geodaetica*, **18**: 227-241.

Harris, F J (1978): "On the Use of Windows for Harmonic Analysis with the Discrete Fourier Transform", *Proceedings of the IEEE*, **66**(1).

Harrison, J C & Dickinson M (1989), "Fourier Transform Methods in Local Gravity Field Modelling", *Bulletin Geodesique*. **63**: 149-166.

Heiskanen, W A & Moritz H (1967), *Physical Geodesy*, W.H. Freeman & Co., San Francisco and London.

Jackson, L B (1986), *Digital Filters and Signal Processing*, Kluwer Academic Publishers, Norwell, USA.

Keckler, D (1995), *Surfer for Windows Users Guide*, Golden Software, Golden, Colorado, USA.

Kotsakis C and Sideris M G (1999), "On the adjustment of Combined GPS/Levelling/Geoid Networks", *Journal of Geodesy*, 73(8), 412-421.

Krynski, J (1995), *Geodesy*, University of Natal, Durban, Lecture Notes.

Lemoine, F G, Smith D E, Kunz L, Smith R, Pavlis E C, Pavlis N K, Klosko S M, Chinn D S, Torrence M H, Williamson R G, Cox CM, Rachlin K E, Wang Y M, Kenyon S C, Salman R, Trimmer R, Rapp R H, Nerem R S (1996), *"The Development of the NASA GSFC and NIMA joint Geopotential Model"*, Proceedings, International Symposium on Gravity, Geoid and Marine Geodesy, Tokyo, September 1996, 461-469.

Merry, C L (1977), "Gravity and the South African Height System", *South African Journal of Surveying and Mapping*, 16(1), 44-53.

Merry, C L & van Gysen H G (1987), "A regional geoid for Southern Africa", *Paper presented at the 19th General Assembly, International Union of Geodesy and Geophysics, Vancouver.*

Merry, C L & Rens J (1989), "Transformation Parameters for the Cape Datum", *South African Journal of Surveying and Mapping*, **20**(3), 95-102.

Merry, C L (1993), "GPS and Heights", *South African Journal of Surveying and Mapping*, **22**(2), 81-87.

Merry, C L (1998), "A Precise Quasi-Geoid for the South-Western Cape", *South African Journal of Surveying and Mapping*, **24**(4), 155-164.

Merry, C L & Amod A (2001), "Proposals for a new Southern African Quasi-Geoid Model", *Paper presented at the 12th Conference of Southern African Surveyors, Cape Town.*

Milbert, D G & Smith D A (1996), "Converting GPS Height into NAVD 88 Elevation with the GEOID96 Geoid Height Model", *http://www.ngs.noaa.gov/PUBS_LIB/gislis96.html.*

Milbert, D G (1999), National Geodetic Survey, Personal Communication.

Moritz, H (1966), "Linear Solutions of the Geodetic Boundary Value Problem", Ohio State University, Department of Geodetic Science, Report No. 79.

Moritz, H (1968), "On the Use of the Terrain Correction in Solving Molodensky's Problem", Ohio State University, Department of Geodetic Science, Report No. 108.

Moritz, H (1989), *Advanced Physical Geodesy*, Herbert Wichmann Verlag, Karlsruhe Druch und Verarbeitung: E. Lokay, Reinheim.

Rapp, H R & Pavlis N K (1990), "The Development and Analysis of Geopotential Coefficient Models to Spherical Harmonics Degree 360", *Journal of Geophysical Research*, **95**(B13), 21 885-21911.

Schwarz, K P (1984), *Data Types and their Spectral Properties*, In: Proceedings of the International Summer School on Local Gravity Field Approximation, Beijing, China, August 21-September 04.

Schwarz, K P, Sideris M G & Forsberg R (1990), "The Use of FFT techniques in Physical Geodesy", *Geophys. J. Int.*, **100**: 485-514

Sideris, M G and Schwarz K P (1986), "Solving Molodensky's Series by Fast Fourier Transform Techniques", Bulletin Geodesique, **60**: 51-63.

Sideris, M G & Forsberg R (1990), "Review of Geoid Prediction Methods in Mountainous Regions", In: *Determination of the Geoid Present and Future* (Eds. Rapp R H, and Sanso F), Springer-Verlag, New York Inc.

Sideris, M G (1994), *Geoid Determination by FFT Techniques*, In: Lecture Notes: International School for the Determination and Use of the Geoid, International Geoid Service, Milan.

Sideris, M G (2001), University of Calgary, Alberta, Canada, Personal Communication.

Sjö berg, L E (1994), "Techniques for Geoid Determination", In: *Geoid and its Geophysical Interpretations* (Eds. Vaní'ček, P, and Christou N T), CRC Press, Inc.

Smith, D A (1998) "There is no such thing as 'the' EGM96 geoid: subtle points on the use of a global geopotential model", *IGeS Bulletin No. 8*.

Strang van Hees, G (1990) "Stokes formula using Fast Fourier Techniques", *Manuscripta Geodaetica*, **15**: 235-239.

Torge, W (1991), *Geodesy*, Walter de Gruyter, Berlin, New York.

Tsiavos, I N (1996), "Comparisons of Spectral Techniques for Geoid Computations over large regions", *Journal of Geodesy*, 70, 357-373.

Vaní'ček, P (1974), *Brief Outline of the Molodenskij Theory*, Lecture Notes No.23, University of New Brunswick Fredericton N.B. Canada.

Vaní'ček, P & Krakiwsky E (1987), *Geodesy, the Concepts*, North Holland, Amsterdam, New York, Oxford, Tokyo.

van Gysen, H G and Merry C L (1985), "A Preliminary Gravimetric Geoid for Southern Africa", *Proceedings, Eight Conference of Southern African Surveyors, Durban.*

van Gysen, H G and Merry C L (1987), "The Gravity Field in Southern Africa", University of Cape Town Department of Surveying Technical Report TR-3.

van Gysen, H G (1991): "Thin-Plate Spline Quadrature of the inner zone contribution to Stokes' formula", Presented, IAG Symposium on Geoid Determination Techniques, XX IUGG General Assembly, Vienna, August 1991.

van Gysen, H G (1992): "Levelling, Gravity and the Geoid", Presented, Workshop on Surveying and Photogrammetry with Emphasis on the Lesotho Highlands Water Project, Pretoria, October 1992.

van Gysen, H G & Krynski J (1993): The Geoid in South Africa, In: *Measure for Measure: A Festschrift in Honour of Basil Maurice Jones* (Eds. Hoogsteden C, and C van Zyl), Otago University Press, Dunedin.

Vella, J P & Featherstone W E (1999), "A gravimetric geoid model of Tasmania, computed using the one-dimensional fast Fourier transform and a deterministically modified kernel", *Geomatics Research Australia*, No. 70, 53-76.

Vermeer, M (1998), "The geoid as a product", *Proceed. 2nd* International Symposium on the Geoid in Europe, Budapest, Hungary.

Vermeer, M (1992), *Geoid determination using frequency domain techniques*, In: Lecture Notes, NKG Autumn School in Helsinki, Sept. 7-13, 1992.

Weaver, H J (1983), *Applications of Discrete and Continuous Fourier Analysis*, John Wiley and Sons, New York.

Wonnacott, R T (1986), "A Comparison between the Geodetic Triangulation and Traversing and the Doppler Survey in South Africa", *Proceedings, Symposium on Geodetic Positioning for the Surveyor, Cape Town.*

Zakiewicz, T (1997), "The African Arc of the 30th Meridian", *South African Journal of Surveying and Mapping*, **24**(2), 65-82.

APPENDIX A

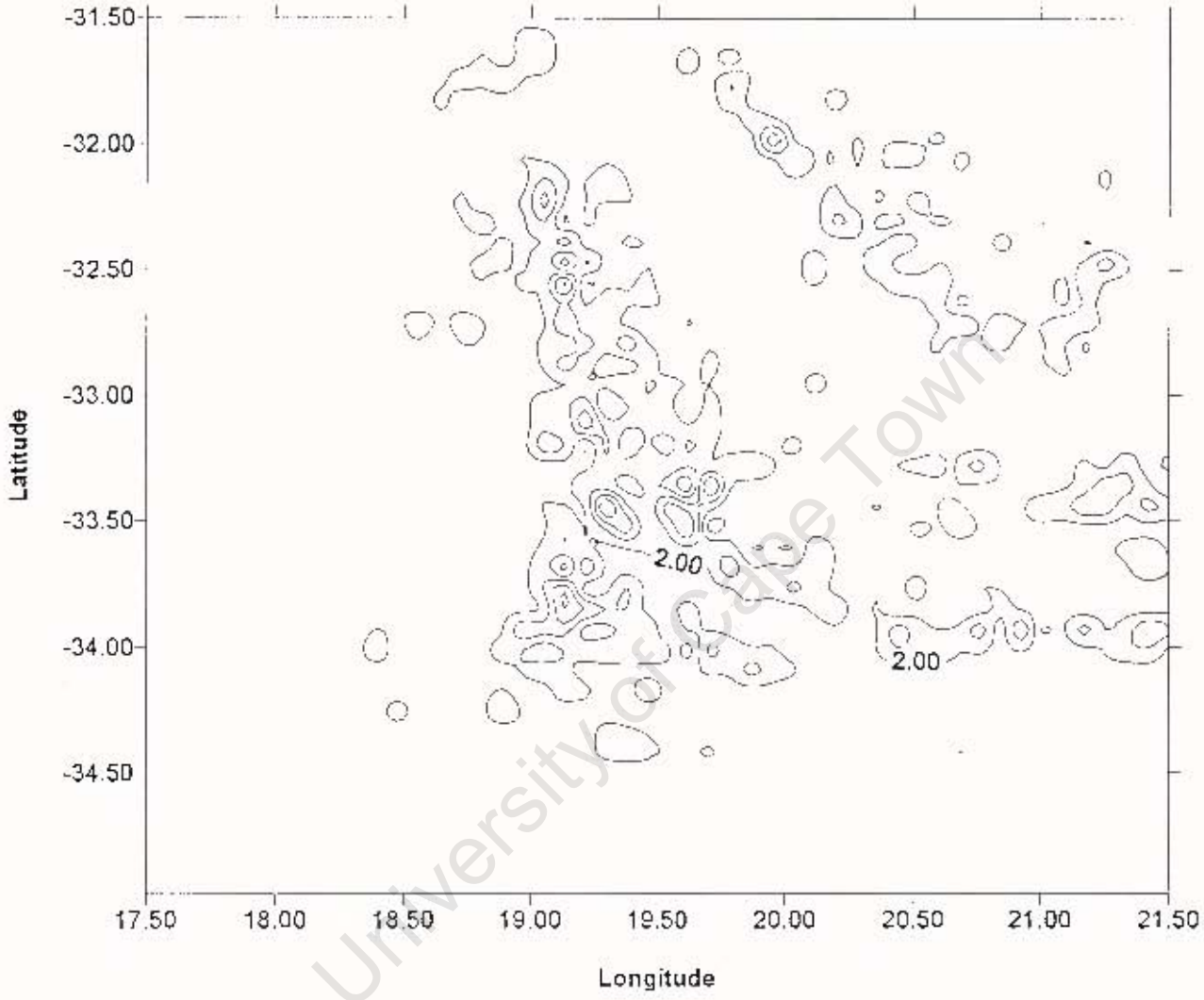

Figure A.1: Evaluation of the G_1 Contrbution via Quadrature
Grid Interval – 1 minute
(Contour Interval 5mgal)

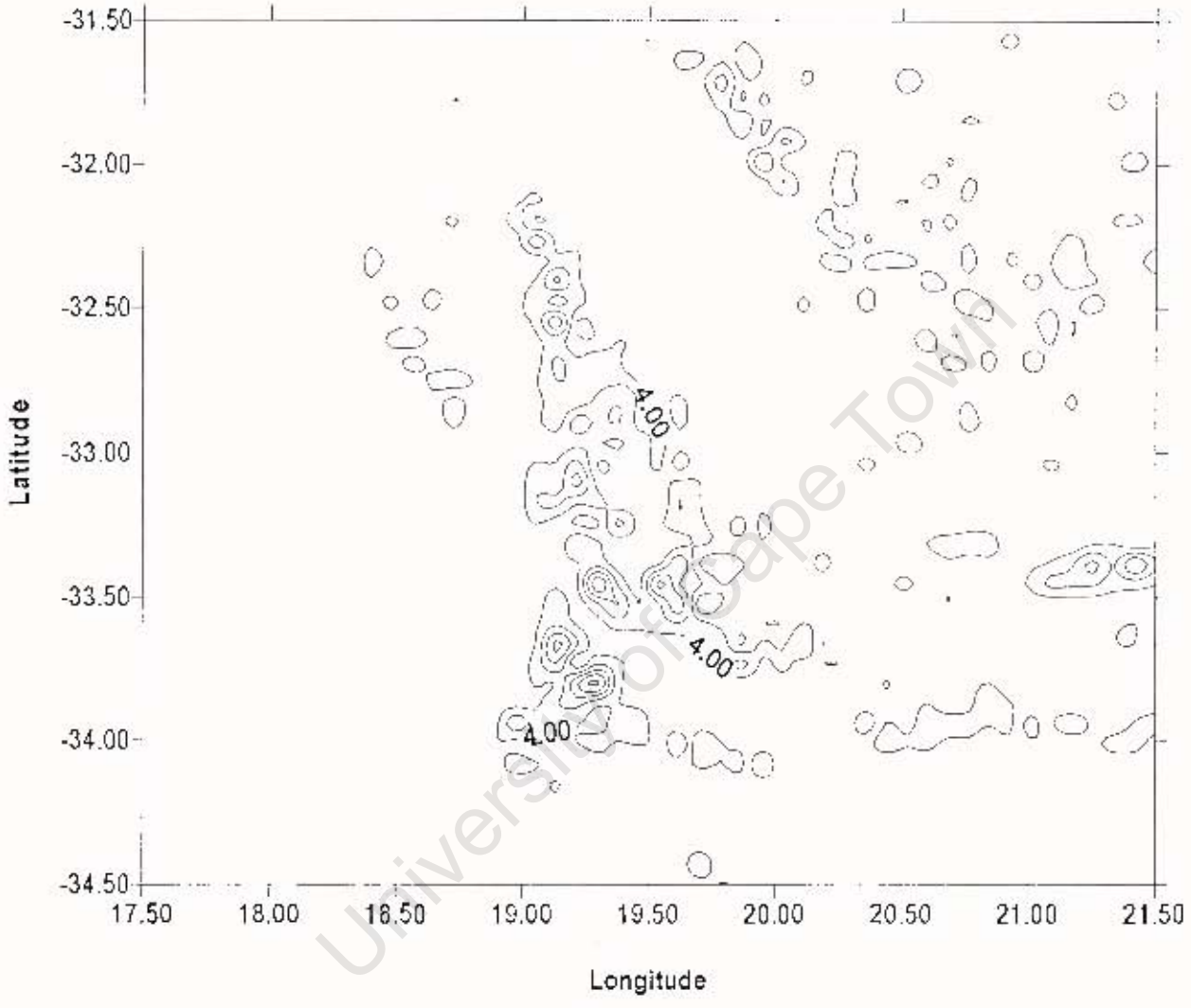

Figure A.2: Evaluation of the G_1 Contribution via Convolution
Grid Interval – 1 minute
(Contour Interval 5mgal)

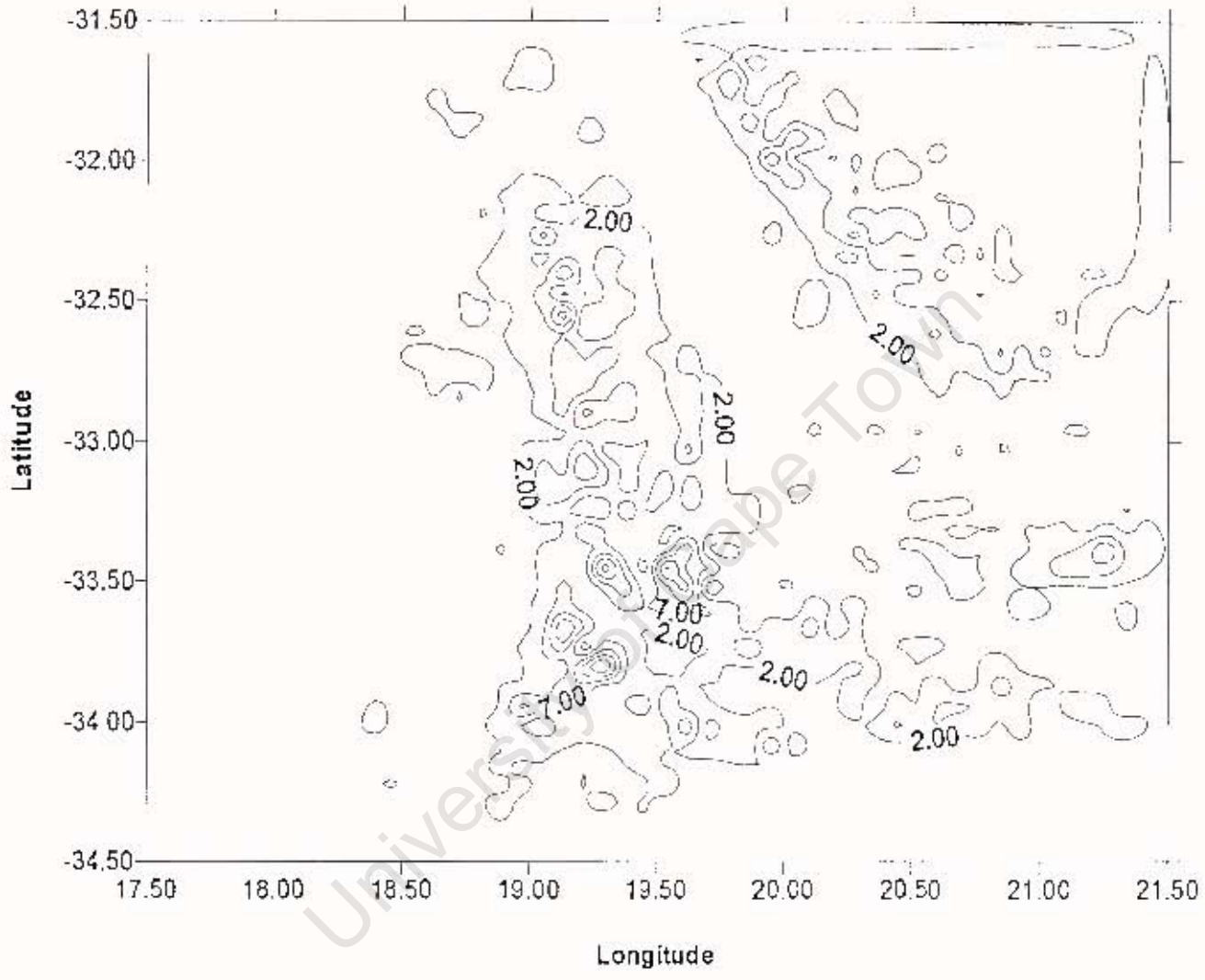

Figure A.3: Evaluation of the G_1 Contribution via FFT
Grid Interval – 1 minute
(Contour Interval 5mgal)

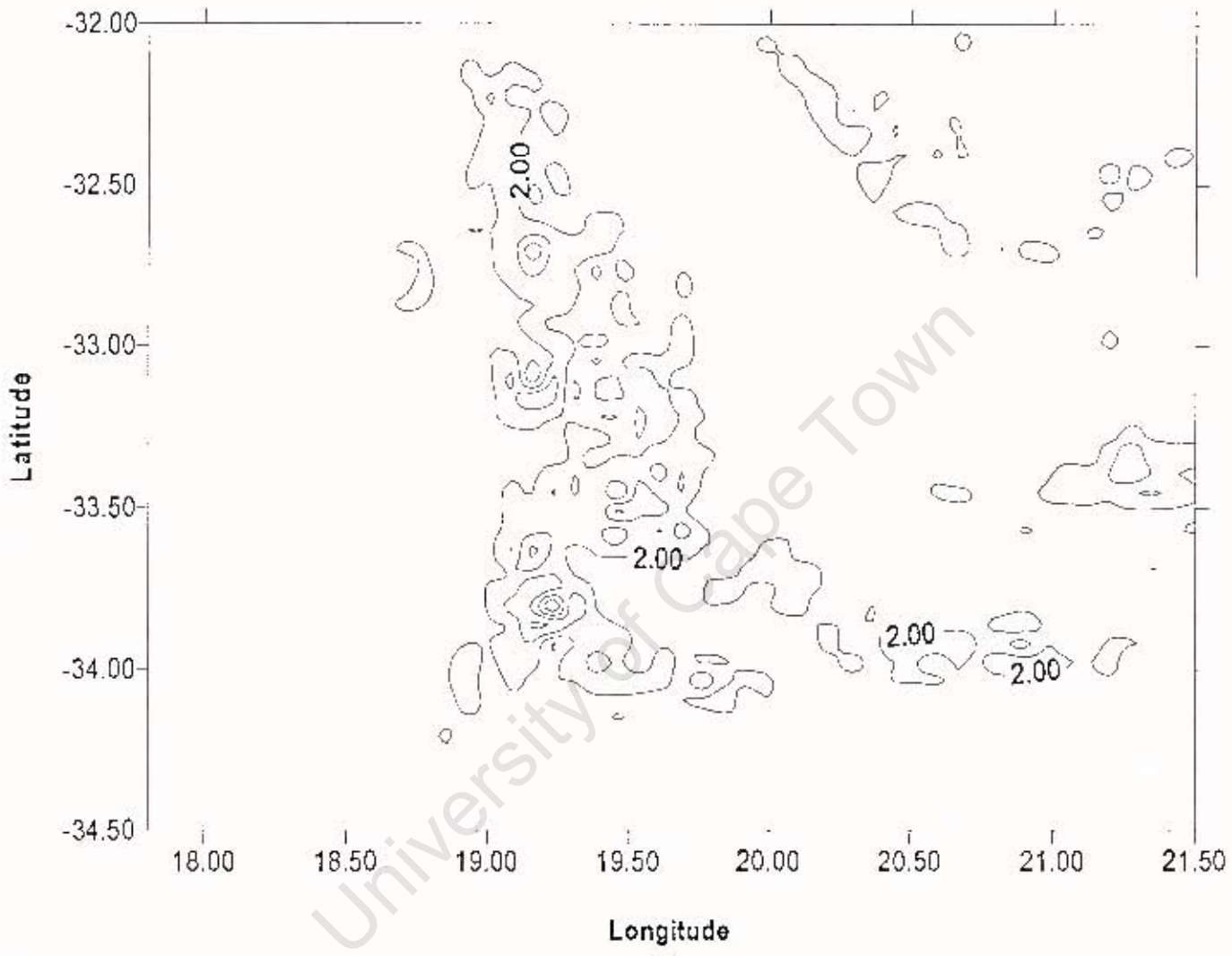

Figure A.4: Evaluation of the G_1 Contribution via Quadrature
Grid Interval – 2 minutes
(Contour Interval 5mgal)

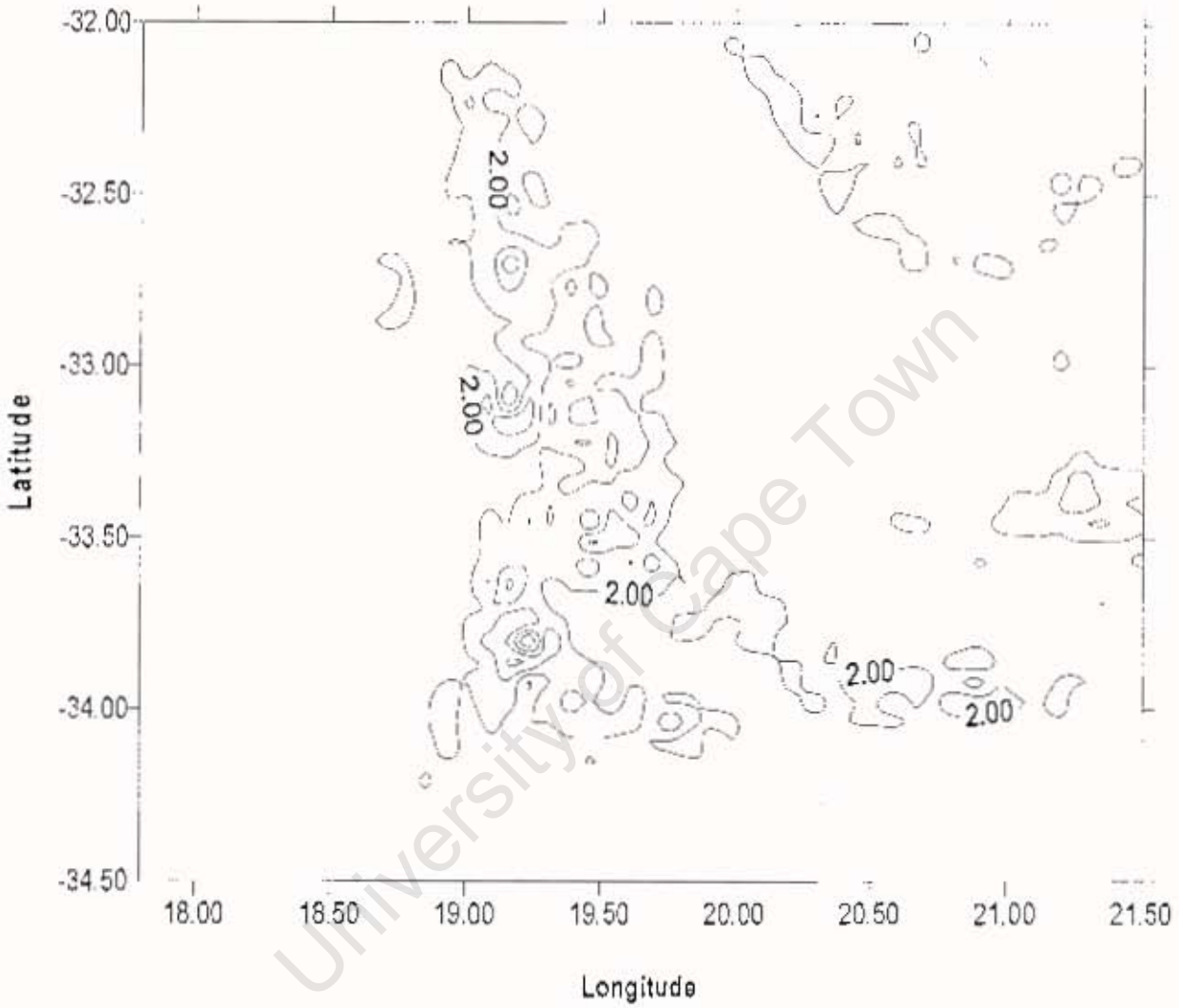

Figure A.5: Evaluation of the G_1 Contribution via Convolution
Grid Interval – 2 minutes
(Contour Interval 5mgal)

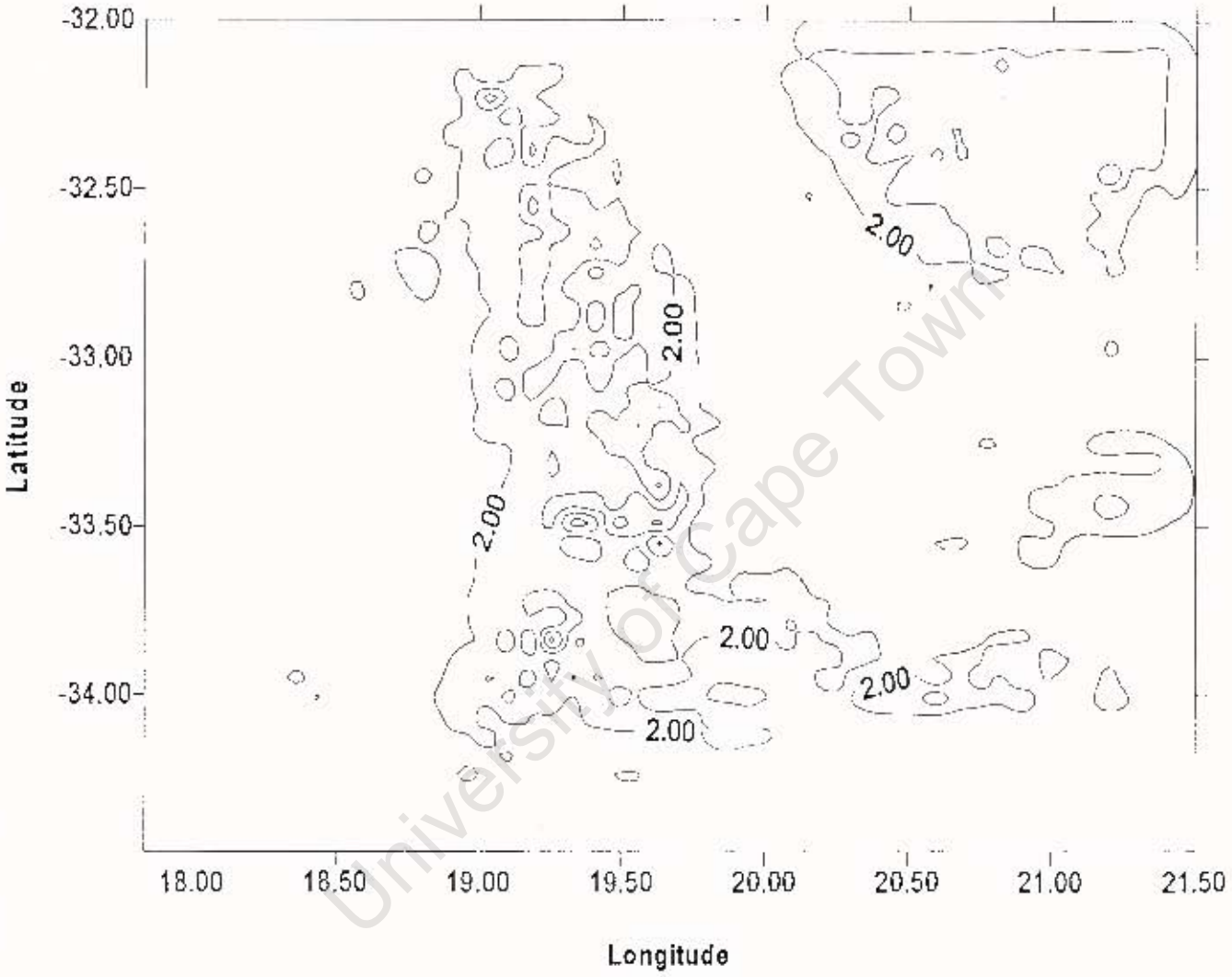

Figure A.6: Evaluation of the G_t Contribution via FFT
Grid Interval – 2 minutes
(Contour Interval 5mgal)

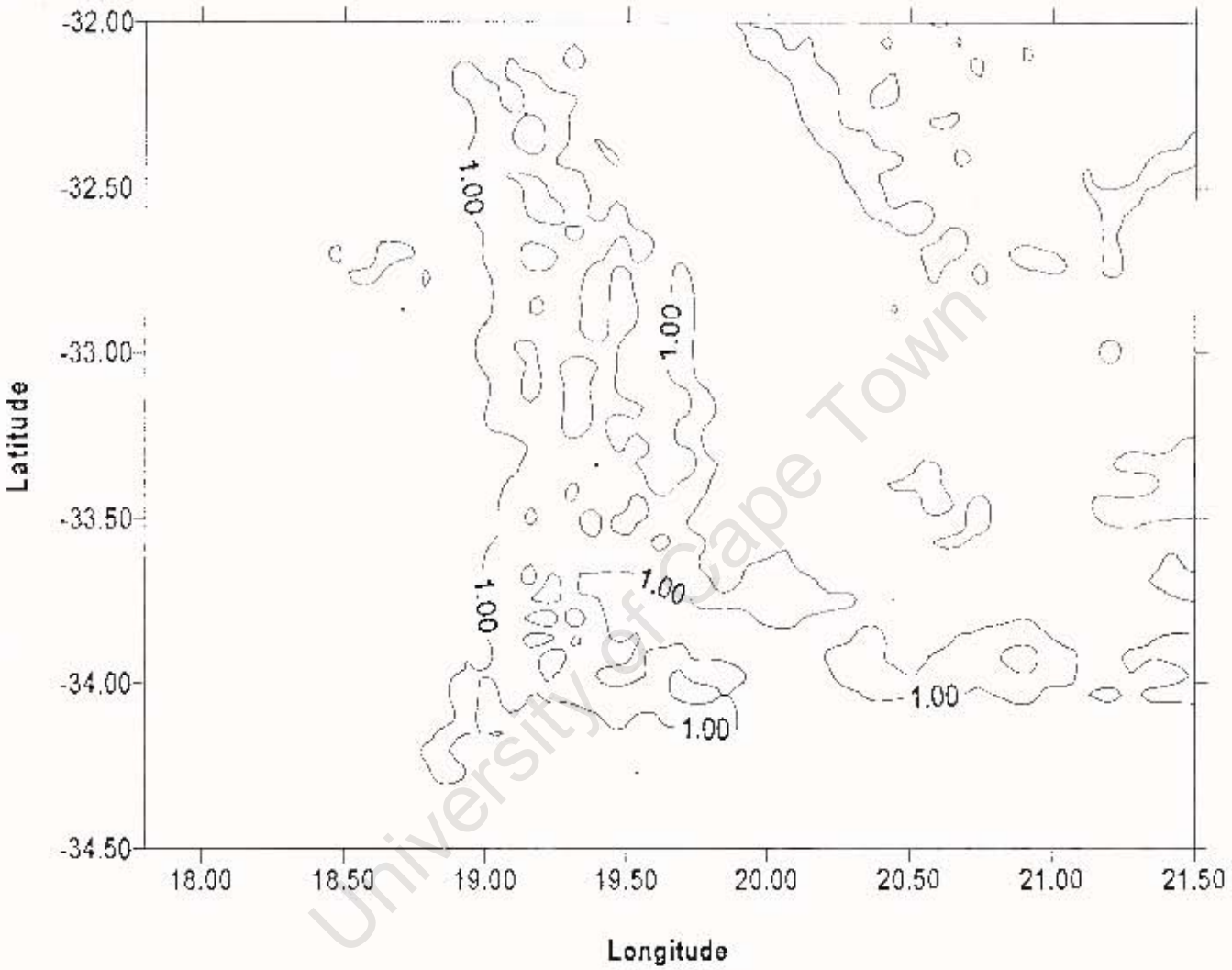

Figure A.7: Evaluation of the G_1 Contribution via Quadrature
Grid Interval – 3 minutes
(Contour Interval 5mgal)

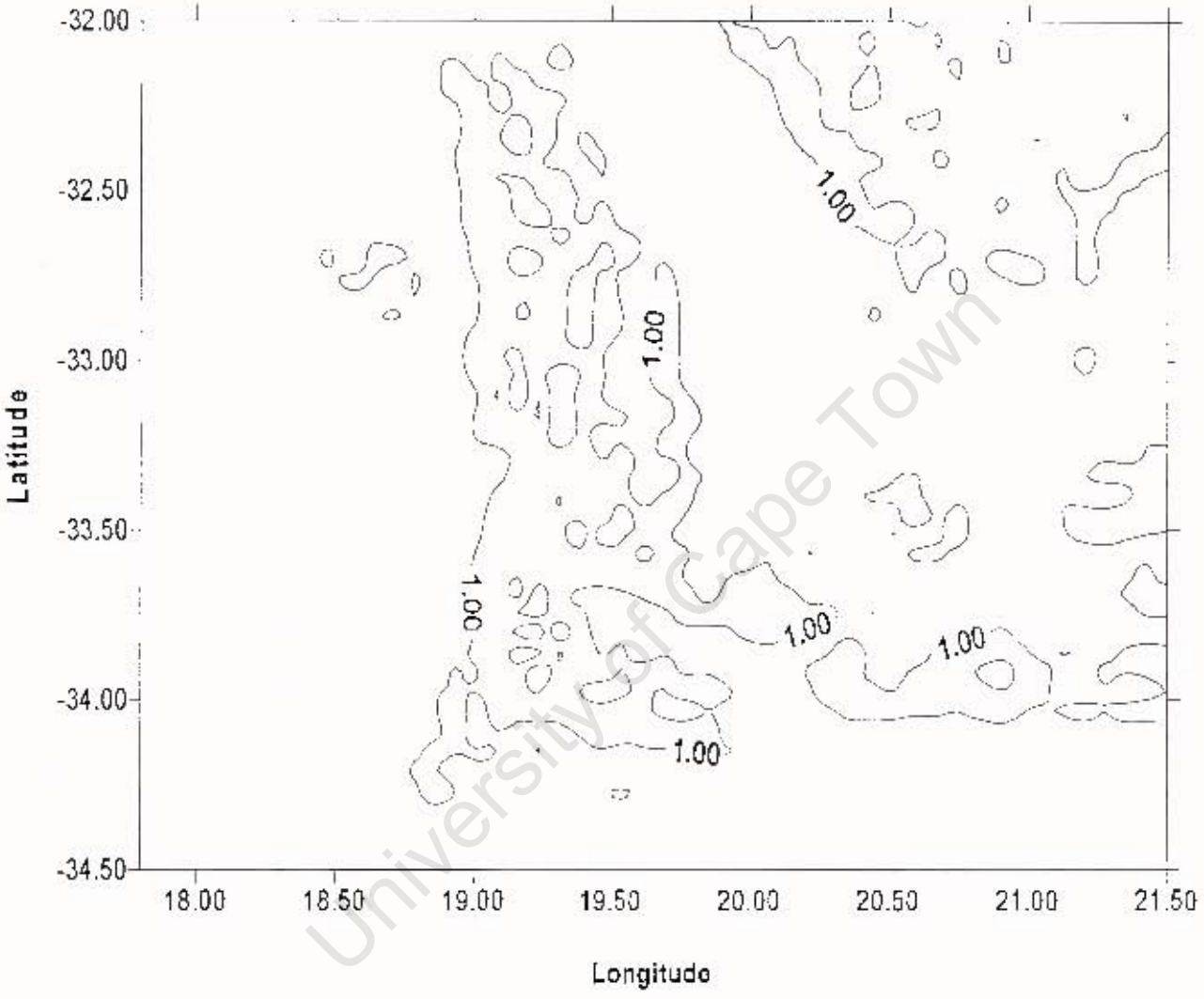

Figure A.8: Evaluation of the G_1 Contribution via Convolution
Grid Interval – 3 minutes
(Contour Interval 5mgal)

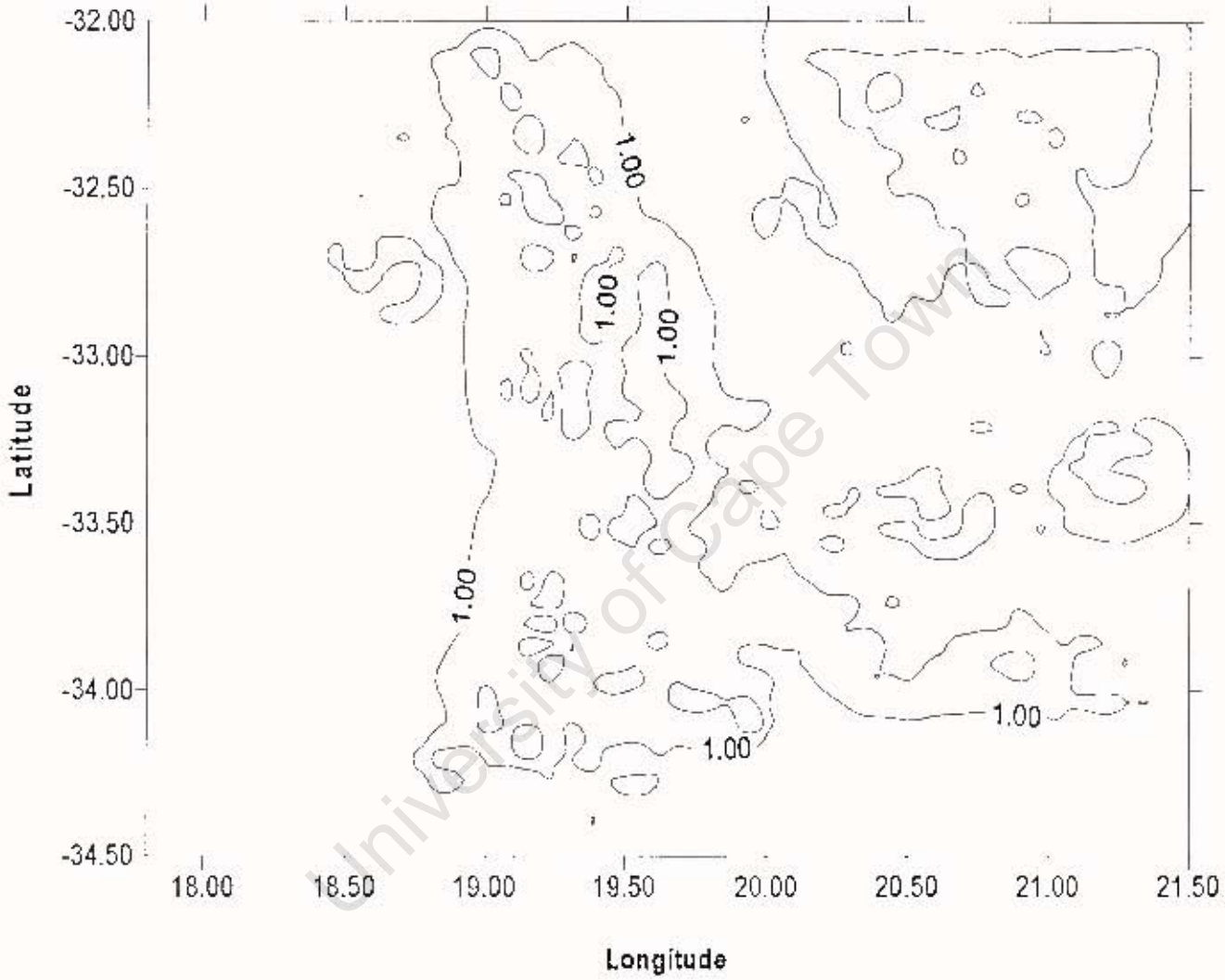

Figure A.9: Evaluation of the G_1 Contribution via FFT
Grid Interval – 3 minutes
(Contour Interval 5mgal)

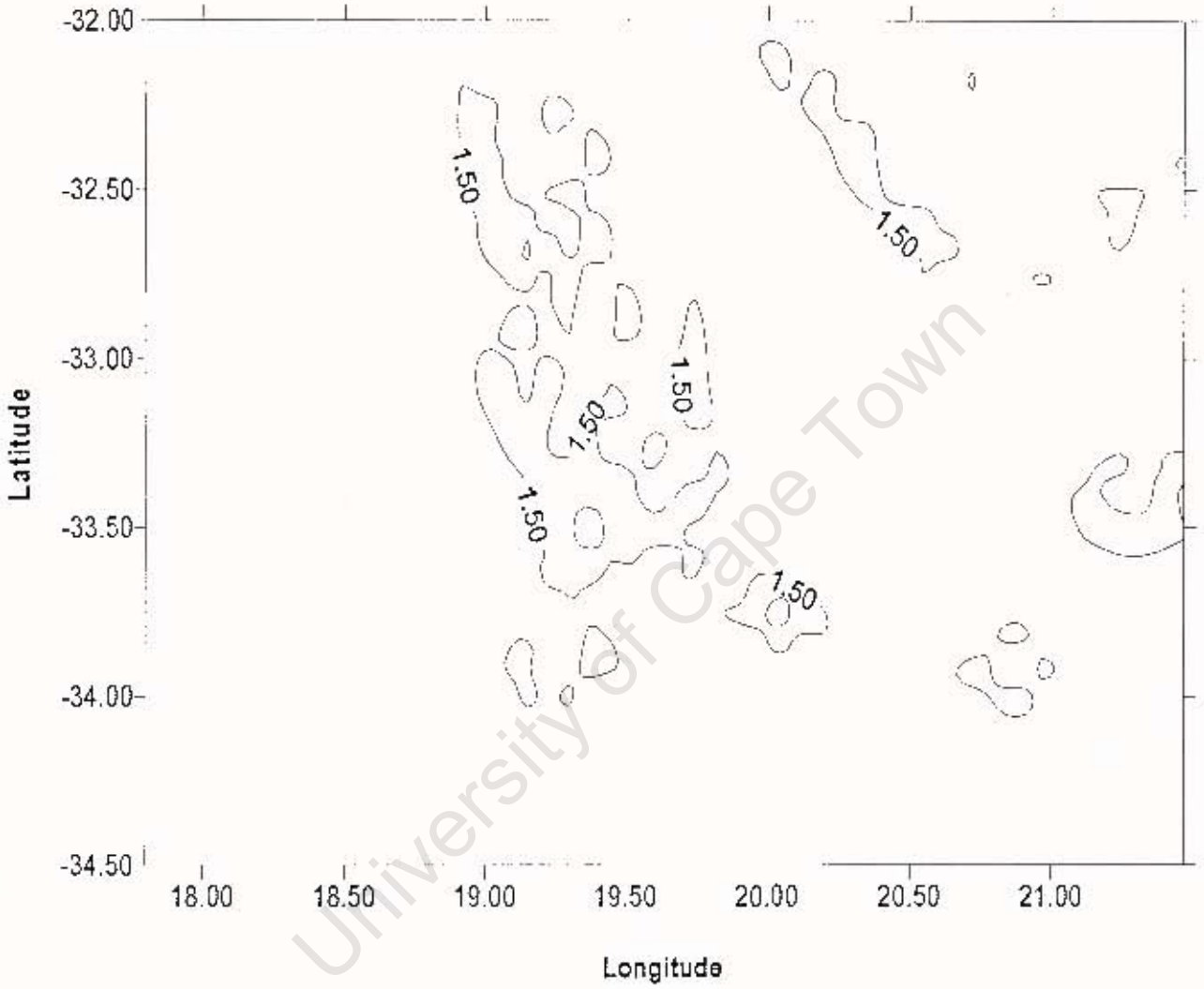

Figure A.10: Evaluation of the G_1 Contribution via Quadrature
Grid Interval – 5 minutes
(Contour Interval 5mgal)

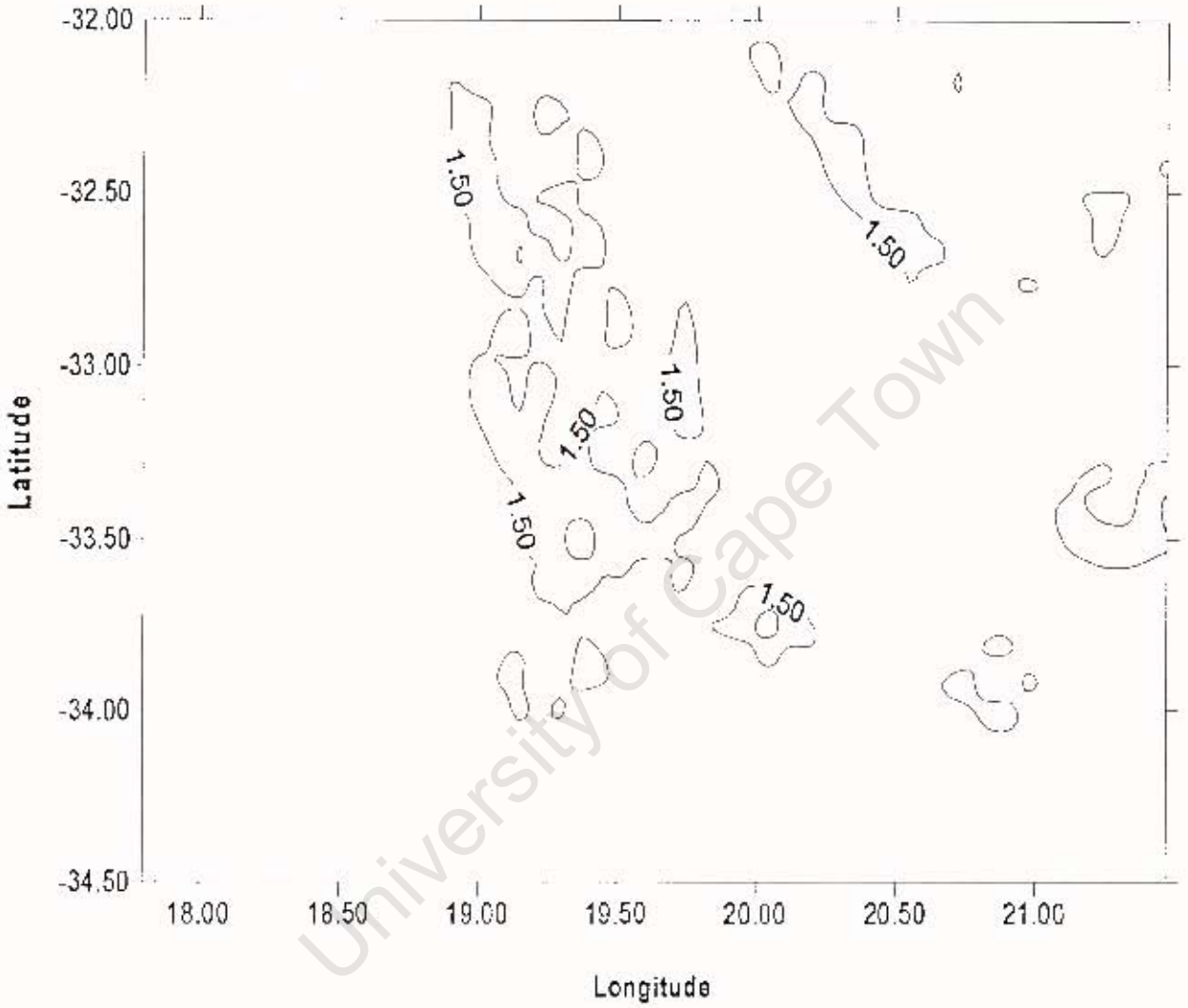

Figure A.11: Evaluation of the G_1 Contribution via Convolution
Grid Interval – 5 minutes
(Contour Interval 5mgal)

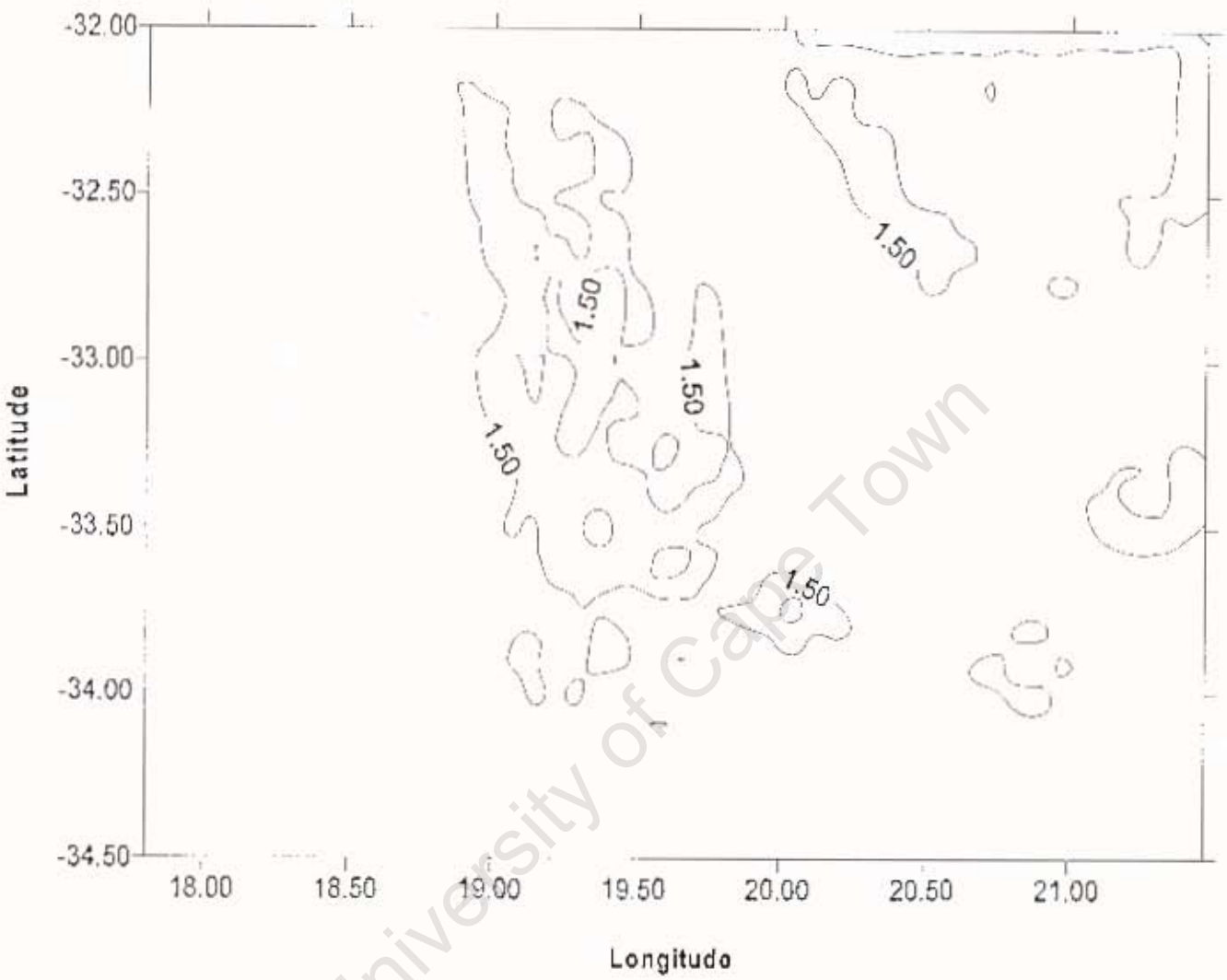

Figure A.12: Evaluation of the G_1 Contribution via FFT
Grid Interval – 5 minutes
(Contour Interval 5mgal)

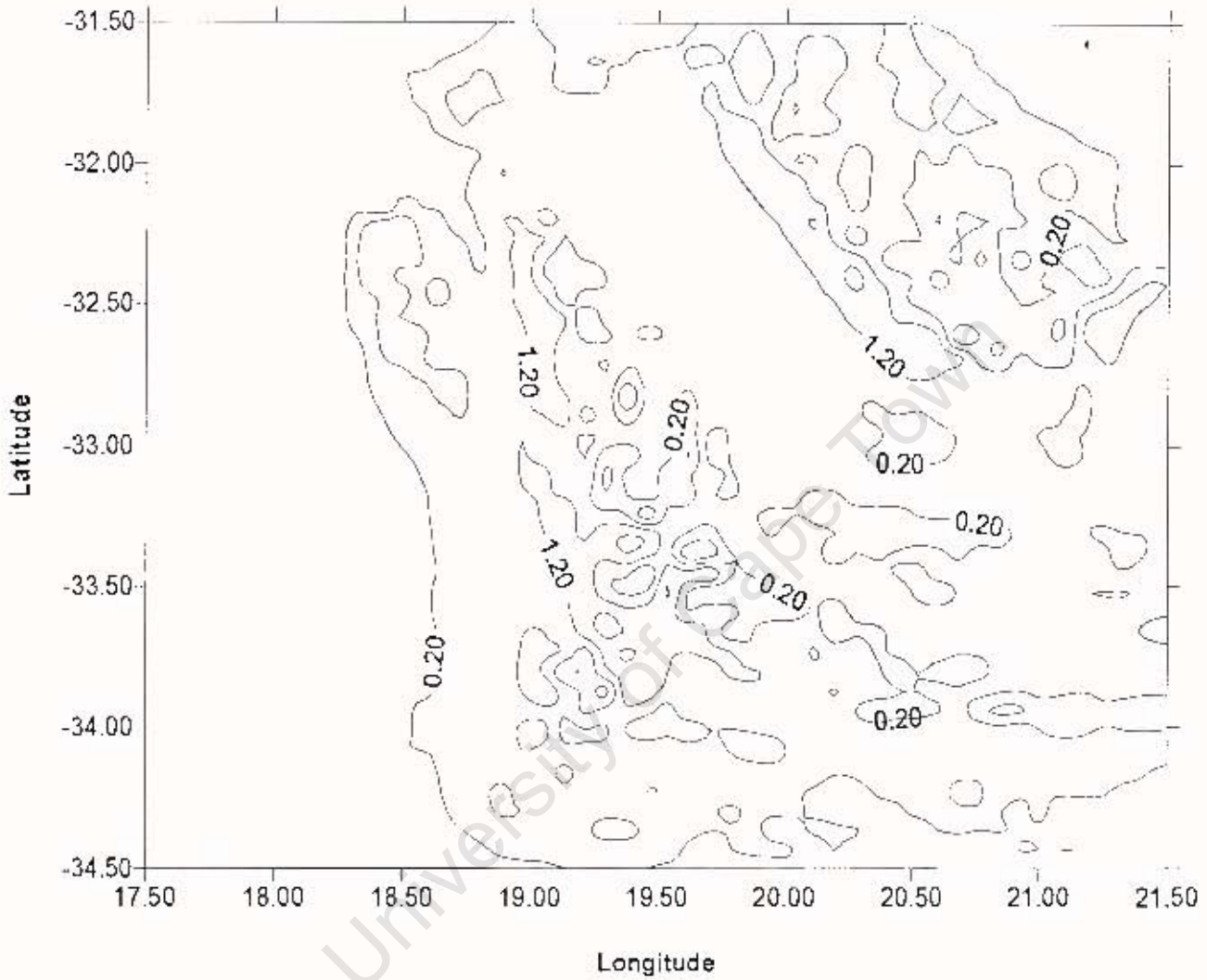

Figure A.13: Differences between the use of a full distance and limited radius kernel
Grid Interval – 1 minute
(Contour Interval 1 mgal)

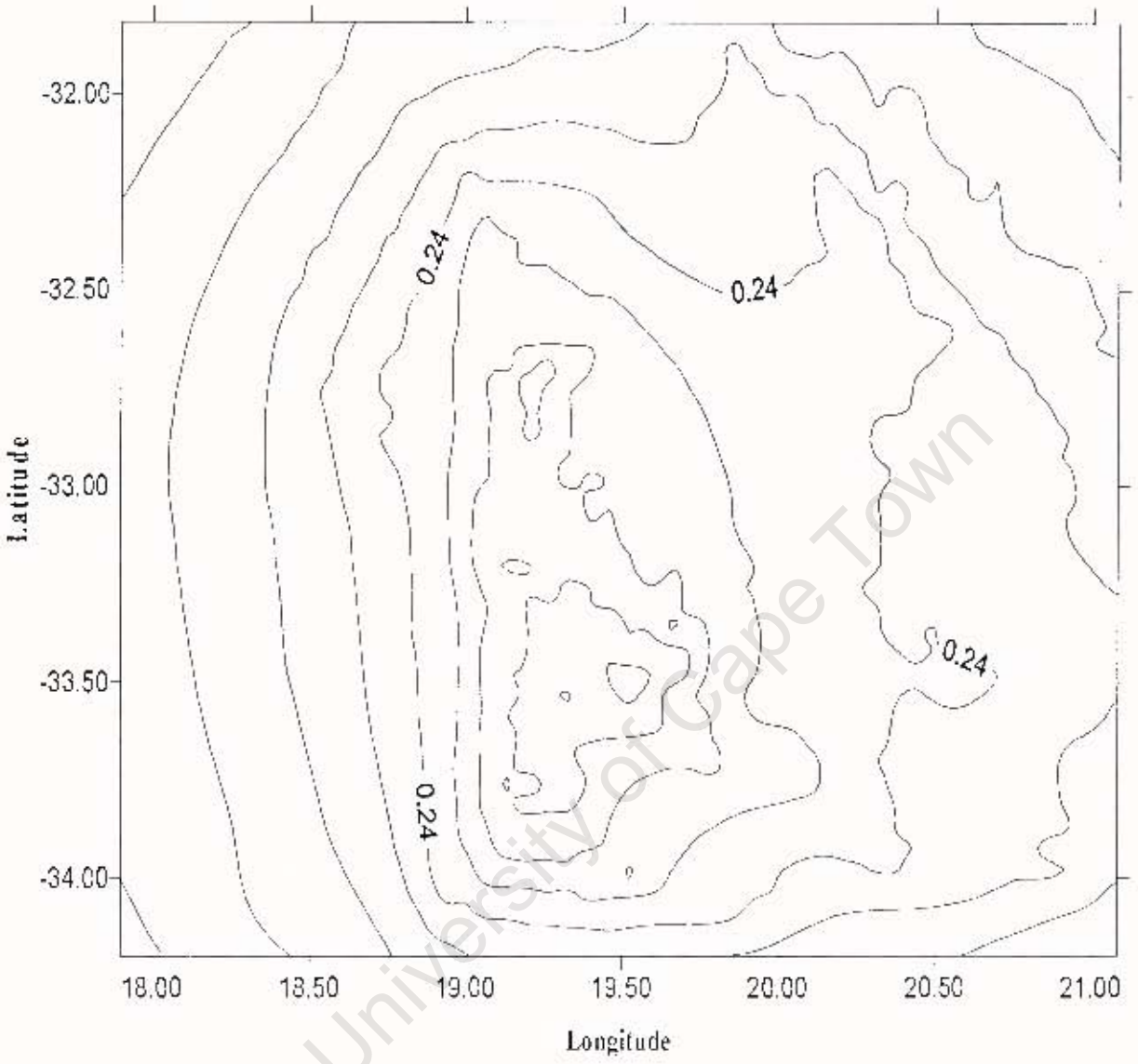

Figure A.14: G_1 Contribution to the Quasi-geoid
Grid Interval – 1 minute
(Contour Interval 0.04m)

APPENDIX B

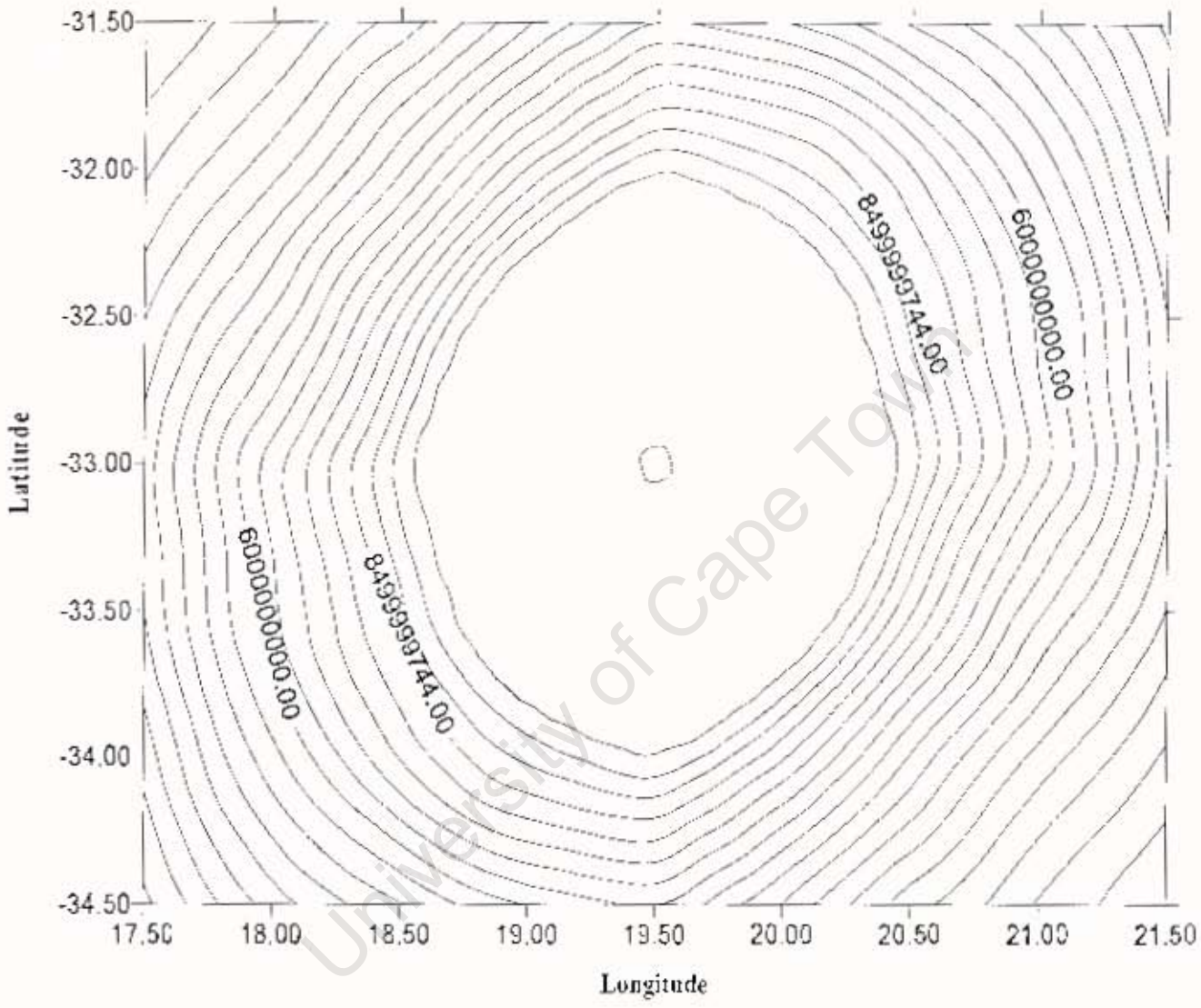

Figure B.2: Height Autocorrelation Function - South Western Cape

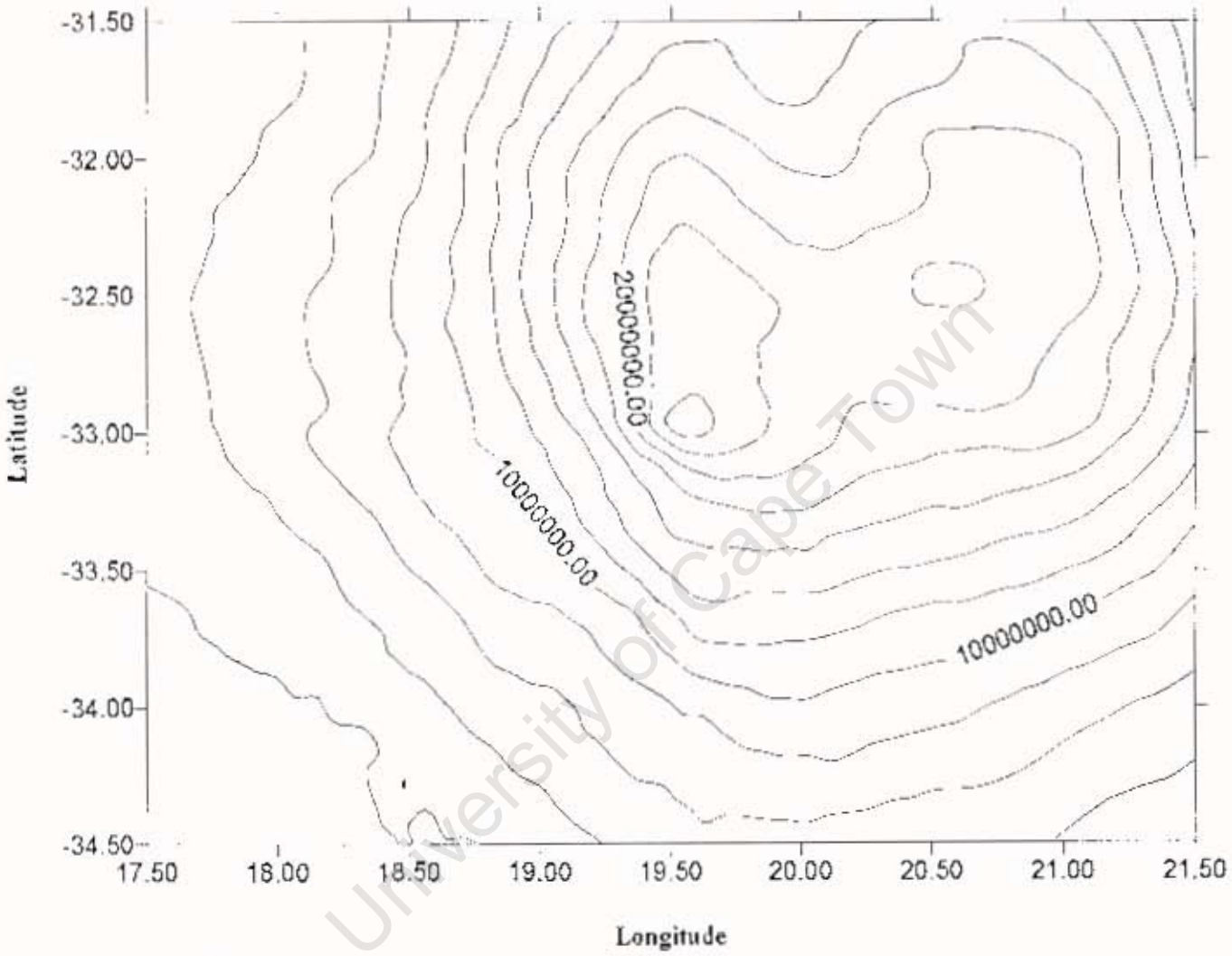

Figure B.2: G_1 Autocorrelation Function – South Western Cape

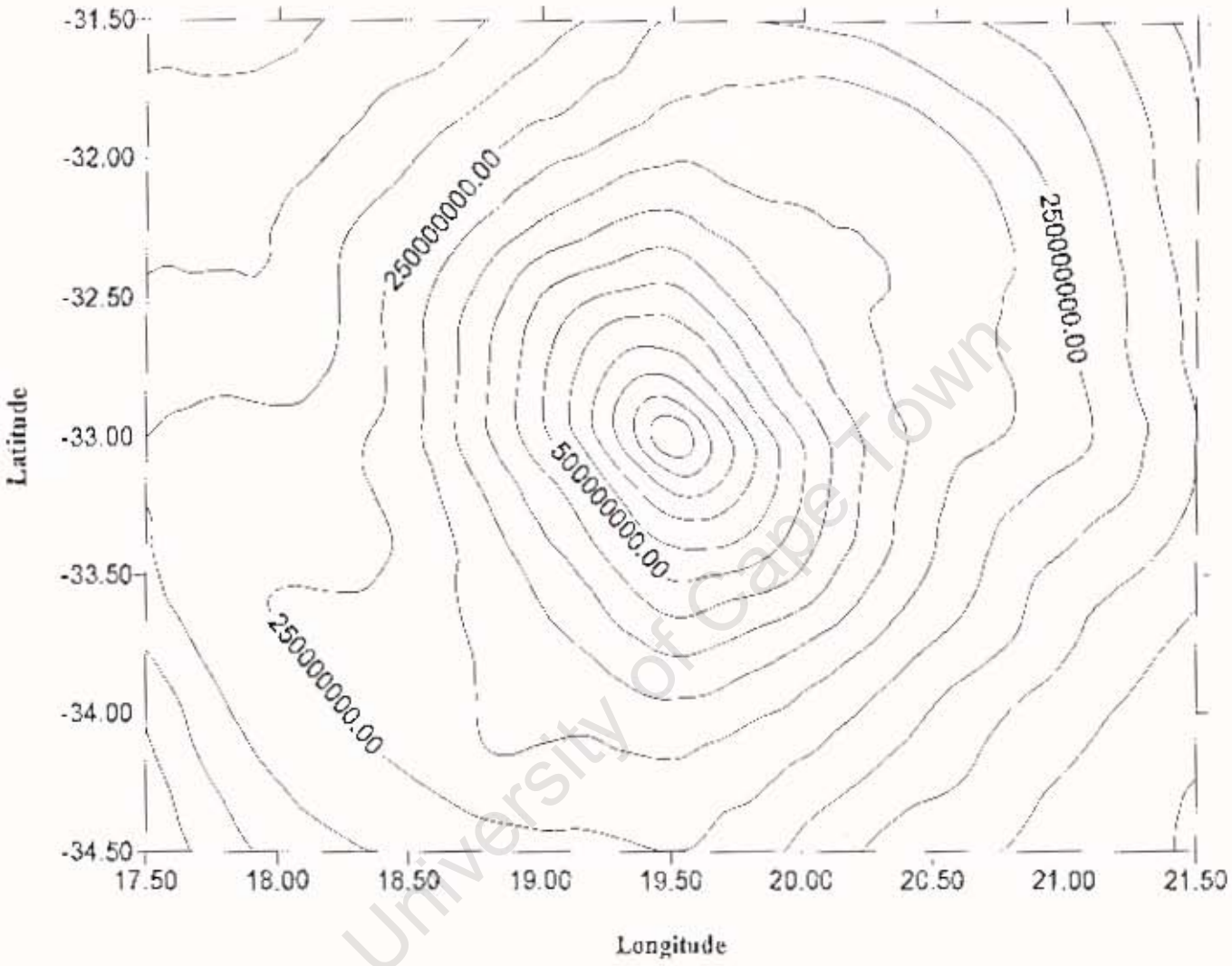

Figure B.3: Free Air Anomaly and Height Cross Correlation Function – South Western Cape

APPENDIX C

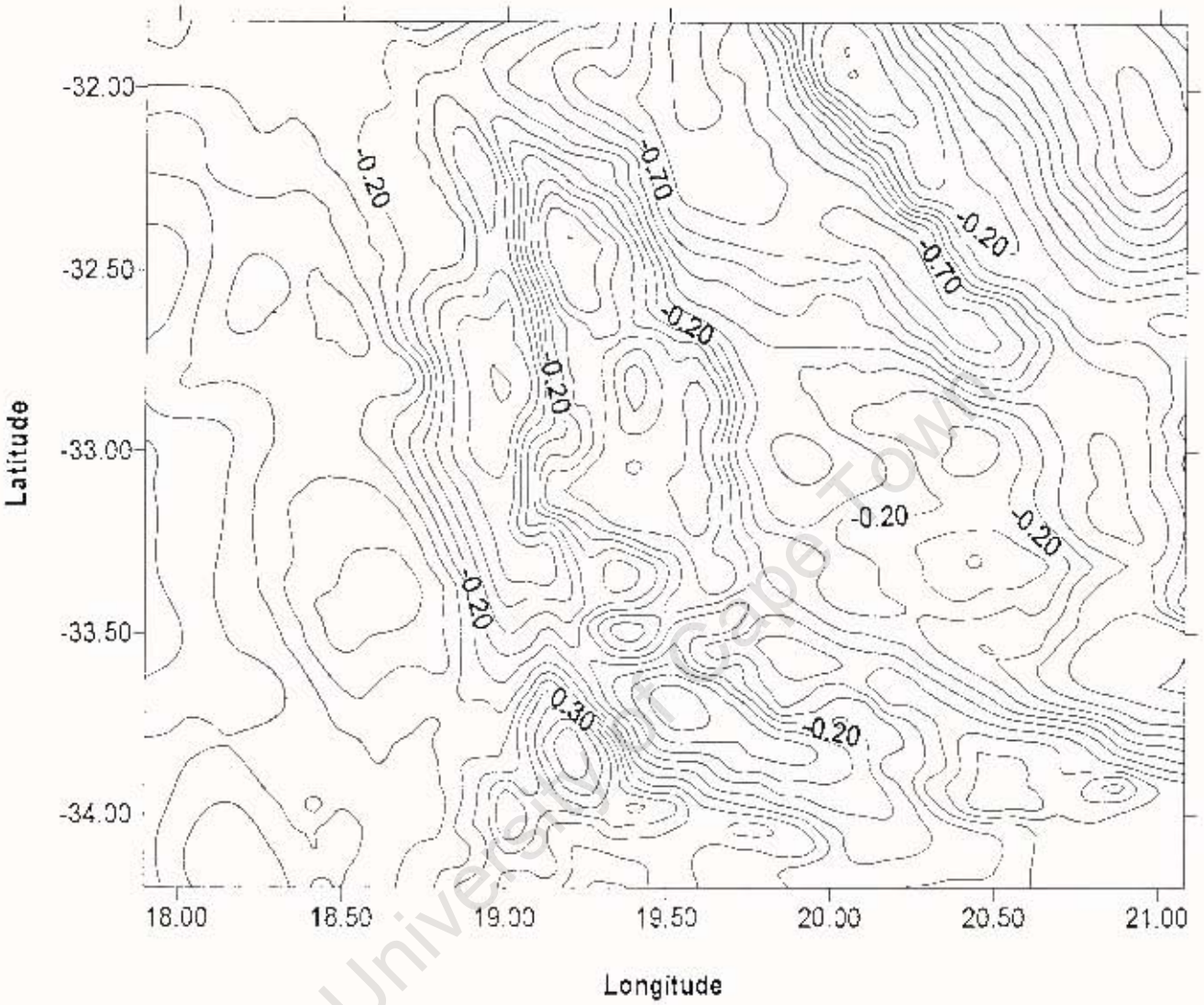

Figure C.1: Residual Quasi-Geoid for the South Western Cape via planar FFT (Contour Interval 0.1m)

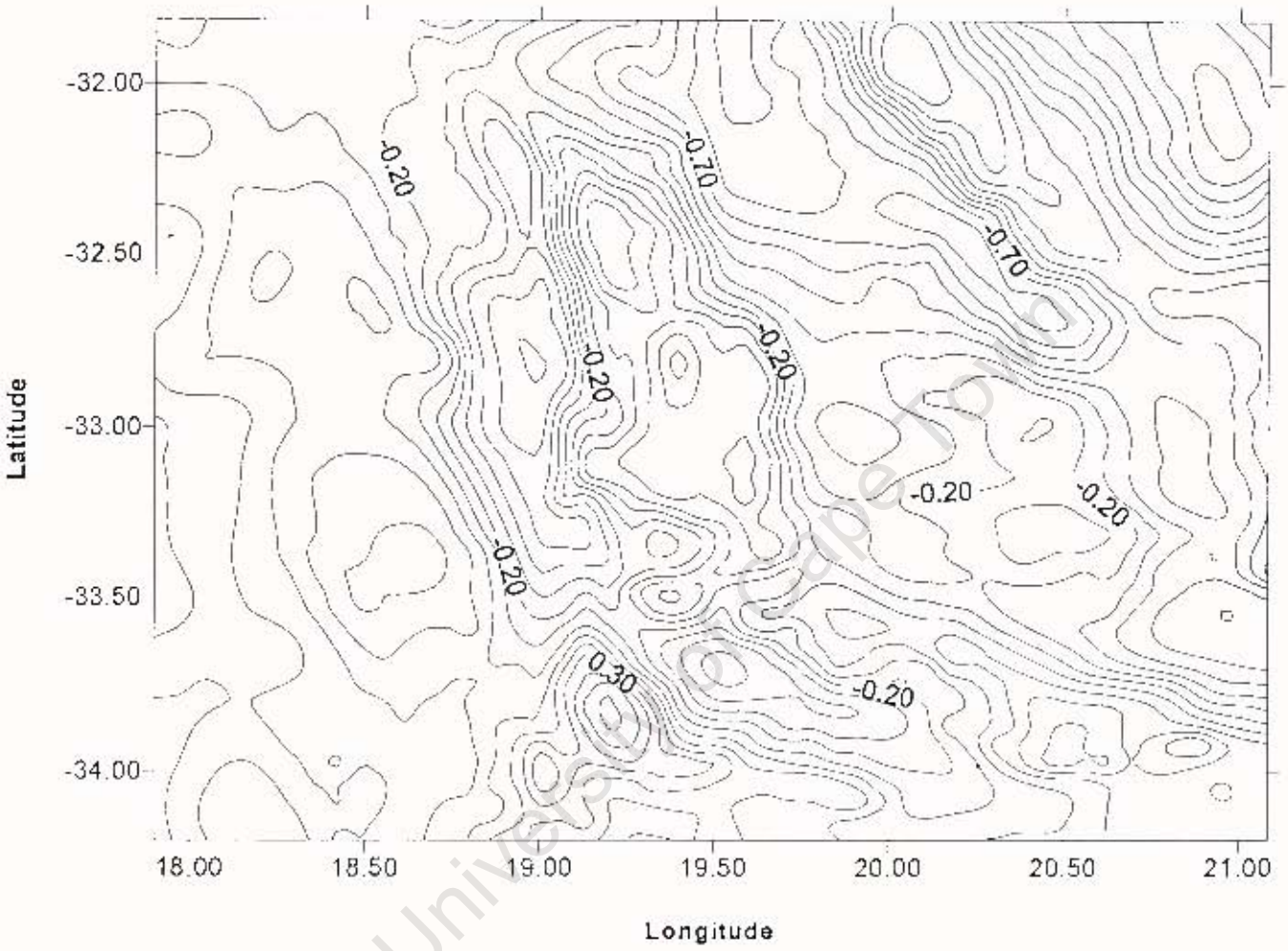

Figure C.2: Residual Quasi-Geoid for the South Western Cape via Spherical FFT (Contour Interval 0.1m)

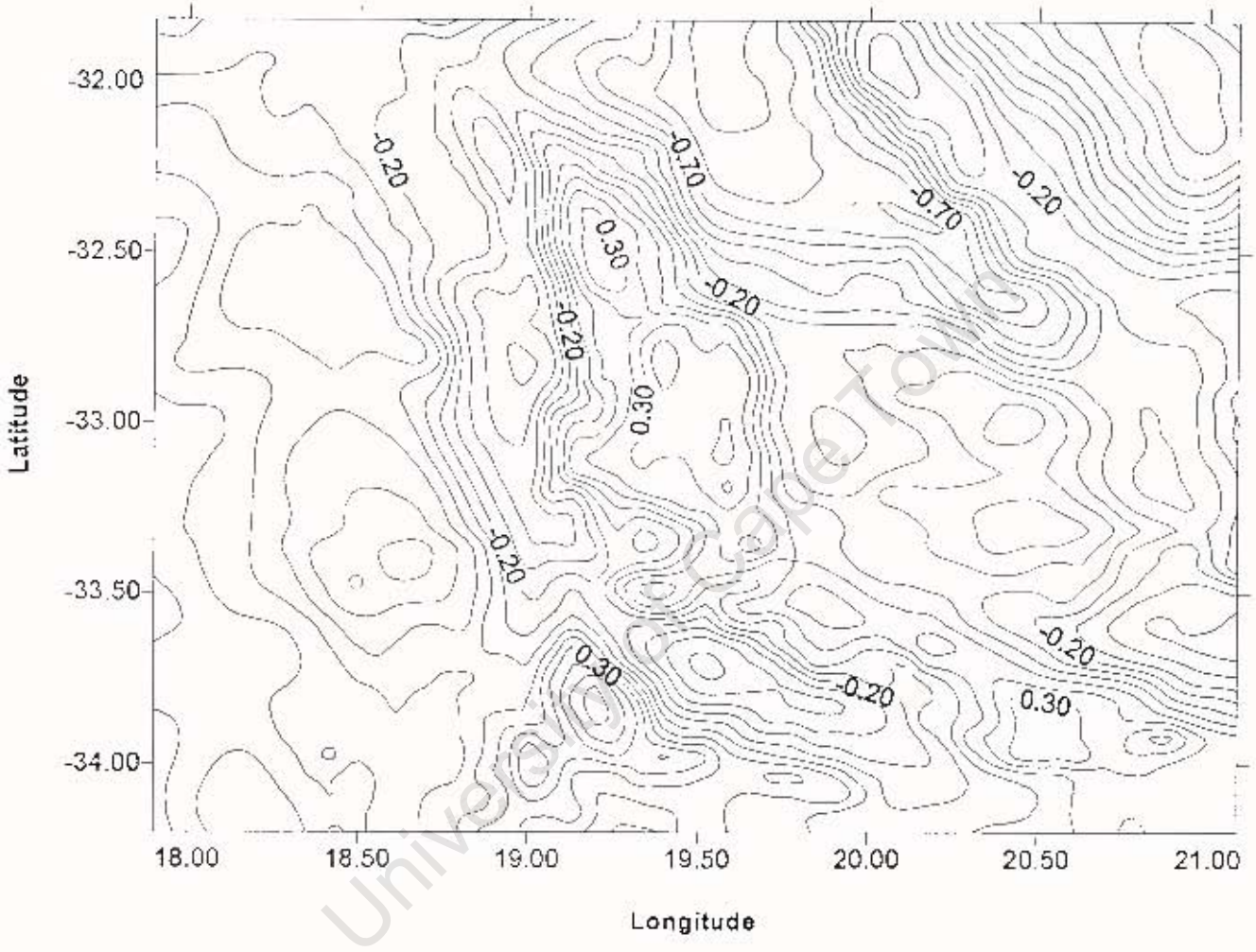

Figure C.3: Residual Quasi-Geoid for the South Western Cape via Multi-band SFFT (2 bands, 20 minute overlap) (Contour Interval 0.1m)

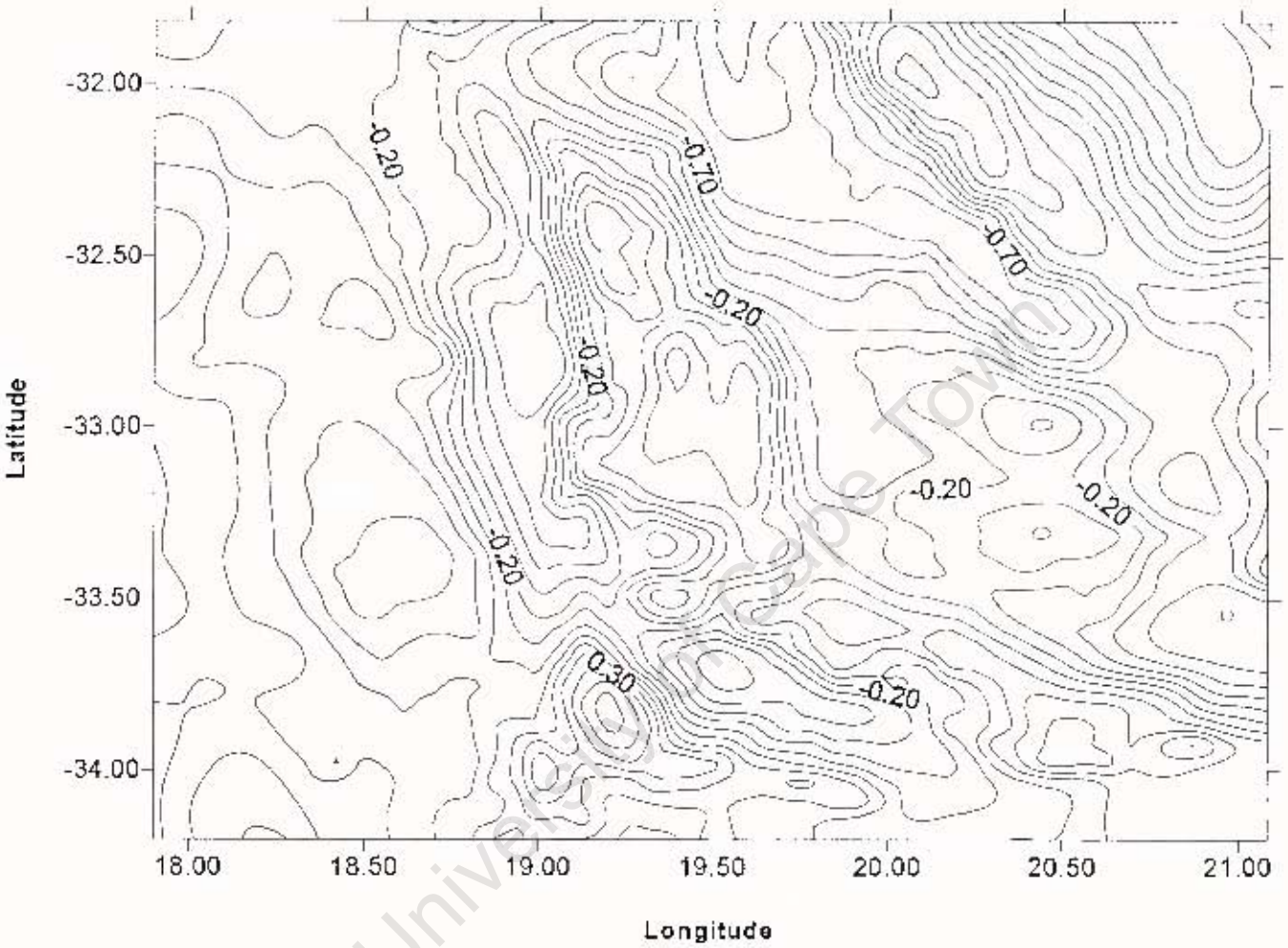

Figure C.4: Residual Quasi-Geoid for the South Western Cape via Multi-band SFFT (2 bands, 80 minute overlap) (Contour Interval 0.1m)

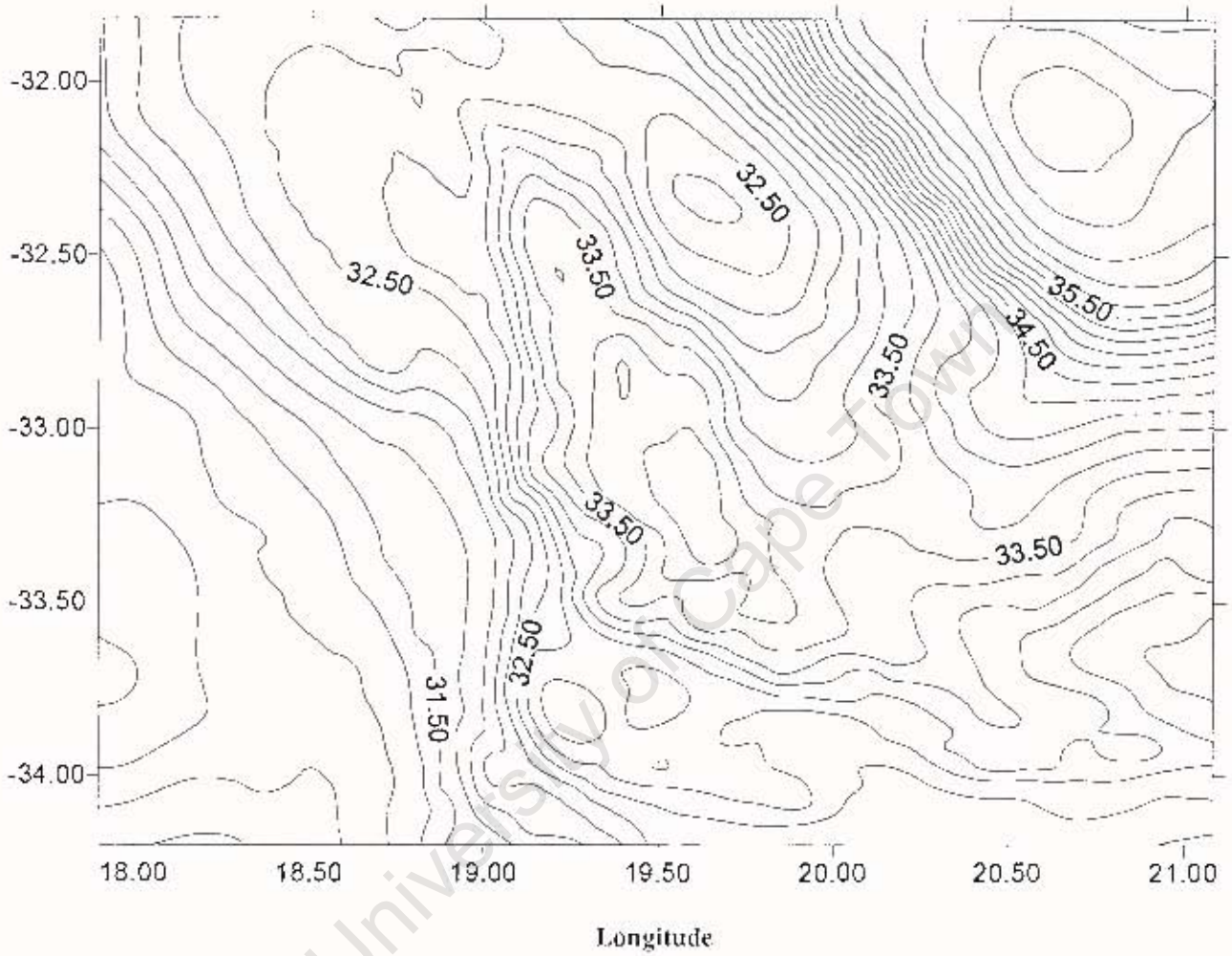

Figure C.5: Quasi-Geoid for the South Western Cape via Spherical FFT (Contour Interval 0.2m)

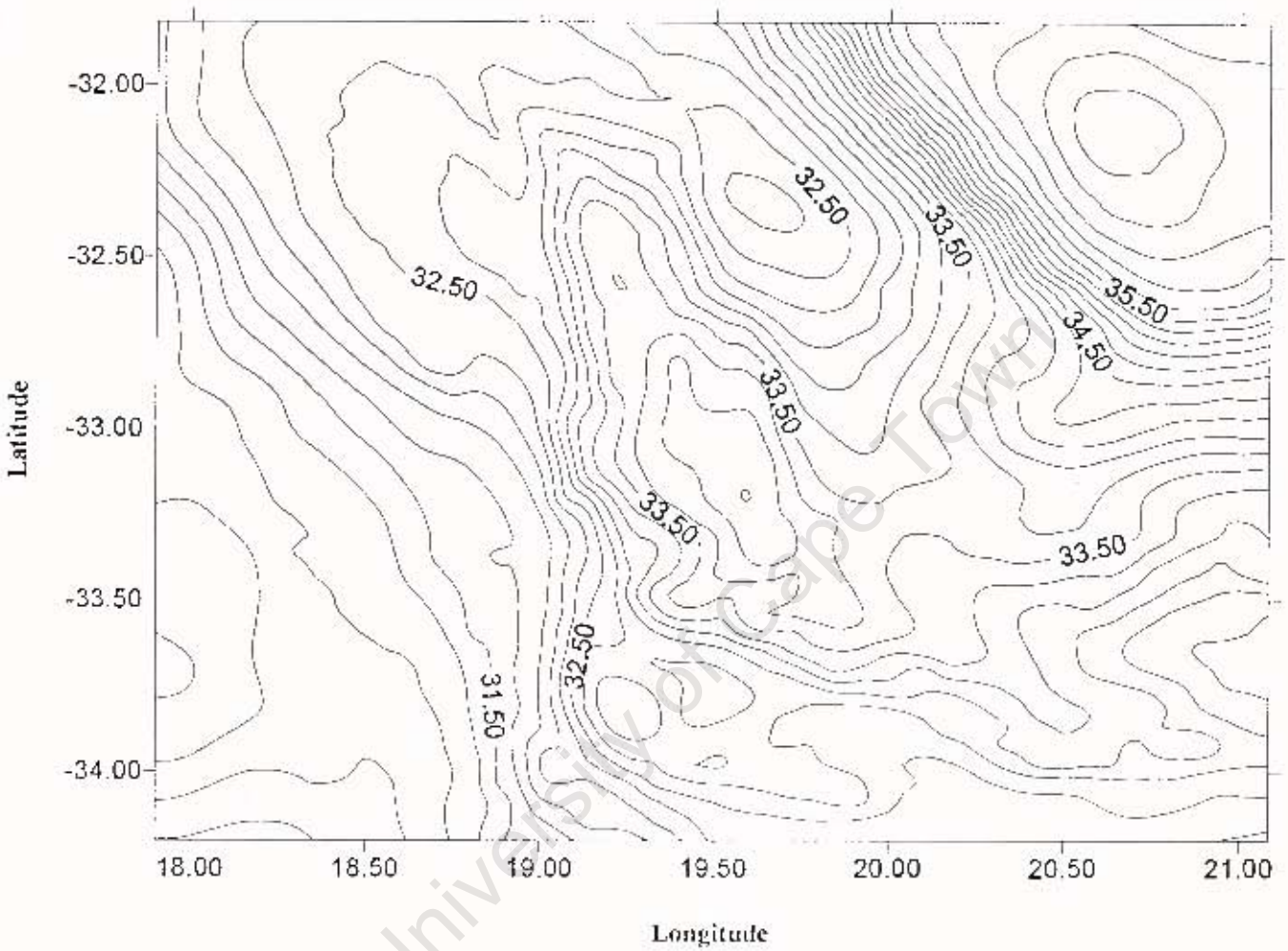

Figure C.6: Quasi-Geoid for the South Western Cape via Multi-Band SFFT (2 band, 80 minute overlap) (Contour Interval 0.2m)

APPENDIX D

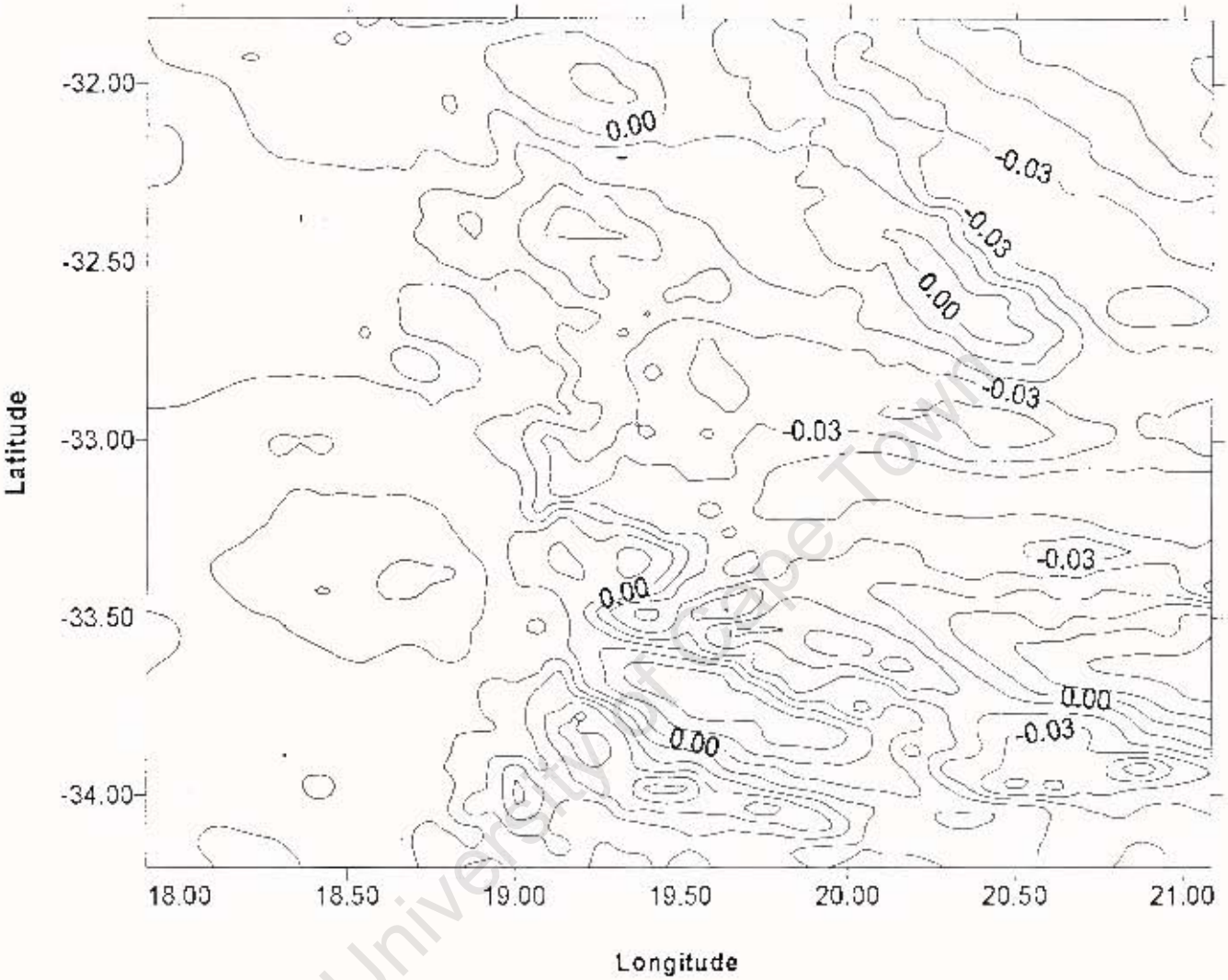

Figure D.1: Quasi-geoid Differences between Planar FFT and Spherical FFT – South Western Cape
(Contour Interval 0.01m)

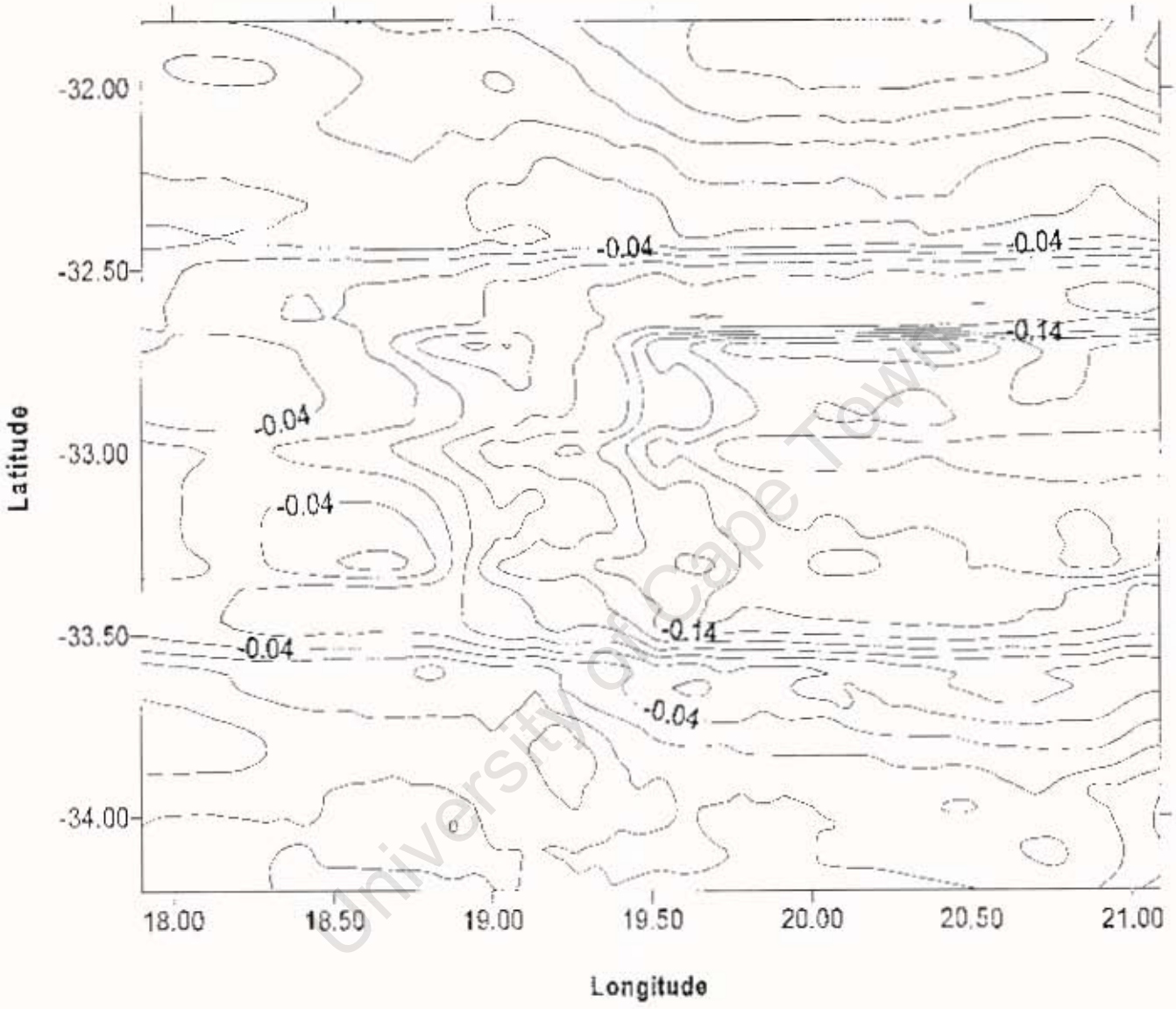

Figure D.2: Quasi-geoid Differences between Planar FFT and Multi-band Spherical FFT (2 bands 20 minute overlap)– South Western Cape (Contour Interval 0.02m)

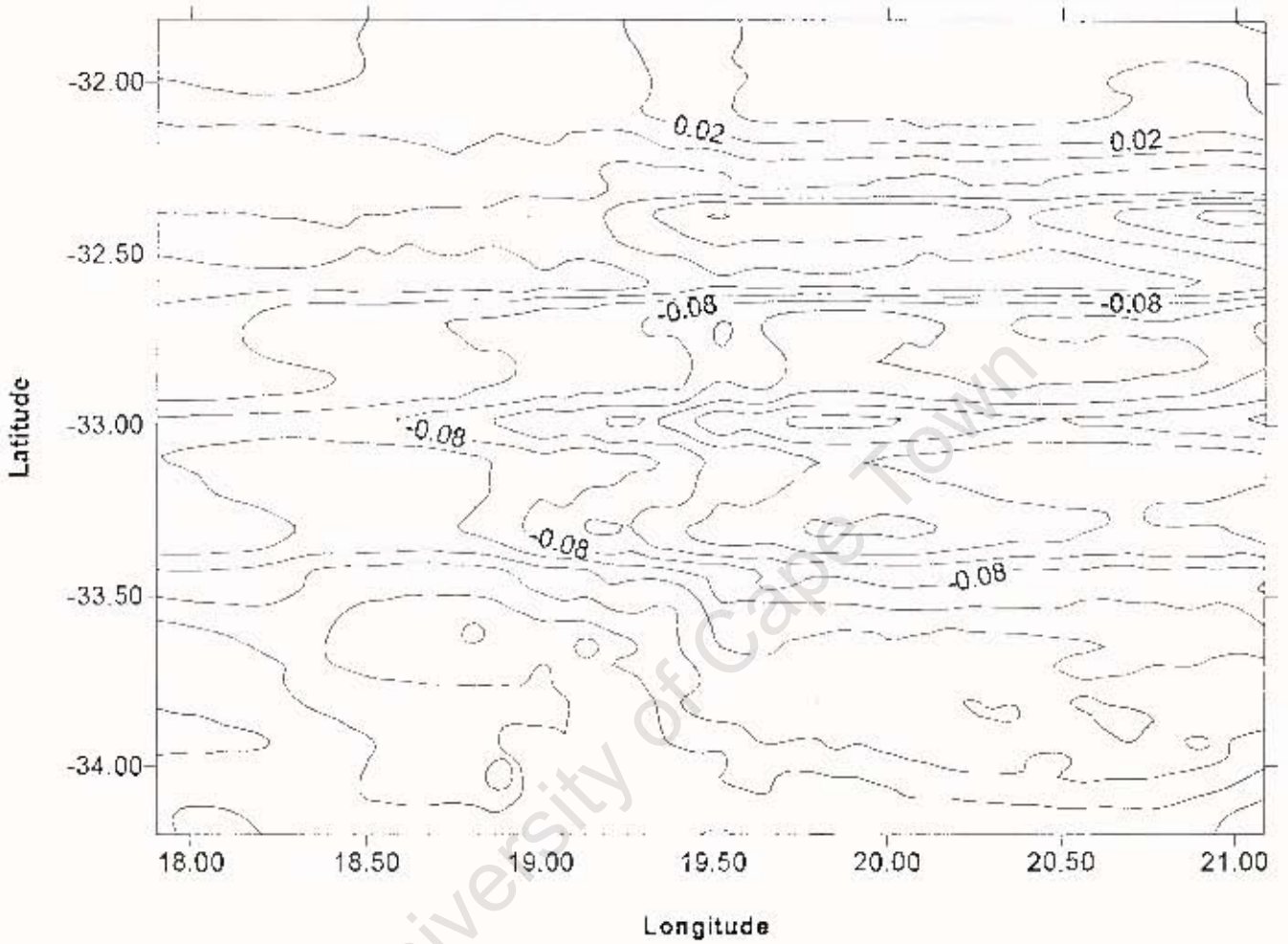

Figure D.3: Quasi-geoid Differences between Planar FFT and Multi-band Spherical FFT (2 bands 40 minute overlap) - South Western Cape
(Contour Interval 0.02m)

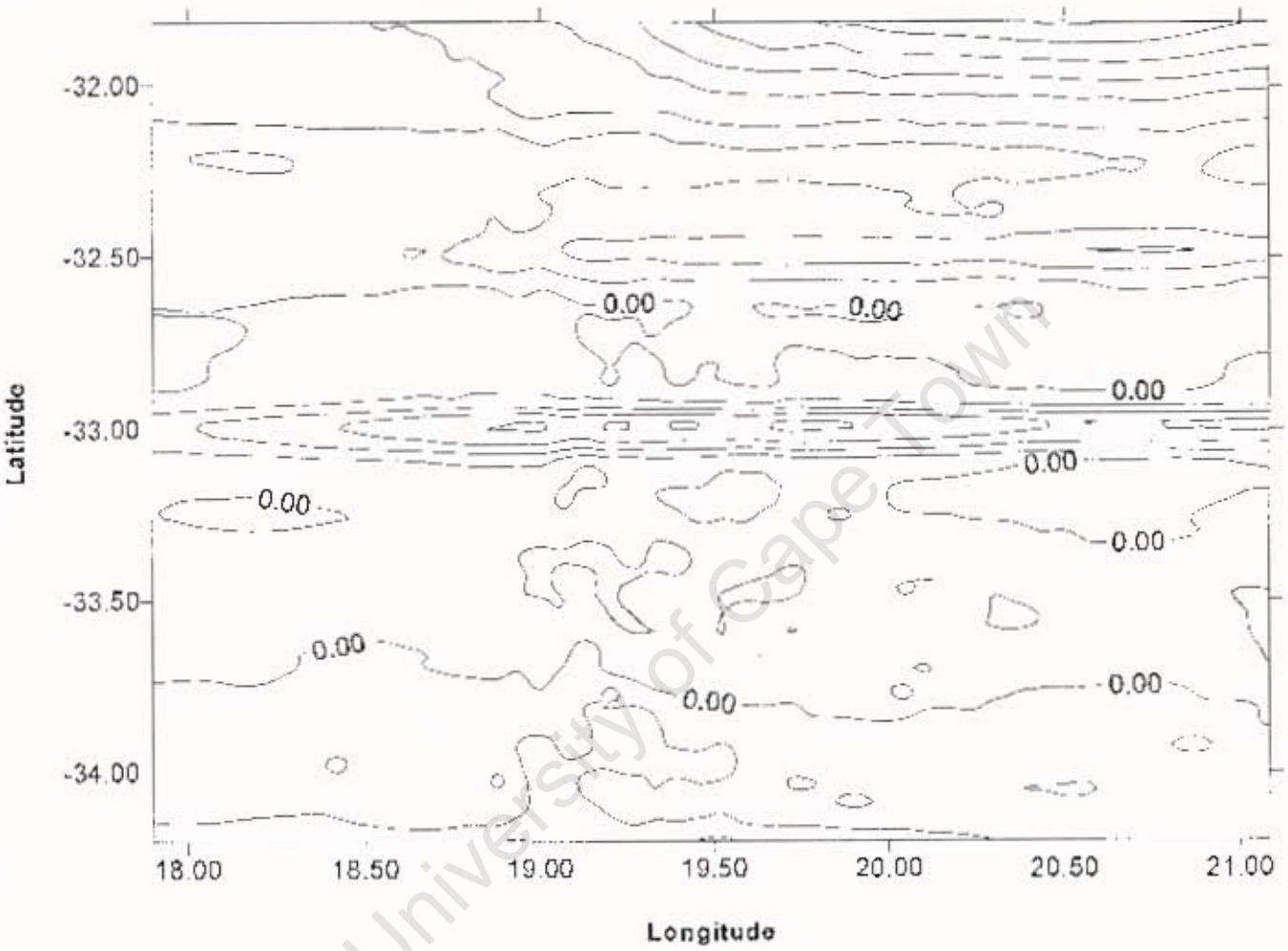

Figure D.4: Quasi-geoid Differences between Planar FFT and Multi-band Spherical FFT (2 bands 80 minute overlap)– South Western Cape
(Contour Interval 0.02m)

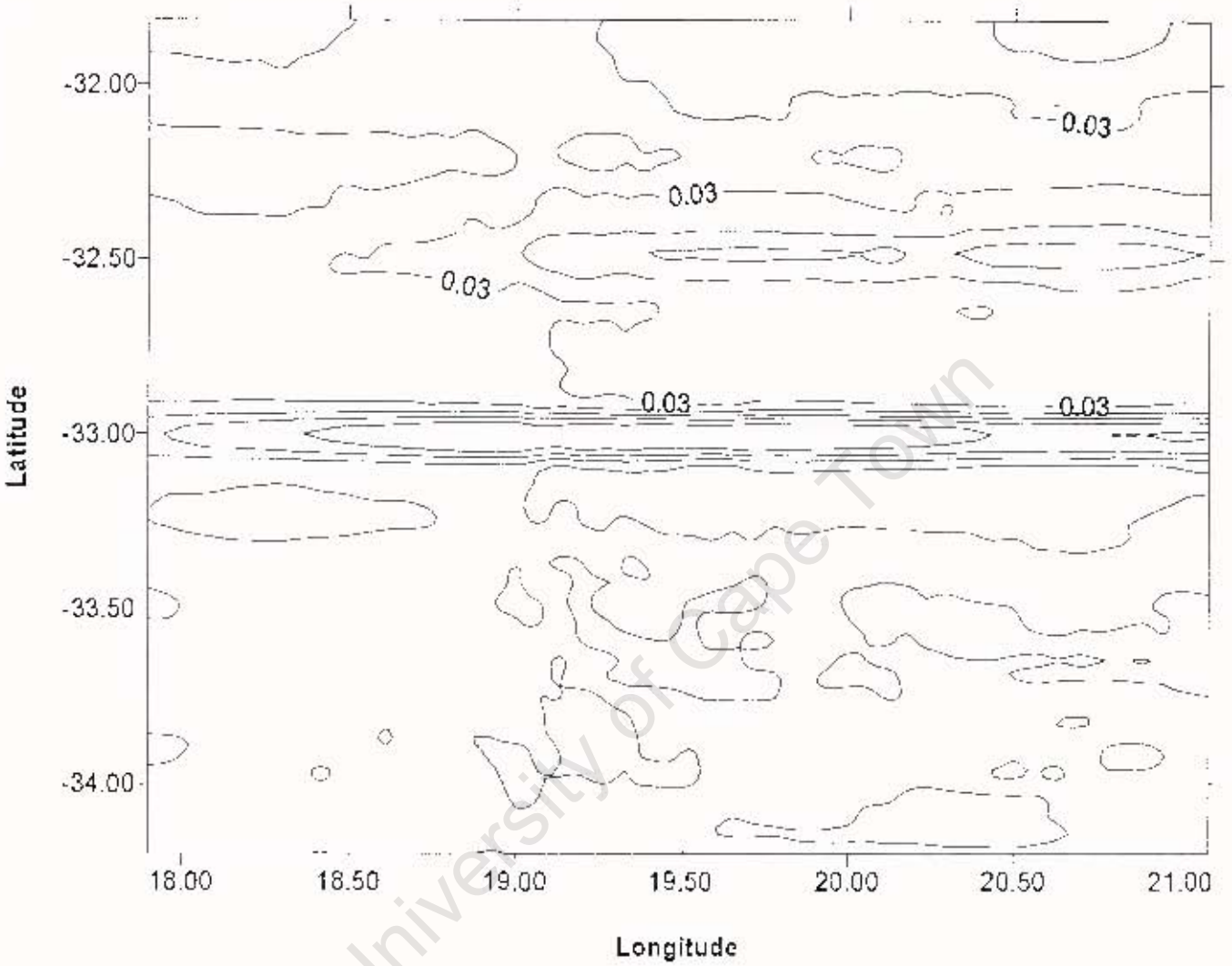

Figure D.5: Quasi-geoid Differences between Planar FFT and Multi-band Spherical FFT (2 bands 80 minute overlap with *no interpolation*)– South Western Cape
(Contour Interval 0.02m)

APPENDIX E

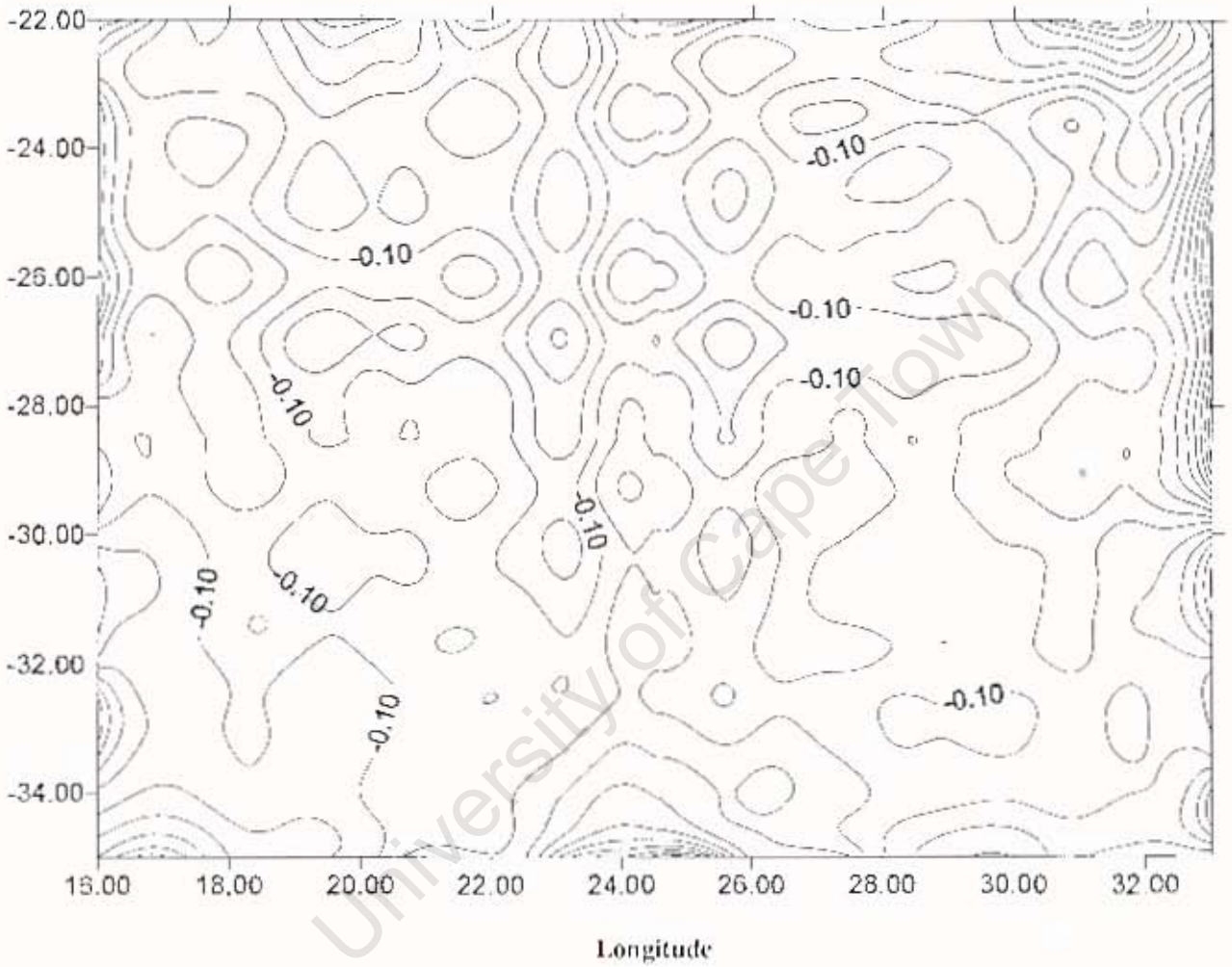

Figure E.1: Differences between Planar FFT and EGM96 Quasi-geoids (Contour Interval: 0.1m)

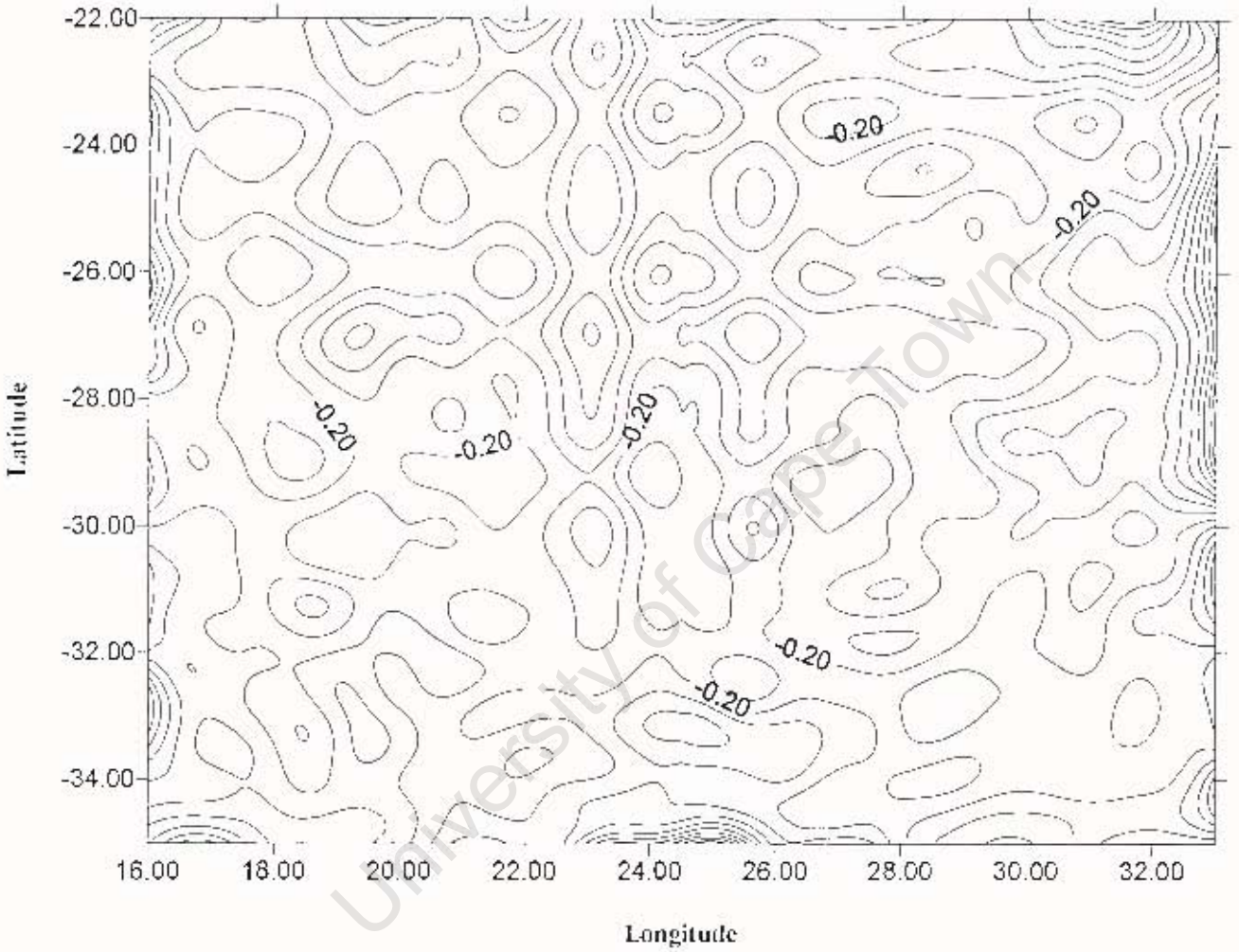

Figure E.2: Differences between Spherical FFT and EGM96 Quasi-geoids
(Contour Interval: 0.1m)

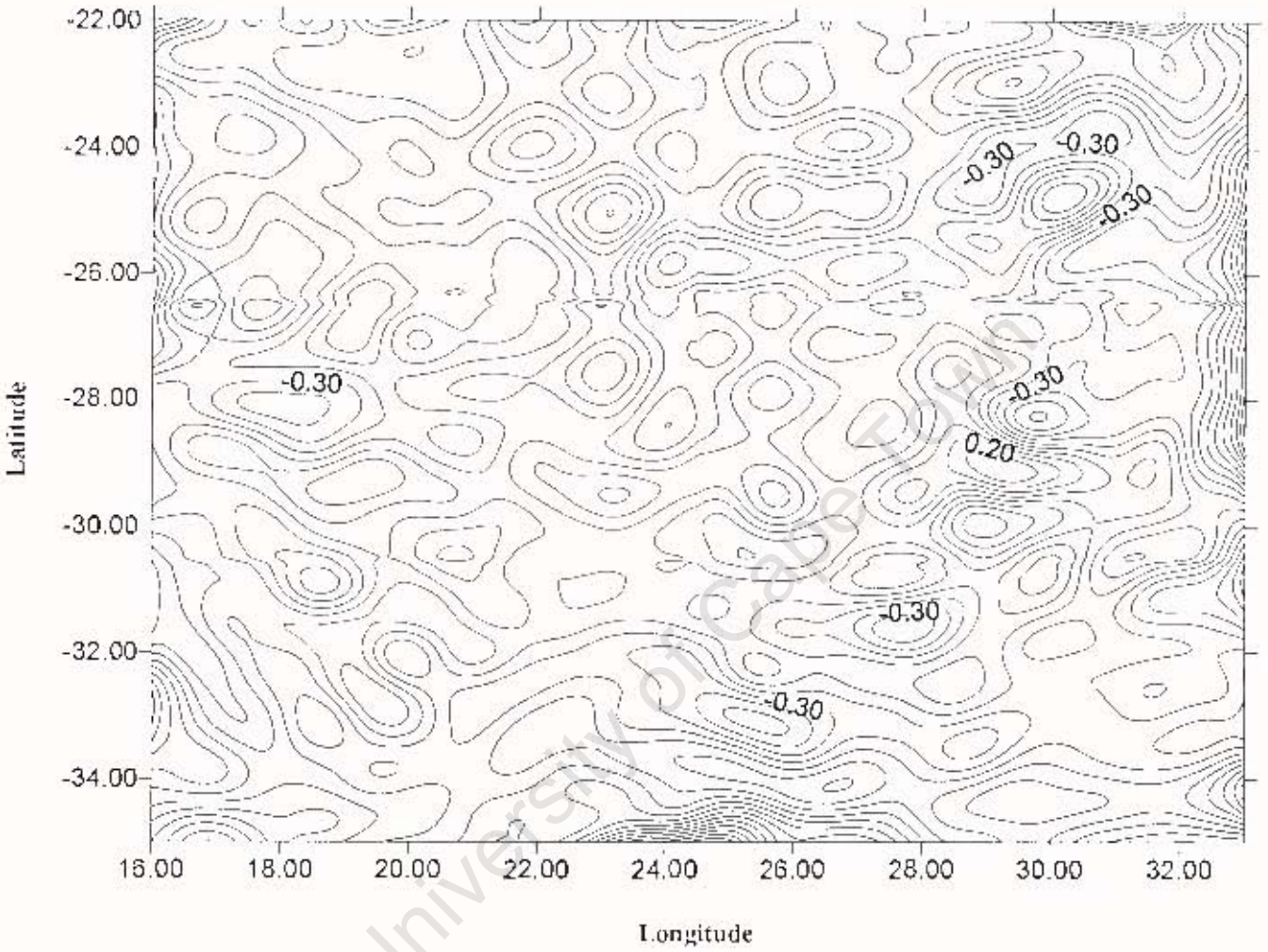

Figure E.3: Differences between multi-band FFT (2band/2deg.) and EGM96 Quasi-geoids (Contour Interval: 0.1m)

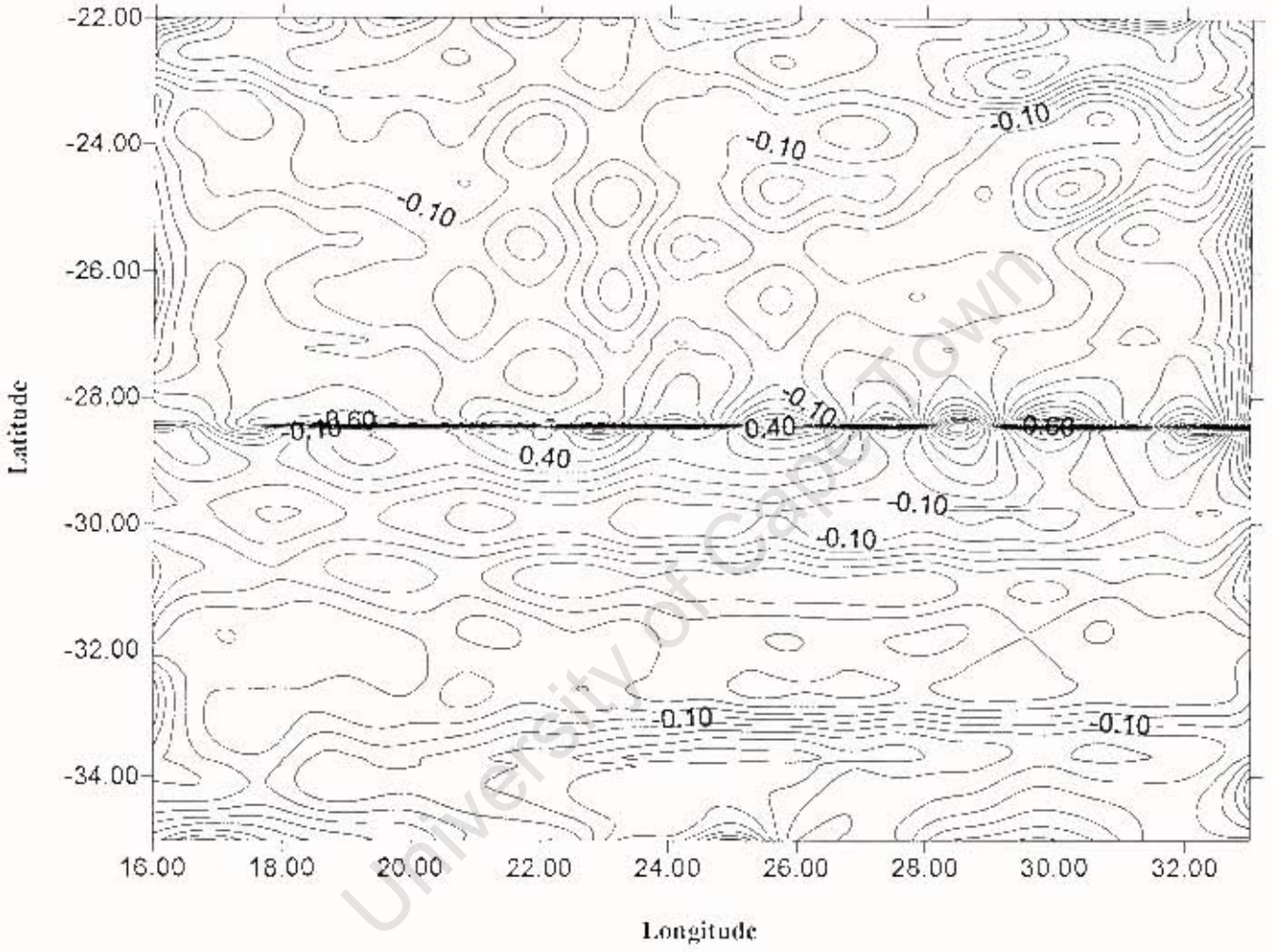

Figure E.4: Differences between multi-band FFT (4band/2deg.) and EGM96 Quasi-geoids (Contour Interval: 0.1m)

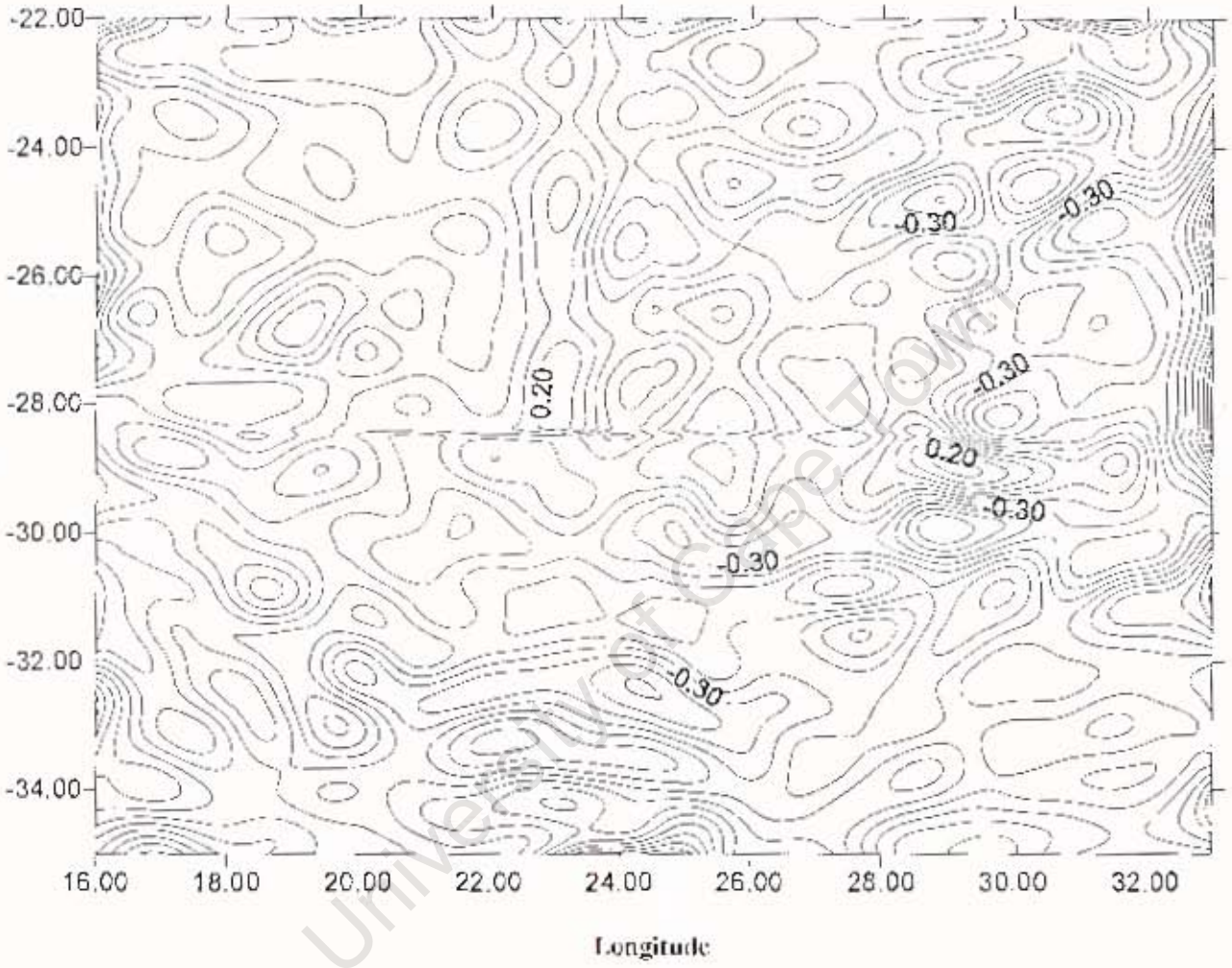

Figure E.5: Differences between multi-band FFT (2band/3deg., no interpolation) and EGM96 Quasi-geoids (Contour Interval: 0.1m)